Imperial College

London

Nanocapsules via Layer-by-Layer Self-assembly Technique

Li Ye

A Thesis submitted in partial fulfilment of the requirements for the degree of Doctor of Philosophy

Imperial College London

Department of Chemical Engineering and Chemical Technology December 2011

Imperial College London

Department of Chemical Engineering and Chemical Technology

Nanocapsules via Layer-by-Layer Self-assembly Technique

©2011 Ye Li

y.li05@imperial.ac.uk

This publication may be distributed freely in its entirety and its original form without the

consent of the copyright owner.

Use of this material in any other published works must be appropriately referenced, and, if necessary, permission sought from the copyright owner.

Published by: Ye Li

Department of Chemical Engineering and Chemical Technology

Imperial College London

South Kensington Campus

London SW7 2AZ

December 2011

www3.imperial.ac.uk/chemicalengineering

DEDICATION

This work is dedicated to my beloved parents for their unconditional love…

Content

List of Figures 5

List of Tables 10

Abstract 12

Acknowledgements 13

Abbreviations 14

Chapter 1 Introduction 17

Chapter 2 Literature Review 21

2.1 Drug delivery systems 21

2.2 Review of Other Hollow Capsule Synthesis Methods 24

2.3 Nanocapsules Synthesised via the Layer-by-Layer Self-assembly Method 27

2.3.1 The Principles of the Layer-by-Layer Method 27

2.3.2 Application of Layer-by-Layer Self-assembly Method on Preparation of Micro- and Nano-capsules 29

2.3.3 Advantages of Layer-by-Layer Self-assembly Strategy 32

2.3.4 Encapsulation 33

2.3.5 Releasing of Loaded Components 37

2.3.6 Core Templates and Coating Materials 42

2.4 Summary of the Motivation and Innovation of this PhD Project 47

Chapter 3 Characterization Methods 48

3.1 Zeta-Potential Measurement 48

3.2 Dynamic Light Scattering 53

3.3 Electron Microscope 55

3.3.1 Scanning Electron Microscope 56

3.3.2 Transmission Electron Microscope 58
3.4 Disc Centrifuge 60
3.5 X-ray Powder Diffraction 61
Chapter 4 Nanocapsules Based on Silica Core Templates 65
4.1 Materials 65
4.2 Methodology 66
4.2.1 Synthesis of Silica Nanoparticles 66
4.2.2 Polyelectrolyte Preparation Process 68
4.2.3 Layer-by-layer Self Assembly Process 68
4.2.4 Core Removal Process 69
4.3 Results and Discussions 70
4.3.1 Sizes of Silica Particles 70
4.3.2 Polyelectrolyte Assembly Process 75
4.3.3 Core Removal Process 80
4.4 Conclusion 84
Chapter 5 Nanocapsules Based on Large Polystyrene Core Templates 86
5.1 Materials 86
5.2 Methodology 87
5.2.1 Synthesis of Polystyrene Nanoparticles 87
5.2.2 Layer-by-Layer Self-assembly Process 89
5.2.3 Core Removal 93
5.3 Results and Discussion 93
5.3.1. Polystyrene Core Particles 93
5.3.2 Layer-by-Layer Self-assembly 94

5.4 Conclusion....118
Chapter 6 Nanocapsules Based on Small Polystyrene Core Templates....119
6.1 Materials....119
6.2 Methodology....120
6.2.1 Synthesis of Polystyrene Nanoparticles....120
6.2.2 Fabrication of Nanocapsules via Layer-by-Layer Self-assembly Method 120
6.3 Results and Discussion....125
6.3.1 Polystyrene Nanoparticles Synthesized with Surfactant....125
6.3.2 Nanocapsules Consisting of Polyelectrolyte and Laponite....128
6.3.3 Functionalization of the Nanocapsules....134
6.4 Conclusion....145
Chapter 7 Nanocapsules Consisting of Proteins and Polyelectrolyte....146
7.1 Nanocapsules Consisting of Proteins via Polystyrene Nanoparticles....146
7.1.1 Materials....146
7.1.2 Methodology....147
7.1.3 Results and Discussion....150
7.2 Fabrication of Encapsulated Insulin Nanoparticles....160
7.2.1 Materials....160
7.2.2 Methodology....160
7.2.3 Results and Discussion....162
7.3 Conclusion....169
Chapter 8 Conclusions and Recommendations for Future Work....170
8.1 Conclusions....170
8.2 Recommendation for Future Work....173

Appendix.....176

Reference 186

List of Figures

Fig. 2.1 Different structures of the nano-scale delivery system [47] 23
Fig. 2.2 The diagram shows the process of the LbL method [93] 29
Fig. 2.3 shows procedures for hollow nanospheres production via Layer-by-Layer self-assembly methods [1]. 31
Fig. 2.4 Techniques for encapsulating therapeutics: A) loading after the capsule formed; B) encapsulate crystal particles C) components preloaded in porous particles [107]. 34
Fig. 2.5 The fabrication of biocompatible hollow capsules and the loaded protein releasing system [131]. 37
Fig. 2.6 Demonstration of burst release of nanocapsule consisting of polyelectrolyte and gold nanoparticles triggered by laser [107] 39
Fig. 2.7 Release figure of FITC-albumin from hollow capsules of different polyelectrolyte combination at different temperatures, CT and Dex in the figure correspond to CHI and DS in this thesis [131]. 41
Fig. 3.1 A schematic of the Double Layer of Colloidal Particles [185] 48
Fig. 3.2 The relationship of the electric potential and the distance from the particle surface [189]. 49
Fig. 3.3 Graph of zeta-potential of CHI and ALG depositing on PS particles [113] ... 50
Fig. 3.4 The machine (ZetaPALs) used to measure the Zeta-potential of the nanoparticles 51
Fig. 3.5 Graph of the inner structure of a SEM [206] 57
Fig. 3.6 Leo 1525 Gemini Field Emission Gun SEM 58
Fig. 3.7 Graph of working principle of TEM [210] 59
Fig. 3.8 JEOL 2010 TEM 60
Fig. 3.9 Illustration of principle of the Disc Centrifuge [211] 60
Fig. 3.10 The diagram of the principle of the X-ray powder diffractometer [216] 62
Fig. 3.11 The Philips PW1700 X-ray diffractometer 64
Fig. 4.1 Diagram of the dialysis process 67
Fig. 4.2 Particles size distribution of the silica particles from the method: 50 ml Ethanol 4 ml TEOS and 2.4 ml NH4OH with reaction time of 4 hr. 70
Fig. 4.3 Particle size distribution of the silica particles with the method of 2.4 ml NH4OH. 71
Fig. 4.4 SEM micrographs of the silica particles from the method: 1.4 ml NH4OH/4 ml TEOS 73
Fig. 4.5 SEM micrographs of the silica particles from the method: 1.6 ml NH4OH/4 ml TEOS 73
Fig. 4.6 SEM micrographs of the silica particles from the method: 2.4 ml NH_4OH/4 ml TEOS 73
Fig. 4.7 SEM micrographs of the silica particles from the method: 2.8 ml NH_4OH/4 ml TEOS 74

Fig. 4.8 SEM micrographs of the silica particles from the method: 3.2 ml NH_4OH/4 ml TEOS 74
Fig. 4.9 The first layer (CHI) deposition at different salt concentration (from left to right 0.1 M, 0.3 M, 0.5 M) 76
Fig. 4.10 The zeta-potential of each polyelectrolyte layer coated on 95 nm silica particles (CHI/DS) 78
Fig. 4.11 The zeta-potential of each polyelectrolyte layer coated on 114 nm silica particles (CHI/DS) 78
Fig. 4.12 SEM micrograph of silica nanoparticles 95 nm (from 1.4 ml NH_4OH/4 ml TEOS system) coated with 9 layers polyelectrolyte with a sequence: CHI/DS/CHI. . 79
Fig. 4.13 SEM micrograph of silica nanoparticles 114 nm (from 1.6 ml NH_4OH/4 ml TEOS system) coated with 9 layers polyelectrolyte with a sequence: CHI/DS/CHI. . 80
Fig. 4.14 SEM micrograph of nanocapsules consisted of CHI and DS, based on silica nanoparticles 95 nm (from 1.4 ml NH_4OH/4 ml TEOS system) 81
Fig. 4.15 TEM micrograph of nanocapsules consisted of CHI and DS, based on silica nanoparticles 95 nm (from 1.4 ml NH_4OH/4 ml TEOS system) 82
Fig. 4.16 SEM micrograph of nanocapsules consisted of CHI and DS, based on silica nanoparticles 114 nm (from 1.6 ml NH_4OH/4 ml TEOS system) 82
Fig. 4.17 TEM micrograph of nanocapsules consisted of CHI and DS, based on silica nanoparticles 114 nm (from 1.6 ml NH_4OH/4 ml TEOS system) 83
Fig. 5.1 Inhibitor removal column 87
Fig. 5.2 3-neck Round-bottom reactor for polymerization 88
Fig. 5.3 Geometry of Laponite disk [230]. 90
Fig. 5.4 Phase Diagram of Laponite suspensions [232] 90
Fig. 5.5 SEM micrographs of the polystyrene particles with different magnifications 94
Fig. 5.6 Zeta-potential of the polymer layers (polystyrene/PDADMAC/DS/PDADMAC) at different salt concentration. 96
Fig. 5.7 The zeta-potential of the each coating layer ($(PDADAMAC/PSS)_5$ 1 mg/ml PE, 0.1 M NaCl) 97
Fig. 5.8 SEM micrograph of 10 layers (5 PDADMAC/PSS bi-layers) coated polystyrene particles 98
Fig. 5.9 SEM micrographs of different magnifications of particles composed of 3 layers (PDADMAC/PSS/PDADMAC) 100
Fig. 5.10 TEM micrographs of the polystyrene particles with 10 layers after 24 hours of core removal 101
Fig. 5.11 SEM micrographs of the particles composed of (a) 8 coating layers (3 Laponite layers), (b) 13 coating layers (5 Laponite layers) 104
Fig. 5.12 The zeta-potential of the each coating layer (synthetic polyelectrolyte and Laponite). 105
Fig. 5.13 SEM micrographs of the particles coated with 18 layers 107
Fig. 5.14 TEM micrographs of nanocapsules consisting of 5 layers of polyelectrolyte and Laponite before (a,b) and after (c,d) the THF dissolving 108
Fig. 5.15 TEM and SEM micrographs nanocapsules consisting of 8 layers

(5PE/3Laponite) after the core removal process, (a) (b) SEM and (c) (d) TEM 109
Fig. 5.16 TEM micrographs of the nanocapsules consisting of 9 layers of polyelectrolyte and Laponite (6PE/3Laponite) after the core removal process..... 110
Fig. 5.17 TEM micrographs of the nanocapsules consisting of 12 layers of polyelectrolyte and Laponite (7PE/5Laponite) after the core removal process..... 110
Fig. 5.18 TEM micrographs of nanocapsules consisting of 13 layers of polyelectrolyte and Laponite (8PE/5Laponite) after the core removal process..... 111
Fig. 5.19 SEM micrographs (at different magnification) of polystyrene particles coated with 10 layers of biocompatible polymers 114
Fig. 5.20 SEM micrographs of polystyrene particles coated with 11 layers of biocompatible polymers and one layer (outer layer) of Laponite particles, a) b) represent different magnifications 115
Fig. 5.21 The zeta-potential of the each coating layer (biocompatible polymers and outer layer Laponite)..... 116
Fig. 5.22 SEM micrographs of coated polystyrene particles after treated with THF. (a) coated with 10 layers(5 bi-layers CHI/DS); (b) coated with 12 layers (5 bi-layers CHI/DS plus bi-layer CHI/Laponite)..... 117
Fig. 6.1 Dark-aged HAuCl4 solution..... 122
Fig. 6.2 Gold nanoparticle suspension..... 123
Fig. 6.3 SEM micrograph of polystyrene particles prepared by polymerization of styrene monomers with the presence of surfactant..... 127
Fig. 6.4 Zeta-potential of layers of nanocapsules consisting of 10 layers biocompatible polyelectrolyte ((CHI/DS)5);The values are given in the appendix Table A.7..... 129
Fig. 6.5 Zeta-potential of layers of nanocapsules consisting of 9-layer of biocompatible polyelectrolyte (CHI/DS) and laponite (the 4th layer); The values are given in the appendix Table A.8..... 129
Fig. 6.6 SEM micrograph of polystyrene particles coated with 10 layers of biocompatible polyelectrolyte..... 130
Fig. 6.7 SEM micrograph of polystyrene particles coated with 10 layers of biocompatible polyelectrolyte and where the 4^{th} layer is laponite..... 131
Fig. 6.8 TEM micrographs of nanocapsules derived from 10-layer coated polystyrene nanoparticles of different magnification (no laponite attendance), the size of the left scale bar is 200 nm and the size of the right scale bar is 50 nm 132
Fig. 6.9 TEM micrographs of nanocapsules derived from 10-layer coated polystyrene nanoparticles of different magnifications (the 4^{th} layer is laponite), the size of the left scale bar is 100 nm, and the size of the right scale bar is 50 nm 133
Fig. 6.10 TEM micrographs with different magnifications of gold nanoparticles; the scale bar of the left micrograph is 20 nm and it is 5 nm for the right one 135
Fig. 6.11 TEM micrograph of polystyrene particles (8 layers polyelectrolyte and the 4th layer is laponite) coated with gold nanoparticles, the scale bar in the graph is 20 nm 136
Fig. 6.12 TEM micrographs of nanocapsules (after dissolving by THF for 48 hr) of 8-layer polyelectrolyte (CHI/DS), one layer laponite (4^{th} layer) and the outer layer is gold, the scale bar in the left graph is 100 nm and the scale bar is 20 nm in the right

graph 137
Fig. 6.13 The test of the magnetic property of the magnetite nanoparticles. (a) The magnetic particle suspension; (b) The magnetic particle suspension stimulated by a permanent magnetic stirrer.....138
Fig. 6.14 The XRD patterns of magnetic particles with or without sodium oleate. (Blue line: without sodium oleate; red line: with sodium oleate; the straight vertical black line: pure magnetitie) 139
Fig. 6.15 The XRD pattern of the magnetite prepared by Sun et al. [222].....140
Fig. 6.16 The TEM micrographs of the magnetic nanoparticles (a) prepared with sodium oleate (b) prepared without sodium oleate 142
Fig. 6.17 TEM micrographs of 10-layer coated polystyrene sample coated with one layer of magnetite nanoparticles (prepared with sodium oleate), the scale bar is 50 nm 143
Fig. 6.18 TEM micrographs of nanocapsules consisting of 9-layer polyelectrolyte, one layer of laponite and one layer of magnetic nanoparticles, the scale bar in both graphs is 200 nm.....144
Fig. 7.1 The general structure of BSA [241].....148
Fig. 7.2 The general structure of lysozyme [244] 149
Fig. 7.3 Zeta-potentials of the first protein coating (4th and 5th layer of the coating process) at different pH values (pH7.4, pH9.2, pH10) (a) BSA (b) Lysozyme; 152
Fig. 7.4 The zeta-potential results of protein (BSA/lysozyme) coating processes started from different layers of polyelectrolyte (PDADMAC/DS) precursors (0, 1, 3 layers).....154
Fig. 7.5 SEM micrographs of polystyrene particles coated with 5 layers of proteins ((lysozyme/BSA)$_2$/lysozyme) without any polyelectrolyte layers.....155
Fig. 7.6 SEM micrographs of polystyrene particles coated with 7 protein layers and 1 polyelectrolyte (PDADMAC/(BSA/lysozyme)$_3$/BSA) pre-coating layer 156
Fig. 7.7 SEM micrographs of polystyrene particles coated with 5 protein layers and 3 polyelectrolyte pre-coating layers (PDADMAC/DS/PDADMAC/(BSA/lysozyme)$_2$/BSA) 156
Fig. 7.8 SEM micrographs of capsules prepared from polystyrene particles pre-coated with 3 polyelectrolyte layers and 5 protein layers a) and b) core-removed capsules (deflated) larger than 700 nm, (c)-(e) core-removed capsules smaller than 500 nm.158
Fig. 7.9 SEM micrographs capsules prepared from polystyrene particles pre-coated with 1 polyelectrolyte layer and 7 protein layers. (a) and (b) are of different magnitude. 159
Fig. 7.10 SEM micrograph of insulin micro-aggregates salted out from suspension (0.6 M NaCl, pH 1.1).....163
Fig. 7.11 Scheme of the LbL adsorption of negatively charged polyelectrolyte (black strings) and positively charged polyelectrolyte (grey strings) on insulin particles [17]. 164
Fig. 7.12 Zeta-potential of the layers (DS/lysozyme) of the coated onto insulin nano-particles.....165
Fig. 7.13 SEM micrographs of 8 layers ((DS/lysozyme)$_4$) coated insulin

nano-particles; (a) (b) represent different magnification 167
Fig. 7.14 The SEM photograph of the insulin–polyelectrolyte nanoparticles with six polyelectrolyte adsorption cycles from Fan et al.'s work [17].....168
Fig. 7.15 Large NaCl crystals formed during the drying out process.....169

List of Tables

Table 3.1 The zeta-potential of each polyelectrolyte layer coated on 95 nm silica particles (CHI/DS 0.1 M NaCl) (First measurement) 52
Table 3.2 The zeta-potential of each polyelectrolyte layer coated on 95 nm silica particles (CHI/DS 0.1 M NaCl) (Second measurement) 53
Table 4.1 Silica particles prepared with different amounts of NH4OH 72
Table 4.2 Zeta-potential of the 1st layer under different NaCl concentration 75
Table 4.3 The zeta-potential of the 1st polyelectrolyte layer at different deposition time span 77
Table 5.1 Zeta-potential of the particles after coating 1 mg/ml PDADMAC for different time 95
Table 6.1 Estimation results of the particle average size of the magnetite particles . 141
Table 7.1 Depositing and re-dispersing solution used in the protein (BSA/lysozyme) deposition experiments (left: dissolving solution, right: re-dispersing solution) 153
Table A.1 The zeta-potential of each polyelectrolyte layer coated on 95 nm silica particles (CHI/DS) 176
Table A.2 The zeta-potential of each polyelectrolyte layer coated on 114 nm silica particles (CHI/DS) 177
Table A.3 Zeta-potential of polyelectrolyte layers (PE 1 mg/ml) on polystyrene particles at different salt concentrations 177
Table A.4 The zeta-potential of each coating layer (consisting of only synthetic polyelectrolytes PDADMAC(odd)/PSS(even)), the concentrations: PE 1 mg/ml, NaCl 0.1 M, Laponite 10 mg/ml 178
Table A.5 The zeta-potential of each coating layer (Consisting of synthetic polyelectrolytes and Laponite particles, PDADMAC/PSS/$(PDADMAC/Laponite)_8$), the concentrations: PE 1 mg/ml, NaCl 0.1 M, Laponite 10 mg/ml 178
Table A.6 The zeta-potential of each coating layer (Consisting of bio-compatible polyelectrolytes and Laponite particles, $(CHI/DS)_5$/CHI/Laponite), the concentrations: PE 1 mg/ml, NaCl 0.1 M, Laponite 10 mg/ml 180
Table A.7 Zeta-potential of nanocapsules consisting of 10 layers of biocompatible polyelectrolyte ($(CHI/DS)_5$) 181
Table A.8 Zeta-potential of nanocapsules consisting of 9-layer biocompatible polyelectrolytes (CHI/DS) and one layer laponite (the 4th layer) 182
Table A.9 The zeta-potential of the first BSA layer (4th layer after 3 polyelectrolyte layers) on PS cores at different pH environments 183
Table A.10 The zeta-potential of the first Lysozyme layer (5th layer after 3 polyelectrolyte layers and one BSA layer) on PS cores at different pH environments 183
Table A.11 The zeta-potential of the coating process on polystyrene particles contained different number of pre-coating polyelectrolyte (PDADMAC/DS) layers the rest layers are proteins (BSA (-)/lysozyme(+)) 184

Table A.12 Zeta-potential of the layers of coated on insulin nano-particles (DS (odd layers)/lysozyme(even layers)) 185

Abstract

Since the drug molecules inside human body (in the blood vessel) are recognised as being alien, and quickly eliminated or degraded, it is necessary to find a way to protect and direct these effective components to the target zone. Therefore, the design and preparation of the therapeutic delivery systems in vivo has attracted considerable attention in recent decades. Nanocapsules, as a relatively new delivery approach, have many advantages. Compared with micron or larger delivery systems, nanocapsules are smaller and hence can migrate to diseased organs without blocking the bloody vessels. Also unlike nanospheres, nanocapsules could provide more capacity space for the therapeutics loading. Therefore, in this thesis the design and preparation of nanocapsules for the drug delivery system is discussed. A Layer-by-Layer self-assembly method onto nanospheres as a template has been developed. This method allows easy control of the size of the capsules and the thickness of the capsule walls; moreover, its flexibility has enabled various types of materials to be used to form the walls of the capsules, such as polyelectrolytes, proteins and various inorganic particles.

In this project, two different core templates (silica and polystyrene nanoparticles) were prepared. Hollow capsules based on silica nanoparticles (95 nm and 114 nm) were obtained from the deposition of 9 layers of Chitosan (CHI) and Dextran sulphate sodium salt (DS), subsequently the silica cores were removed by dissolving in an HF/NH_4F buffer solution. For the nanocapsules based on polystyrene particles (130 nm and 480 nm), a layer of the synthetic inorganic clay, Laponite, was introduced to improve the strength of the nanocapsules. After the core-removal process (by dissolving in tetrahydrofuran THF), a high productivity of hollow nanocapsules was observed for both particle sizes. Gold (4-10 nm) and magnetite (10 nm) nanoparticles were also incorporated into the capsule walls to modify the properties of nanocapsules obtained from the polystyrene nanoparticles of 130 nm; these materials make the particles sensitive to near infer red light and a magnetic field respectively. Furthermore, nanocapsules consisting of proteins (lysozyme and bovine serum albumin BSA) and polyelectrolytes (Poly(diallydimethylammonium chloride) PDADMAC and DS) were also fabricated. In the final part of the thesis, loading materials into the nanocapsules were tried. Instead of directly loading into the nanocapsules, the insulin was first prepared as insulin nanoparticles and these nanoparticles were then coated with the polyelectrolyte/protein layers to form the nanocapsules loaded with drug molecules.

This project has extended the size range of nanocapsules that can be synthesized, and also the range of materials, and hence the properties, that can be included in the walls of the nanocapsules.

Acknowledgements

I would like to thank many people who made this thesis possible.

First and foremost, I would like to express my highest gratitude to my supervisor, Prof. Paul F. Luckham. Apart from giving a great opportunity to do this project, I am really grateful to him for his guidance and support throughout my whole PhD. I have been privileged to be associated with him, and without his patience, inspiration and encouragement, this thesis would not be finished as it is now.

Many thanks are to my parents for their financial support and giving me such a precious opportunity to study at Imperial College. Their endless love had made me through all the tough time during my PhD.

In this department, I would like to thank Dr. Joao Cabral who is my collaborating academic for his advices during my research work. I would also like to thank Dr. Jerry Heng who lets me use some equipment for my experiment. Special thanks must be given to Mrs Susi Underwood who helped me to sort out the registration documents of my PhD. Also I would like to thank all the members involved in MET group at Imperial College London who gave me plenty of help and suggestions.

Last but not least, I want to thank all the friends around me especially my girl friend Lulu. Without them, I would not be able to have a great and joyful life throughout my PhD time.

Abbreviations

AFM	Atomic force microscopy
AH	Acridine hydrochloride
ALG	Alginate
BSA	Bovine Serum Albumin
CDDS	Colloid drug delivery system
CHI	Chitosan
DOPC	1,2-dioleoyl-sn-glycero-3-phosphocholine
DOX	Doxorubicin hydrochloride
DS	Dextran Sulphate Sodium Salt
Fe(II)-MEPE	Fe(II) metallosupramolecular polyelectrolyte
FITC	Fluorescein isothiocyanate
FRAP	Fluorescence recovery after photobleaching
FS	Freely suspended
HA	Hyaluronic acid
ICP- OES	Inductively Coupled Plasma-Optical Emission Spectroscopy
IEP	Isoelectric point
IG	Isotropic gel
IgG	Immunoglobulin G
IL	Isotropic liquid

LC	Liquid crystalline
LbL	Layer-by-Layer
MF	Melamine formaldehyde
NG	Nematic gel
PAH	Poly(allylamine hydrochloride)
PBS	Phosphate buffered saline
PCR	Polymerase chain reaction
PEG	Poly(ethylene glycol)
PEI	poly(ethylene imine)
PDADMAC	Poly(diallydimethylammonium chloride)
PGA_{ALK}	Alkyne-functionalized poly(L-glutamic acid)
PL	Poly(lysine)
PS	Polystyrene particles
PSS	Poly(sodium 4-styrenesulfonate)
PVPON	Poly(N-vinyl pyrrolidone)
SAXS	Small angle X-ray scattering
SDBS	Sodium dodecylbenzene sulphonate
SEM	Scanning Electron Microscopy
SP	Spermidine
SPLS	Single Particle Light Scattering
TEOS	Tetraethy orthosilicate

TEM	Transmission Electron Microscopy
THF	Tetrahydrofuran
THPC	Tetrakis(hydroxymethyl)phosphonium Chloride
XRPD	X-Ray Powder Diffraction

Chapter 1 Introduction

Recently, there has been intense research into the preparation of uniformly-sized hollow capsules. Controlled release of material of for various purposes has been the main driving force behind the research into these hollow spherical structures [1]. Such structures have found application in various research fields including petrochemicals, pharmaceutics, agrochemicals and cosmetics [2, 3]. Hollow capsules can also be used in catalysis, acoustic insulation, developing low dielectric constant materials and piezoelectric transducers, and in the preparation of advanced materials et al [1, 4].

Nanocapsules are one type of hollow capsules with a size range from tenths of nanometers to 1000 nm [5, 6]. Due to the small size of these hollow capsules, one of the most important applications of nanocapsules is for use in drug delivery systems, because the size of the colloid drug delivery systems (CDDS) is one of the most important parameters affecting the performance of CDDS in vivo, furthermore it can also influence the interaction of CDDS with the environment and the target field [7]. Nano-sized capsules can be injected directly into the human body without blocking blood vessels [8, 9]. Furthermore, it has been reported by many researchers [10-12] that their small size is an advantage, in that smaller CDDS were removed more slowly from blood circulation [13]. In addition, it was found that nanoparticles under 200 nm have a longer circulation time in the body than larger particles because the high radius of curvature of the particle surface prevents the efficient binding of opsonins [13]. The combination of long circulation time and small size of the nanocapsules has been shown to increase the accumulation of the loaded drugs into the tissues [5]. Also, it may be possible to put some targeting ligands [14, 15] onto the capsules and so target the drug loaded capsules to directly go to the diseased cells, and reduce the side-effect of the drug to the normal tissues. Because of the importance of nanocapsules in drug

delivery systems, how to prepare nanocapsules with these demanding properties has aroused immense interest.

There are various methods to prepare a wide size range (nanometre to millimetre) of stable hollow capsules consisting of different composite materials, including nozzle reactor processes, emulsion/phase separation procedures(often combined with sol-gel processing) and sacrificial core techniques [4]. However, there are still many limitations of these techniques, which prevent the commercialisation of the hollow spheres. Some of these limitations come from the process of preparing the hollow spheres, e.g. the harsh conditions involved in some methods, and the difficulty in introducing materials into the capsules; others are from the properties of the capsules, e.g. the lack of control over size, geometry, wall thickness and wall uniformity [1]. The sacrificial core technique is the only method that could potentially be used to prepare nanometre sized capsules.

An alternative way has been developed to fabricate nanocapsules of uniform size, wall thickness, geometry and composition etc., which combines the so called Layer-by-Layer self-assembly method onto colloidal particles which act as templates, and is then followed by removal of that colloidal particle (the sacrificial core) [1]. In this method a charged particle acts as a template and alternating layers of oppositely charged polyelectrolytes are successively built up on the particles and finally the particle template is removed to leave a capsule. The mono-dispersed colloidal templates determine the diameter of the nanocapsules, and the number of polyelectrolyte layers controls the wall thickness of the capsules. Also by the Layer-by-Layer method, various composite materials can be combined together to form nanocapsules of different physical or chemical properties [16].

At the outset of this project this technique was limited to producing small microcapsules, 1-100 μm in diameter rather than nanocapsules dozens of nanometers to 1000 nm. This thesis reports attempts to produce genuine nanocapsules which could be usefully used as drug delivery vehicles. Different core templates (silica and polystyrene nanoparticles) and capsule materials (polyelectrolytes, inorganic nanoparticles and proteins) were utilised in the experiment to make nanocapsules with diverse characteristics. The method of synthesizing such capsules was confirmed applicable, although no studies of the release of materials have been conducted in this study; an outline of the thesis is given below.

In Chapter 2, firstly different therapeutics delivery systems are reviewed and the reason for choosing nanocapsules as the drug delivery system is also discussed. Then, various methods of preparing nanocapsules are compared and based on the advantages and disadvantages of these methods, the Layer-by-Layer (LbL) self-assembly method was selected as the main approach in this work to prepare nanocapsules. Thirdly, the principles of the LbL method and the mechanism of loading and releasing therapeutics are reviewed. Also the core templates and coating materials of the LbL method ware discussed. Finally, the motivation and innovation of this PhD project is presented.

In Chapter 3, the characterization methods (zeta-potential measurement, dynamic light scattering, CPS disc centrifuge, SEM , TEM, and powder x-ray diffraction) used in this project were discussed (including the experiment details, and data and error analysis).

In Chapter 4, the preparation of nanocapsules based on silica nanoparticles templates is discussed. Two biocompatible polyelectrolytes were used as the capsule materials in the Layer-by-Layer assembly process. Silica nanoparticles with different size ranges

were produced in the experiment. The silica core was then removed by HF dissolution to make the hollow nanocapsules.

In Chapters 5 and 6, two sizes of polystyrene particle templates were manufactured. Both of the polystyrene particles were employed to prepare hollow nanocapsules. For the particles with a size of around 480 nm, both synthesis and biocompatible polyelectrolyte were used as the capsule materials and the effect of adding the synthetic clay, Laponite on the mechanical strength of the capsules was qualitatively investigated. For the particles with a smaller size (130 nm), only biocompatible polyelectrolytes were employed, moreover the capsules were functionalized with gold and magnetite nanoparticles. Nanocapsules of different size were obtained by dissolving the polystyrene particles in tetrahydrofuran.

In Chapter 7, the nanocapsules consisting of biomolecules were fabricated. Two different core templates: polystyrene and insulin nanoparticles were used in this section. For the nanocapsules based on polystyrene particles, 2 protein molecules (bovine serum albumin/lysozyme) were used as coating materials and they were added onto the polyelectrolyte pre-coated polystyrene nanoparticles. The nanocapsules were formed by dissolving the polystyrene template with THF. The insulin particles were prepared via a salting out process [17]. After coating with polyelectrolyte and protein, single and well dispersed insulin particles were observed in the suspension.

Finally, in Chapter 8, some general conclusions are given and suggestions for further research work are provided.

Chapter 2 Literature Review

Before we introduce the main topic of this PhD project, it is wise to review the progress of the current development of the drug delivery systems to answer this question why choose nanocapsules?

2.1 Drug delivery systems

Oral taken and subcutaneous or intravenous injection are traditional drug delivery methods to introduce drug molecules into human body. By either way, the medicine will be absorbed into the blood circulation and circulated all over human body. However, because the effective components of drugs are in their molecular state in the blood, there are more possibilities for them to meet any situation which could arouse their degradation. Thus, only a very small amount could reach the ill tissues and most of them are degraded [18]. Therefore, to protect and target these effective components attracted many research interests.

The concept of drug delivery and targeting system comes from the works and ideas of German chemists in 19^{th} century and they named the system as "magic bullet". One representative icon of them is Paul Ehrlich, who described this system as a compound could target an abnormal organism and toxin from the abnormal organism could also be delivered by some agent [19]. A drug delivery system as Petkar et al. concluded is to help dissolve hydrophobic drug in vivo, reduce drug toxicity, target to specific organisms and reinforce the bioavailability and stability of the drugs [20]. To overcome the problems of drug uptake encountered in the traditional delivery system, packaging the drug molecules with designed carrying system is considered to be one of the most

effective ways. So far, many types of drug carrier systems of different size ranges and compositions (like micelles and dendrimers [21-23], liposomes [24-26] and biodegradable particles [27-30] etc.) have been researched and developed and many of them (e.g. micelles (Knakion MM™), liposomes (AmBisome™), microemulsions (Neoral™), liquid scrystalline structures (Elyzol™) and so on) have been commercialized.

During the last two decades, many works have been done on micro-scale drug delivery system to either increase drugs' efficiency or decrease drugs' side effects [31-34]. However, due to the size issue, there are some limitations for the micro-scale drug delivery systems. Firstly, for the oral taken system, the size limitation prevents some large particles into the lymphatic system through intestinal absorption. Secondly, if the drug molecules need to reach certain organism, intraveneous administration is generally required and particles as large as micro-meters would easily clog small capillary vessels and form aggregation [35, 36]. It is also found nanoparticles with size around 200-500 nm are proper for the intraveneous delivery [37]. Also, as aforementioned, smaller size of the nanoparticles provide longer circulation time in vivo, which can provide the ability of sustained releasing [13, 38]. Therefore, in recent years, considerable attention has been focused on the various nanotechnology platforms used in the diagnostic and therapy areas [39], and although most of the products are still in the research state, nano-scale delivery system (e. g. nanospheres [40, 41], solid lipid nanoparticles [42, 43] and nanocapsules [44, 45]) have aroused massive research interests.

The nano-scale drug delivery system normally refers to nanoparticles less than 1 micrometer [46] and the nanoparticles could be classified as nanospheres and nanocapsules [47]. The composition of the nanoparticles is displayed in the Fig. 2.1. In

Fig. 2.1, 5 types of nanoparticles are demonstrated and the first three (from left) belong to the category of nanospheres, and the other two on the right are nanocapsules.

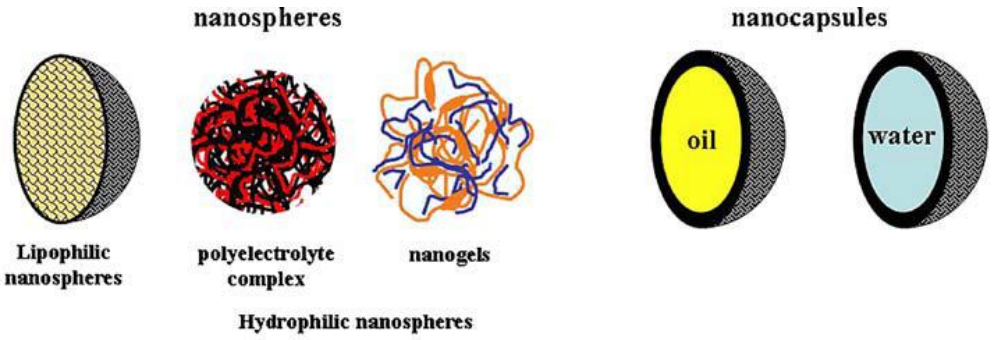


Fig. 2.1 Different structures of the nano-scale delivery system [47]

Nanocapsules are a pool form comprising of a shell structure and a core template. Normally, the cores are liquid or semisolid at room temperature (15-25 ^{o}C). The oily or aqueous medium inside the nanocapsules provide the nanocapsules with abilities to encapsulate hydrophobic (lipo-soluble) or hydrophilic (water-soluble) compounds. Likewise, nanospheres, as described in Fig. 2.1, are nanoparticles with entire mass solid. These nanoparticles are generally of spherical shape but other kinds of shapes are also reported [48-50]. As drug delivery systems, the drug molecules can be either loaded inside or attached on the surface of the nanoparticles.

Compared with nanospheres, nanocapsules provide more advantages for drug delivery. Considering the drug loading dosage, for nanocapsules, the drug/polymer ratio could reach 5:1 when the core is of pure drugs; while for nanospheres, this number is as low as 1:10 [51]. Also low content of polymers and protecting activity of loading stuffs (such as enzymes and proteins) by providing cavitary space are another two benefits when nanocapsules are applied [51].

In summary, since there is so many important advantages and applications for the nanocapsules in drug delivery system, thus in this PhD project, the preparation of nanocapsules of size under 200 nm will be discussed.

2.2 Review of Other Hollow Capsule Synthesis Methods

Lipid liposomes and vesicles which are fabricated from the self-assembly of phospholipids which form closed bilayer systems are a special kind of hollow spherical nanocapsules and Liposomes became commercialized in 1986 by Dior [52]. Liposomes can be classified as large and small unilamellar vesicles, as well as large multilamellar liposomes, depending on the size and number of lipid bilayers [53]. Water-soluble compounds can be encapsulated in the interior of the vesicles, and amphiphilic and lipophilic compounds can be associated with the lipid bilayers [53]. There are many methods to prepare liposomes sizes from 50 nm to a few hundred nanometers. The most common ways include extrusion, sonication, solvent injection and reverse-phase evaporation [39, 54]. In 1962, Saunders et al. introduced the classical method of sonicating a dispersion of phospholipids to form optically clear small unilamellar vesicles suspensions [55]. In 1965, Bangham et al. first reported the preparation of liposomes with entrapped solutes [56]. Later Bangham and his colleagues (1974) pointed out the fact that large multilamellar liposomes can form spontaneously in aqueous solutions [57]. In 1978, Szoka et al. prepared large unilamellar vesicles via water-in-oil phospholipid emulsions and the system buffered in an over saturated organic phase. The excess organic phase was removed by evaporation under reduced pressure [58]. Aboofazeli and Lawrence (1991 and 1993) exploited the preparation of lecithin-based microemulsions; because lecithin is likely to form liquid crystalline structures in water solution [59], a cosurfactant was needed to stabilize the emulsion and the system water-lecithin-alcohol-isopropyl myristate was employed in their research [60, 61]. Later, Lawrence et al. extended their research on the lecithin and used either an alkanoic acid, amine, alkanediol, polyethylene-glycol alkyl ether or alcohol as

the co-surfactant [62] and the influence of the surfactant was also exploited [63]. Due to the very low toxicity of the liposome systems for in vivo applications [39], DNA/RNA, proteins and drug delivery system using liposomes as carriers [64-68] have been developed. Therefore, liposomes are widely used in biophysics, pharmacology and medicine, cosmetics, chemistry and protein studies, food industry and etc [69].

However, there are some limitations related with the stability and permeability of liposomes, which restricts the applications of liposomes [1]. The main limitations of the liposome system are listed below: 1) easily degraded by lipases or flagellated by opsonin followed by macrophage uptake; 2) thermodynamic instability, vesicles are not usually in an equilibrium state, and could be easily trapped in a meta-stable shape during formation [70]; 3) low permeability of polar molecules [71]; 4) poor storage of water soluble components in bloodstream [72].

Therefore, compared with liposomes, polymeric materials which can provide more stability of encapsulation and controlled releasing have aroused extensive research interest [72].

As was mentioned in the introduction, there are several chemical and physiochemical ways to prepare the hollow spherical structures of different size ranges. These methods were summarised and reviewed by Caruso [1] and Wilcox et al[4]. A brief description is presented in the following paragraphs:

The sacrificial core method: the core templates are firstly coated with the required materials via surface reaction or controlled precipitation of molecular precursors. Then the hollow spherical shell could be obtained by a core-removal process, either by

thermal (volatilization) or chemical (dissolving) means [1, 4]. In 1991, Kawahashi et al. prepared hollow spheres consisting of yttrium compounds by the core-sacrificial methods[73]. They prepared polystyrene particles (170 nm) with positive surface charges and adsorbed particles of yttrium basic carbonate on their surface. Then the polystyrene particles were removed by calcination in air and hollow capsules of yttrium oxides which transformed from yttrium basic carbonate were obtained[73].

Nozzle reactor methods: The prepared liquid is quickly pushed through a spray drying nozzle and liquid droplets of 10-500 μm can be produced. Then by heating (spray drying) or cooling (freeze drying) the droplets created previously the moisture of the liquid is removed, and the shape of the spheres could be consolidated [1, 4]. Bruinsma et al. prepared mesoporous fibres and hollow capsules by rapid spray-drying hydrolyzed silicon alkoxide solutions. Then the fibres and capsules were calcined [74]. They also used different ratios of silica-to-surfactant in the solution to modify the pore size of both the mesoporous fibres and hollow capsules. However, the size of the hollow particles was widely distributed (from 1 micron to tens of microns) and certain part of the capsules collapsed after the calcinations [74].

The emulsion/phase separation approach (often combined with sol-gel processing): This technique firstly involves the formation of an emulsion based on the principles of surface and interfacial tension forces and immiscibility between phases. Then, the spheres are separated from the liquid medium, which is then followed by methods to convert them into rigid hollow spheres. The separation is normally of different chemical or physical ways, such as liquid extraction etc [1, 4]. For example, in 1996, Schacht et al. prepared hollow silica capsules by hydrolysing tetra-ethoxysilane (TEOS) at the oil-water interface[75]. In their experiment, a mixture of mesitylene, water, surfactant and TEOS was stirred and the TEOS molecules were encapsulated within the formed mesitylene droplets. Then the TEOS molecules were hydrolyzed at the surface

of oil-water and a silica shell was gradually formed. Finally, hollow capsules consisting of silica were obtained [75].

However, there are several disadvantages in all of the methods mentioned above [1, 76]. Because of the harsh conditions in some methods, it is inappropriate for loading sensitive materials such as pharmaceuticals. Once the capsules formed, it is difficult to encapsulate any new materials into the capsules. Others issues include lack of control over wall thickness, size, geometry, and wall uniformity of capsules, which will in turn affect the potential use of the hollow capsules.

To overcome the disadvantages of these methods of synthesising hollow capsules, a new technique, the Layer-by-Layer self assembly method, has been introduced. The concept and development of the technique will be discussed in the following sections.

2.3 Nanocapsules Synthesised via the Layer-by-Layer Self-assembly Method

2.3.1 The Principles of the Layer-by-Layer Method

The Layer-by-Layer self-assembly method has many advantages for making thin polymeric layers on surfaces and hence capsules, such as this method is easy and cheap and is capable of employing various different materials. The basic principle of the Layer-by-Layer (LbL) method is to utilise electrostatic interactions between oppositely charged polyelectrolytes, or other materials, to fabricate thin uniform multilayers onto the original substrates.

In 1941, Langmuir discussed the idea of adsorption of ions onto a surface to form a single layer, and also demonstrated the experiment by adsorbing a single layer of thorium ions onto a monomolecular layer of barium stearate [77]. In the 1960s, Iler utilised this strategy to build up alternating layers of positively charged alumina fibrils and negatively charged silica colloids onto a smooth glass surfaces [78]. In the early 1990s, Decher and colleagues exploited this method and prepared multilayers of thin films by immersing a charged planar surface (silicon wafer or quartz) alternately into anionic and cationic polyelectrolyte or bipolar ampholyte solutions [79-81]. They used macroscopic planar silicon wafers and quartz surfaces, which are negatively charged, as the templates, and immersed the substrate initially into a solution containing a cationic polyelectrolyte. After that, a monolayer of polyelectrolyte was found to be adsorbed onto the surface of the solid. After rinsing, the solid was then immersed into another solution with an anionic polyelectrolyte. Again a monolayer was adsorbed and the original surface charge was restored [79, 80]. The Layer-by-Layer self-assembly method may be simply demonstrated in Fig. 2.2. Decher et al. demonstrated that multilayers films composed of at least 100 consecutively alternating layer can be assembled in this way. After the build up of the multilayer film UV/vis spectroscopy and small angle X-ray scattering (SAXS) were employed to investigate the property of the film [82]. Then Decher et al. applied this method to fabricate smectic multilayer films by transferring freely suspended (FS) or liquid-crystalline (LC) layers onto the solid support [83].

After that, the LbL method was adapted by many other groups and more and more materials such as functional polymers, orientable chromophores, inorganic particles, clays, dyes, and biomolecules such as DNA and proteins, were employed to fabricate these multilayers [1, 84-87]. Because many diverse materials could be involved in the LbL method, and since the LbL method can be combined with other assembly processes, there is a high application potential for the LbL process in materials development [88-90]. The multilayer structure can be used as matrix materials for

functional or biological molecular entities, such as separation membranes, sensor applications and customised surface modification [88, 91, 92].

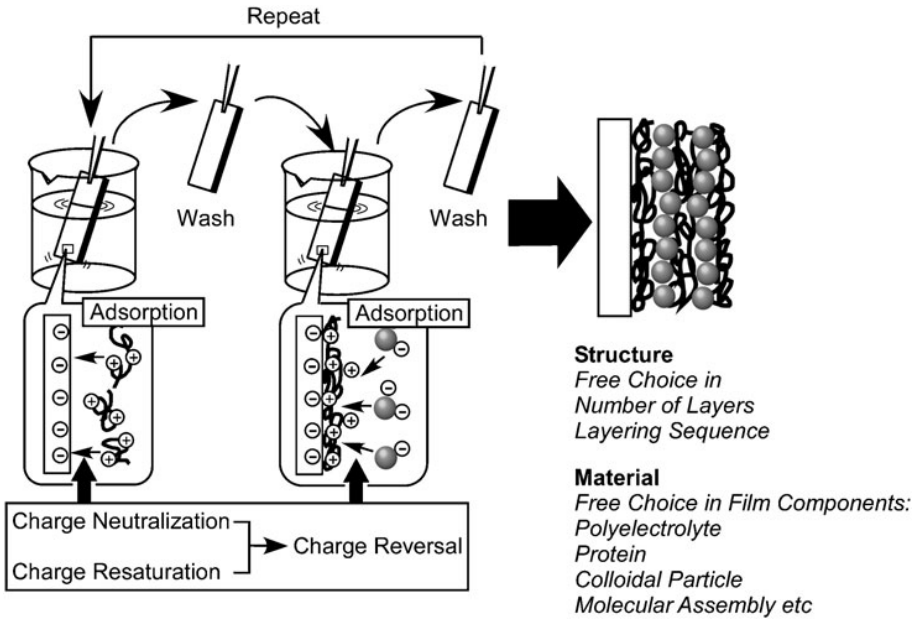


Fig. 2.2 The diagram shows the process of the LbL method [93]

2.3.2 Application of Layer-by-Layer Self-assembly Method on Preparation of Micro- and Nano-capsules

Due to the versatility of the LbL methods, it seems possible to build the multilayer onto higher dimensional surfaces, i.e. non planar surfaces. However, as it was mentioned in the last section, after Decher's pioneer works in the utilizing LbL self-assembly method to prepare multi-layer thin films, there has been a plethora of studies using various materials as layer components to prepare multilayer films [94-99] and most of the research works were based on charged planar surfaces such as quartz or silicon wafers. It was not until 1998 that Sukhorukov [100] and Donath [71] demonstrated their work on transferring the Layer-by-Layer method from macro planar templates to charged colloidal particles in aqueous solution. Their work introduced one of the most

important adaptions of the LbL methods: the application of preparing micro- or nano-capsules. Since 1998, many research works focusing on the application of Layer-by-Layer method on colloidal templates have been undertaken and colloidal cores of various composition (latexes, inorganic oxides, carbonates, phosphates and even cells) and size (nanometre–micrometer range) have been coated with multilayer of diverse composition and controllable thickness [71, 101, 102]. A common application of the core–shell particles produced via the LbL strategy is the formation of hollow multilayer capsules, obtained after removal of the templating cores by either, chemical, or thermal means [71, 101, 102]. The credit of building up the whole process has been given to Caruso and his co-workers' pioneer work in this area [71, 100, 102, 103].

The basic principle of the LbL method is to sequentially deposit oppositely charged macromolecule pairs onto charged colloidal particles. It is comprised of several steps as outlined in Fig. 2.3.

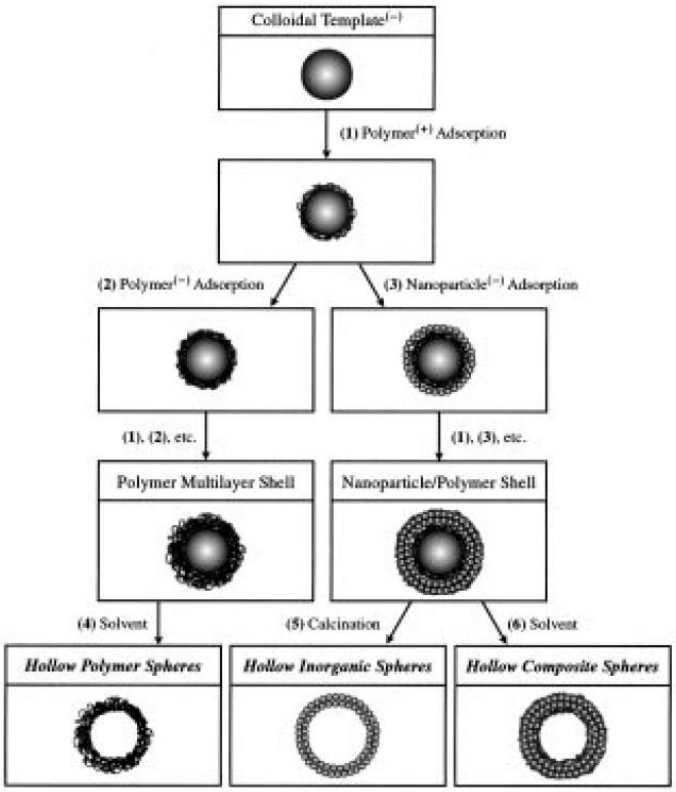


Fig. 2.3 shows procedures for hollow nanospheres production via Layer-by-Layer self-assembly methods [1].

In Fig. 2.3, before step one is the process of preparing the colloidal templates. For the LbL method, the colloidal templates can have different sizes (ranging from sub-micrometer to micrometer regime), composition, and shapes. The first step (1) is the deposition of charged polyelectrolyte onto the charged particle surface. The polymer layer which has the opposite charge to the particle surface adsorbs onto the particle by electrostatic forces. The excess unadsorbed polymers are removed by a centrifugation and rinse cycle; repeating the cycle in step 1 with polymers (step 2) or nanoparticles (step 3) results in another polymer, or nanoparticle, layer deposition. The rest of the layers can be deposited by repeating steps 2 and step 3. After the core-shell structure with the desired size, shell thickness, and composition has been fabricated, the core templates need to be removed to make the final capsules. Depending on the property of the core templates, the cores can be removed either by thermal (calcination) (step5) or chemical (solvent) process (step 4 and step 6):

1) The thermal method employs calcination where a very high temperature is applied and so can only be used if inorganic nanoparticles (shell materials) have been incorporated into the systems. The organic cores and any polymers are burnt out. After the calcination, only hollow inorganic shells can remain [104].
2) The chemical method removes the core templates by dissolving or reacting away the cores. After dissolving, hollow polymer (or inorganic) shells can be obtained [104].

2.3.3 Advantages of Layer-by-Layer Self-assembly Strategy

In summary, according to Caruso et al [71, 105], there are five main advantages of the LbL strategy, and all the advantages are listed below:

The electrostatic and steric interaction involved in the LbL method could pass to the colloids after each layer coating, which could make the colloid more stable to any physical or chemical influence than the colloids prepared from any other approach.

Due to the high flexibility of choosing core templates and shell materials, the composition of the core-shell structure can be controlled and manipulated according to their ultimate usage.

By changing the number of layers, the wall thickness of the capsules can be controlled at nanometre level.

By controlling the template size, the capsule size can be controlled.

The capsules prepared from the LbL process have a relatively more flexible structure and maybe manipulated to be permeable to polar molecules (size up to several nanometers).

2.3.4 Encapsulation

Many techniques have been proposed to encapsulate effective components using the hollow capsules prepared via the LbL self-assembly method. In general, the drug components could be encapsulated by two primary processes: pre-loading and post-loading [106]. Three most used techniques are demonstrated in Fig. 2.4 [107]. In this diagram route A belongs to the post-loading process, while B and C are subject to pre-loading method.

Route A is a straightforward approach to load drug molecules after the hollow capsules have been prepared. In this route, the drug molecules are loaded into the capsules by diffusing from the medium in which the capsules are dispersed. The loading concept behind this route is that if the polyelectrolytes comprising the capsules are sensitive to pH (e.g. poly(allylamine hydrochloride) (PAH)/poly(styrene sulfonate) (PSS)) [108] or ionic strength (e.g. PAH/dextran sulfate) [109], by changing the pH or salt concentration of the medium, there will be the pores formed with the shells and drugs could be loaded through those pores [107]. De Geest et al. also pointed out that when pH of the medium is close to the apparent pKa of one of the polyelectrolyte pair, the binding of polyelectrolyte layers will become weak and lead to increased permeability of the capsules [106]. Many studies has been performed by employing the concept of the route A [108, 110-112]. For example, in 2005, Ye et al. used acridine hydrochloride (AH) as the loading and releasing materials to test the properties of the nanocapsules consisting of chitosan (CHI) and sodium alginate (ALG) at pH 7.4 [113]. Furthermore, it has been reported that low molecular weight substances (less than 5kDa) could freely pass through the wall (in or out) of nanocapsules and any larger macromolecules did not easily pass through [111].

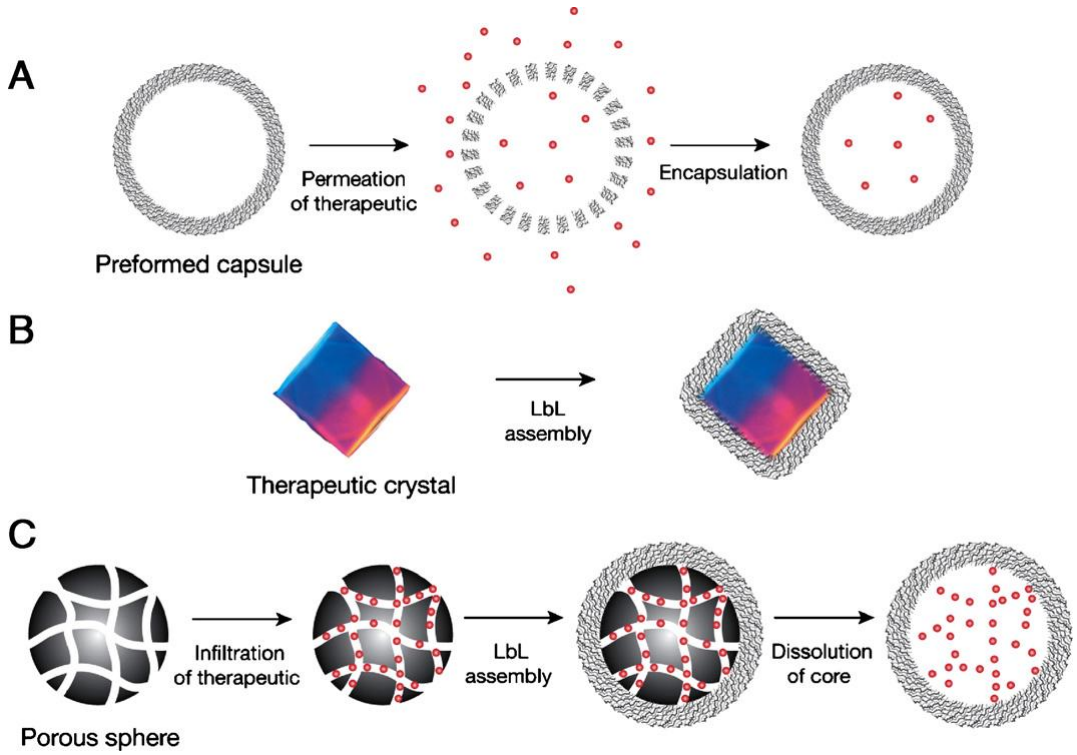


Fig. 2.4 Techniques for encapsulating therapeutics: A) loading after the capsule formed; B) encapsulate crystal particles C) components preloaded in porous particles [107].

To solve this problem, the electrostatic loading mechanism is normally employed [37]. In this mechanism, oppositely charged compounds (in capsule) are utilised to attract the low molecular compounds designed to be encapsulated and the low molecular compounds will accumulate inside the capsules due to electrostatic interaction. Because the molecules to be encapsulated are combined with the opposite charged compounds, the concentration of the "free" molecules is lower than it is in the medium and the drug molecules will continually diffuse into the hollow capsules until reaching equilibrium. Thus in this case, a relatively higher concentration of drug molecules inside the capsules could be obtained. Sukhorukov et al. introduced this method and used this principle to load dyes into hollow capsules (8 μm) [114]. Then, Tao et al. reported the work which introduced the anti cancer drug doxorubicin (DOX) (cationic charged) into hollow polyelectrolyte capsule (7.8 μm) consisting of sodium alginate (ALG) and chitosan where the driving force used was the electrostatic interaction between doxorubicin and ALG [115]. Khopade and Caruso also reported the research work utilising DOX as the loading components and they used a two-step loading

process to achieve the result. In the first step, dextran sulfate (DS) was encapsulated into the hollow capsules (3.5 μm) consisting of poly(styrenesulfonate) (PSS) and a fourth generation poly(amidoamine) dendrimer) by diffusion. Then, DOX which is positively charged, was loaded through the interaction with DS [110]. There is one main challenge for this approach: finding a suitable sequestering agent (the component initially loaded) which not only has a high affinity for the drug molecules but also is biocompatible [107]. In the first part of this thesis (Chapters 4, 5 and 6), the methods for the preparation of hollow nano-capsules, as opposed to micr-capsules, for the post-loading therapeutic will be presented.

Route B indicates the process that polyelectrolyte multilayers could be directly deposited onto the preformed therapeutic particles (e.g. drugs or proteins) [3, 116]. In this route, it is essential for the therapeutic crystal to remain insoluble in the condition of polyelectrolyte multilayers' deposition. Since in most of the situations, the deposition of polyelectrolyte onto the crystal surface occurred in an aqueous environment, the crystals comprised of hydrophobic substances are preferred [107]. Many relevant studies have been reported of this approach [3, 116, 117]. Caruso et al. (2000) reported the encapsulation and release of pre-formed enzyme (catalase) crystal by polyelectrolyte microcapsules consisting of PAH and PSS. The catalase was firstly prepared by salting out method and formed cuboid crystals. These crystals were then alternatively coated with fluorescently labeled (Fluorescein isothiocyanate, FITC) PAH and PSS multilayers and the coated catalase was then released by changing the pH of the solution. Finally, the microcapsules (approx. 20 μm) with minor enzyme residua were obtained [116]. Trau et al. then (2002) reported their work on hydrophobic drug molecules. They encapsulated organic microcrystalline fluorescein diacetate (FDA) (around 1μm) with PAH and PSS multilayers. Then FDA molecules were then released by exposure to a releasing agent containing dimethyl sulfoxide (DMSO) and NaOH solution [117].The main advantage of this method is by encapsulating therapeutic crystals, the therapeutics can be highly concentrated [107]. However, one limitation of

this strategy is that only a few compounds form crystals which can be used as core templates [107]. Hence, to overcome this limit, some groups reported experiments employing protein aggregates (e.g. chymotrypsin [118] and dehydrogenase [119]) as core templates. Many groups had reported their works of this strategy and various materials (e.g. ibuprofen, vitamin K3, biotin) had been used to prepare this core-shell structure [120-124]. All these studies indicate that the existence of the LbL capsules decreased the releasing rate of the drug molecules.

In this work (Chapter 7), encapsulation of protein nano-aggregates have also been carried out. Insulin nano-aggregates were prepared by salting-out procedure and coated with combination of lysozyme and dextran sulfate.

Route C represents a very versatile technique of the LbL self-assembly method. This method employs porous particles and the therapeutics can be loaded into pores of the porous templates before the capsule materials are deposited onto the particles' surface. The large surface area of the particles leads to high loading dosage of therapeutic molecules and this method has been applied to various materials of a wide size range (from protein to some low molecular drugs) [125-130]. The LbL layers can protect the encapsulated components from deactivation or degradation, thereby increase the loading dosage, activity and stability of the therapeutics, e.g. demolishing the access between enzyme and proteolysis [125]. After the coating process, the porous core templates such as silica [130] or calcium carbonate [127] could be removed and the conditions used in core-removal process must be friendly to the loaded components. For example, in 2006, Itoh et al. employed mesoporous silica particles (several microns in diamter) as core-templates and used chitosan and dextran sulphate as capsule materials to prepare biodegradable hollow capsules [131]. They firstly mixed the porous silica particles with protein solution (fluorescein isothiocyanate labelled albumin) to encapsulate protein into the particles. Then the loaded particles were

treated with the LbL process and exposed to chitosan and dextran sulphate alternatively. 6 or 7 layers of biocompatible polyelectrolyte were coated onto the silica particles to encapsulate both silica particles and protein. The core template was then removed by dipping in the aqueous HF solution. The whole process is summarised in Fig. 2.5.

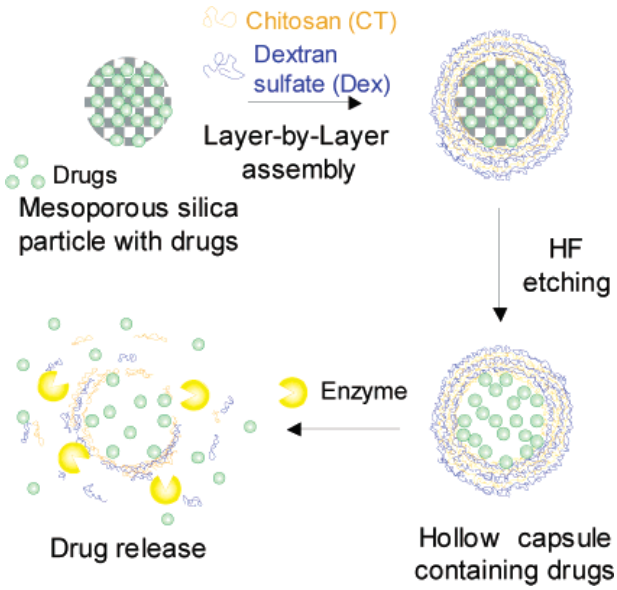


Fig. 2.5 The fabrication of biocompatible hollow capsules and the loaded protein releasing system [131].

2.3.5 Releasing of Loaded Components

Once the capsules are loaded with therapeutic components and delivered to the targeted area, the loaded therapeutics can be released by two methods: immediately (burst release) or gradually over a long period (sustainable release) [107]. Normally, burst release is for a delivery system designed for intracellular uptake (such as chemotherapy and gene transfection) and sustainable release is appropriate for systems releasing effective components outside the cells, in which the instant high concentration of drugs may be dangerous and the concentration of drugs must be kept at certain level (for example, the treatment of diabetes or schizophrenia [132].

2.3.5.1 Burst release

Burst release refers to the release mechanisms of remote functionality [37], in which the degradation of the nanocapsules could be triggered by external forces (e.g. light [133-135], magnetism [136] or ultrasound [137, 138]).

Light stimulation is one of the most popular methods to trigger the "explosion" of the capsules. It was first reported by Tao et al (2004) [139, 140] that hollow capsules consisting of Congo red (an azo dye) and different polyelectrolytes (PSS, PAH and et al) are sensitive to visible light. By illuminating with visible light for 120 min, it was found that the structure of the multilayer was slightly adjusted and the permeability of the capsules was increased to allow fluorescently labeled dextrans (molecular weight up to 464 KDa) to pass through [139]. However, due to the long illumination time (120 min) and low penetration of visible light to human body, the visible light triggering mechanism is not suitable for in vivo application.

Because the human body is almost transparent to the near-infrared laser (800-1200 nm [140]), the utilisation of near-infrared can both remote control the drug release in vivo and eliminate the side-effects of the radiation to the normal tissues [37]. Hence, many recent studies have been undertaken employing near-infrared as a triggering source (Fig. 2.6 simulates a releasing process triggered by near-infrared laser). As is illustrated in Fig. 2.6, to trigger the nanocapsules with near-infrared light, the polyelectrolytes must be incorporated with inorganic nanoparticles [134, 141-145] or infrared dyes [141]. In this process, the inorganic (e.g. gold) nanoparticles/ dyes can absorb and transform the energy to heat which would affect the original integrity of the polyelectrolyte layers [140]. Radt et al [134] and Angelatos et al [133] reported theirs works on gold/polyelectrolyte nanoparticles and according to their results, this composition could absorb heat from a short near-infrared laser shining and the heat

could destroy the capsule itself. In Radt's work, it had also been observed that the energy of the near-infrared light barely affected the activity of lysozyme encapsulated inside of the capsules [134].

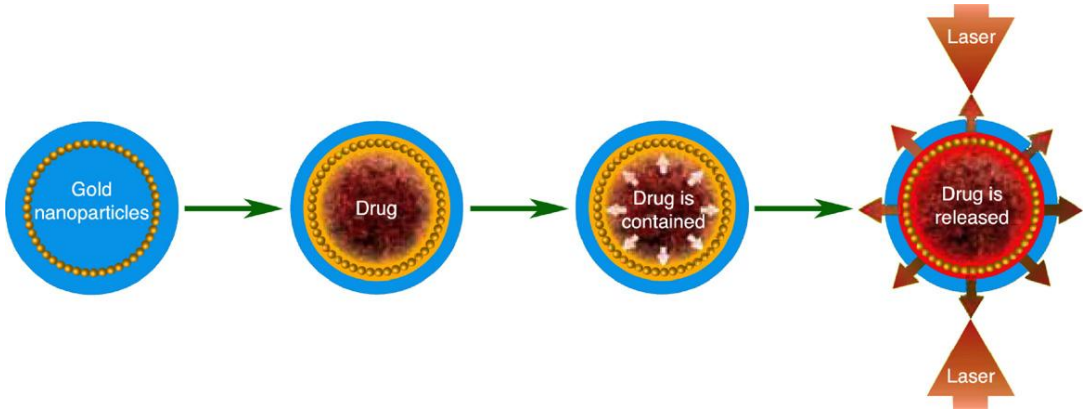


Fig. 2.6 Demonstration of burst release of nanocapsule consisting of polyelectrolyte and gold nanoparticles triggered by laser [107]

Besides near-infrared sensitive polyelectrolyte capsules, there are also other photo-sensitive drug carrier systems (e.g. liposomes and polymer micelles) being developed [146, 147]. For liposomes, the principle of the light stimulating releasing is related to the destabilization aroused by the light irradiation. De Geest et al. based on other group's works summarised the main reasons which induced this destabilization: 1) degradation of lipids due to some reactive species (e.g. singlet oxygen) [148, 149], 2) photo-isomerization [150] or 3) photo-polymerization [151] of lipids. For polymer micelles, the mechanism of burst releasing could be attributed to a photo-chemical reaction which leads to changes of the hydrophobicity of the component polymers [152, 153]. However, most of the photo-sensitive liposomes and polymer micelles are responsive to light sources with wavelengths shorter than near-infrared and in this wavelength range the UV light is harmful and demonstrates nearly no penetration (<0.5 mm) to the human body [140]. Furthermore, it has been reported that the intracellular uptake capsules could also be triggered to release components by the near-infrared laser [143]. By adjusting to an appropriate laser power, the capsules could be collapsed without impairing the cell [154].

In this project, polyelectrolyte nanocapsules incorporated with gold nanoparticles were prepared to endow the nanocapsules with ability of absorbing energy from near-infrared sources.

2.3.5.2 Sustainable release

In general, the drug release rate is dependent on the permeability of the hollow capsules and this permeability is mainly decided by the properties of the constituent polymers. Those properties could be affected by the changes of the environment such as pH, temperature, or ionic strength [108, 155-161]. Therefore, therapeutics could be sustainably released either by changing the conditions of the bulk solution, or by gradual degradation of the capsule itself [107]. The first route is similar with the post-loading process described in the encapsulation section, only with a reverse direction of diffusion. As two main reasons affecting the permeability of the capsules, many studies have been performed on the pH and ionic strength of the capsules dispersion medium [107, 162, 163]. Caruso and Schuler first reported the relationship between the ionic strength and the stabilisation of capsules [164]. They fabricated capsules consisting of DNA and spermidine onto melamine formaldehyde core templates and then the core templates were removed by exposure to an acid environment (pH 1.6). The hollow capsules were found to be sensitive to the ionic strength of the medium and it was observed that the interaction of DNA and spermidine decreased with an increase of the ionic strength. Finally, when the salt concentration reached 5 M, the capsules of DNA/spermidine were found completely dissolved [164]. Then Ibarz et al. reported their research work of permeation of polyelectrolyte capsules at different salt concentrations [112]. In their work, hollow capsules consisting of PSS/PAH were prepared and the polymer PAH labelled with rhodamine B (PAH-rho) was used as loading/releasing material. It was found that along with an increase of the salt concentration in the bulk solution (from 10^{-4} to $2*10^{-2}$ M), both the

loading/releasing speed and amount of PAH-rho increased significantly [112]. However, due to the properties of the capsule materials, sometimes the sudden change of the environment would result a rapid release of the loaded material [128, 160]. Therefore gradually dissolution of the nanocapsules is the other route to achieve sustainable release. A typical example is that reported by Itoh et al. on 2006 [131]. As a continuous part of the experiment which was mentioned previously, Itoh et al. provided a sustainable way to release the loaded material in biodegradable hollow capsules. In this part of the experiment Itoh et al. introduced the enzyme (chitosanase) to degrade the capsule membranes (contains chitosan and dextran sulphate) and a controlled releasing of the loaded protein was achieved (Fig. 2.7).

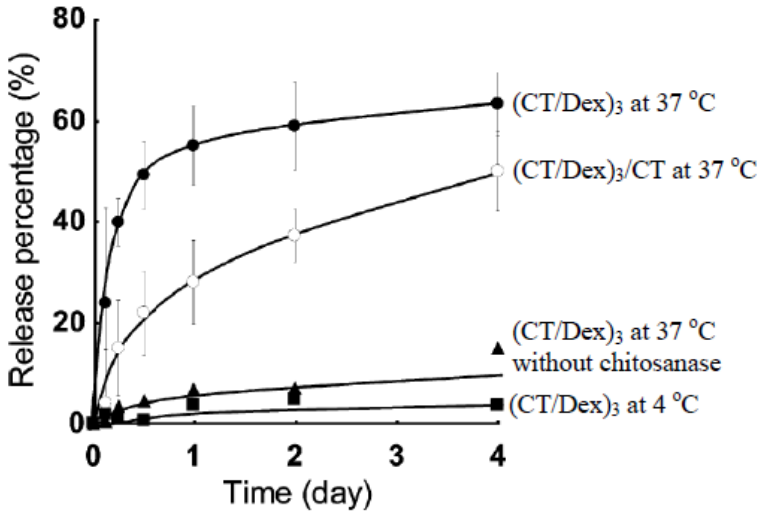


Fig. 2.7 Release figure of FITC-albumin from hollow capsules of different polyelectrolyte combination at different temperatures, CT and Dex in the figure correspond to CHI and DS in this thesis [131].

From Fig. 2.7, it is found that capsules of (CHI/DS)3 at 37℃ presented the highest releasing ability of the four batches of samples. It was explained by Itoh et al. that the negatively charged DS is more likely to attract chitosanase which is positively charged in the solution; therefore in that case more enzymes gathered at the capsules surface and

led a quick release of the loaded proteins. It was also noticed that at the same temperature (37 ℃), addition of the enzymes would result in a faster releasing rate. Furthermore, from Fig. 2.7, chitosanase at 4℃ has a relatively low activity and the releasing rate at this temperature is the lowest in this graph, implies that the protein was prevented from diffusing through the CHI/DS membrane at this temperature.

In this work, the two main polyelectrolyte used are chitosan and dextran sulphate and both of the materials are biodegradable, which ensures various applications for the nanocapsules prepared in this project.

2.3.6 Core Templates and Coating Materials

2.3.6.1 Core Templates

In the LbL method, the size and morphology of the micro- and nano-capsules are mainly affected by the dimension and shape of original core templates. Different colloidal particles have been used as core templates. In this section, the works of the most popular colloidal core templates are reviewed in the following sections. There are mainly two types of colloidal particles (organic and inorganic) that could be used as core templates.

Organic Core Templates

Melamine Formaldehyde

Due to the property of easily being dissolved in acidic environment, melamine formaldehyde colloidal particles are one of the generally used cores for the LbL self-assembly process. As a pioneer scientist in the area of LbL method preparing

micro- or nano-capsules, in 1998, Donath et al. reported the fabrication of microcapsules consisting of polyelectrolyte on weakly cross-linked melamine formaldehyde (MF) colloidal particles [71]. In their experiment, MF particles of 2 and 3.2 μm were used as core templates and poly(sodium styrenesulfonate) (PSS) and poly(allylamine hydrochloride) (PAH) were sequentially added onto MF particles. After the polyelectrolyte's deposition, the MF particles were then removed by exposure to an acidic media (<pH 1.6) [71]. After Donath's work, many studies have been performed with MF core templates [165-169]. In these works, different polyelectrolyte pairs had been used to prepare the hollow capsules for various applications. Caruso et al. (1999) reported experimental work employing a special kind of synthesised polyelectrolyte: metallosupramolecular polyelectrolyte to prepared microcapsules. Fe(II) metallosupramolecular polyelectrolyte (Fe(II)-MEPE) and poly(styrenesulfonate) (PSS) were deposited on MF particles of 1.7 μm and the MF cores of the core-shell structures were also dissolved in acidic solution (pH=1) [165]. Khopade et al. (2004) provided a new method named, the core-mediated LbL process, to prepare microcapsules via MF core templates (1 or 3.5 μm) [166]. In this method, after the first layer (PSS) deposition, the MF cores were gradually dissolved in a mild acidic environment (pH=4) and spontaneously the MF molecules derived from the core decomposition formed the second layer. Then after repeating this cycle, the capsule could be built on the partially dissolved cores and the final core templates were removed in HCl solution (pH=1) [166]. However, most of the hollow capsules produced via MF cores are located within the micron size range, to the best knowledge of the author of this thesis, no works of submicron or nanometre size range had been reported.

Polystyrene

Polystyrene colloid is another organic core template widely used in the LbL method. Like melamine formaldehyde colloidal particles, polystyrene particles are also

relatively easy to be removed. As the first few groups reported the adaption of Layer-by-Layer process onto colloid templates, Sukhorukov et al. (1998) demonstrated that the multilayer films can also be obtained by deposition of polyelectrolyte onto charged latex particles in aqueous solution [100]. They used polystyrene latex particles (from 640 nm to 3 μm) as the core templates and tried two pairs of polyelectrolyte, namely sodium poly(stryrene sulfonate), poly(allylamine hydrochloride) and poly(diallyl dimethyl ammonium chloride) and DNA as the polyelectrolyte layer materials. They also employed a centrifugation-based technique to separate coated polystyrene particles from bulk solution to avoid large particle aggregates and this technique was then widely used in the LbL process. However, as an early work of this area, no hollow capsules were produced [100]. To remove the polystyrene core templates, two methods had been provided including: chemical dissolving and calcination. Chemical dissolving could be used for the capsules consisting of polyelectrolytes and the calcination is for the ones comprised of inorganic materials. As a good example for both core-removal methods, Caruso et al. (1998) prepared silica-polymer spheres on the polystyrene templates of a size scale from720 to 1000 nm. By alternatively adding polymer and silica nanoparticles onto the polystyrene core templates, uniform core-shell structures were fabricated. Then the polystyrene particles were removed by either solvent (tetrahydrofuran THF) dissolution or calcination, two types of hollow capsules were obtained. Silica-polymer hollow spheres were obtained from chemical dissolving and silica hollow capsules were obtained from the calcination. However, both broken and intact hollow capsules were found after both core removal methods[102]. Then, along with the tremendous interests had been put into the preparation of nanocapsules via the LbL method, polystyrene colloid particles were widely used as core templates and hollow capsules of submicron size and various shell composition were prepared [102, 170-173].

However, there is one advantage of the organic core templates. Many studies have mentioned that after the core removal process, a residue of organic cores is likely to

remain inside the capsules and may crosslink with the polymer shell [167, 169]. And due to their relatively large molecular weight and quickly being dissolved, the osmotic pressure is relatively large while the core removal process and might result capsule disruption [174].

Inorganic Core Templates

Compared with the organic core templates, the inorganic core templates are more attractive for the low molecular weight (normally less than 5KDa) of the molecules derived from the core removal process.

Inorganic Carbonates

Many inorganic carbonates had been used as core templates for the LbL process, including cadmium carbonate ($CdCO_3$), manganese carbonate ($MnCO_3$) [175] and calcium carbonate ($CaCO_3$) [176]. All the inorganic carbonates colloidal particles could be removed by ethylene-diamine-tetra-acetic acid (EDTA) and HCl solution [175, 176]. However, so far, as reported most of the hollow capsules prepared via the inorganic carbonates are within micron size range.

Silica nanoparticles

Silica particles (both porous and non-porous) have aroused much attention in the LbL process for two main reasons. One is the mono dispersed sample could be easily obtained from commercial suppliers or laboratory preparation. The other is the particles are stable at all pH's. This is very important for some polyelectrolytes which need acidic solution to dissolve e. g. chitosan or the layer deposition process involves hydrogen bonding [177, 178]. One important limitation for silica core template is the

solvent (HF) used to dissolve the silica cores. HF is very toxic and needs extreme care to remove completely from the system. However, as Shu et al. [38] and Itoh et al. [131] reported, the attendance of HF does not affect the activity of the pre-loaded protein or enzyme and in this project, the post-loading strategy is employed to provide adequate washing cycle to get rid of the HF residue. In this case, the impact to the loading therapeutics and human body could be minimised.

In summary, because the aim of the project is to prepare nano-scale drug delivery system, the core templates must be within the size range of submicron (dozens to hundreds of nanometres). Thus, the silica and polystyrene nanoparticles were selected as the core templates.

2.3.6.2 Polyelectrolytes

Due to the high flexibility of the LbL process, there is a very wide range for the selection of the shell materials. DNA [164], proteins [172], inorganic particles [170], synthesis polyelectrolytes [170] and biopolyelectrolyes [113] are all reported as capsule materials. Since the nanocapsules would be degraded either outside or within the cells [106]. They must be produced under certain requirements (also apply to substances after degradation): non toxic, biodegradable and non immunogenic [47].

The main polyelectrolyte pair in this PhD project is chitosan and dextran sulphate. They are both biodegradable and attractive for biomedical applications [179]. Two synthetic polyelectrolytes PDADMAC and PSS have also used as substitutions for CHI and DS for some special situations and they are both biocompatible [140, 180]. Two proteins BSA and lysozyme are both naturally extracted proteins. The inorganic nanoparticles used in this project are gold, magnetite nanoparticles and both of them were confirmed as biocompatible materials [107, 181]. Laponite nanoparticles which were widely used

for the design of biosensors [182-184] were employed to strengthen the nanocapsules prepared in this project.

2.4 Summary of the Motivation and Innovation of this PhD Project

To ensure the therapeutics could be properly protected in the human blood circulation and to make components more effectively cure the ill organs, a useful drug delivery system is desired to be developed. As it was discussed in section 2.1, compared with other routes there are many advantages of the nano-scale drug delivery system. Thereby, in this thesis, the preparation of drug delivery systems on nano-scale range will be discussed. Due to the advantages such as easy control of the size and wall thickness, various composition and simple process of assembly, the Layer-by-Layer self-assembly method is utilised in this project. In this project, the nanocapsules (100-200 nm) via silica and polystyrene nanoparticle templates were prepared and this size range is an innovation for nanocapsules prepared by LbL process. The combination of low molecular weight chitosan and dextran sulphate gives more flexibility to the nanocapsules produced and is originally from this research. Also the utilising of two oppositely charged proteins and coating the insulin nanoparticles with biodegradable polyelectrolyte (DS) and protein (lysozyme) are both innovations of this project.

Chapter 3 Characterization Methods

In this Chapter, the principles of the main characterization methods utilised in the project are briefly described, together with the specific details which were actually used in making the measurements.

3.1 Zeta-Potential Measurement

In this project, the zeta-potential was used to monitor the deposition of each polyelectrolyte (or other material). Colloidal particles dispersed in a polar solvent such as water, or an electrolyte solution, are generally electrically charged (Fig. 3.1).

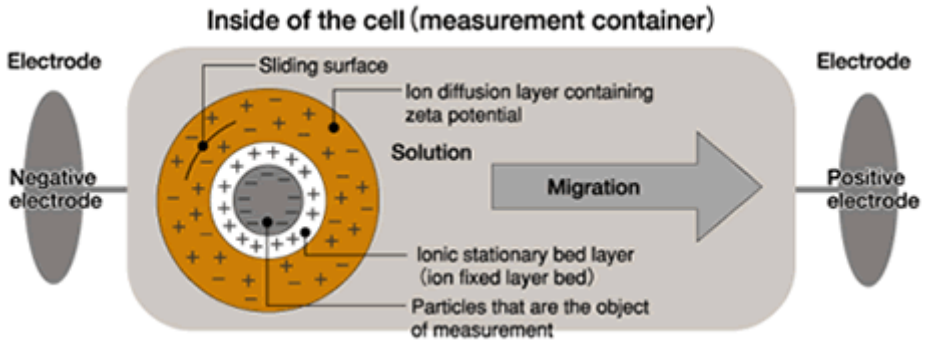


Fig. 3.1 A schematic of the Double Layer of Colloidal Particles [185]

As Fig. 3.1 shows, each particle dispersed in a solution will attract counter ions around it, and these attracted counter-ions form a flexible shell. The innermost part of the shell is a tightly attached layer of counter-ions, known as the Stern Layer [186]. Outside the Stern Layer, there are also some counter-ions that are affected not only by the attraction from the particles but entropy which is trying to disperse the ions. So these counter-ions form a cloud-like area, which has high concentration of counter-ions near

the Stern Layer surface and exponentially decreases with the distance away from the particle surface to infinite until reaching equilibrium, again with the bulk counter-ions in the solution [186, 187]. This region is called the diffuse layer, and the whole system called an electrical double layer [188]. (see Fig. 3.2)

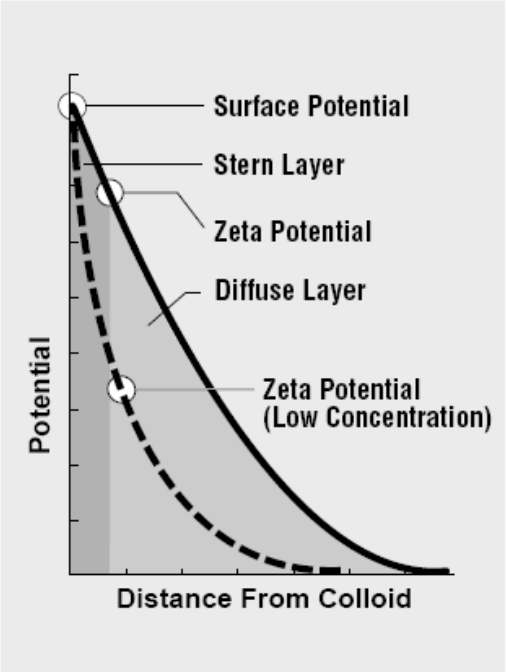


Fig. 3.2 The relationship of the electric potential and the distance from the particle surface [189].

When a voltage is applied to the solution in which particles are dispersed, particles will be attracted by the electrode of the opposite polarity, and they will move to the electrode accompanied by the fixed layer of ions whilst the diffuse double layer consisting of oppositely charged ions moves to the opposite electrode. The term zeta-potential refers the electrical potential at the plane of shear between the particle and diffuse layer. It needs to be noted that zeta-potential is not equal to the potential of the stern layer [190] or particle surface [188]. The zeta-potential may be calculated from the Smoluchowski equation [186] (Equation 3.1).

Equation 3.1 $$\zeta = u\eta/\varepsilon$$

Where u is the mobility of the particle, η is the viscosity of the solution and ε is the permittivity of the solution, respectively.

In this work, zeta-potential measurements were used to track the deposition process of the polyelectrolytes. With the change of the zeta-potential, one can determine whether the polyelectrolyte has adsorbed on the particles. For example, as Fig. 3.3 shows, the polystyrene (PS) particles are negatively charged. When the first layer (chitosan) adsorbed on the particle, the zeta-potential of the coated particle turns positive. Then the second layer (sodium alginate) formed, and the zeta-potential switched to negative. Repeating the cycle, we observe positive zeta-potential for the odd layer, and negative potential for the even layer. Each time of the change of the zeta-potential (from positive to negative and vice versa) confirms each polyelectrolyte layer's deposition.

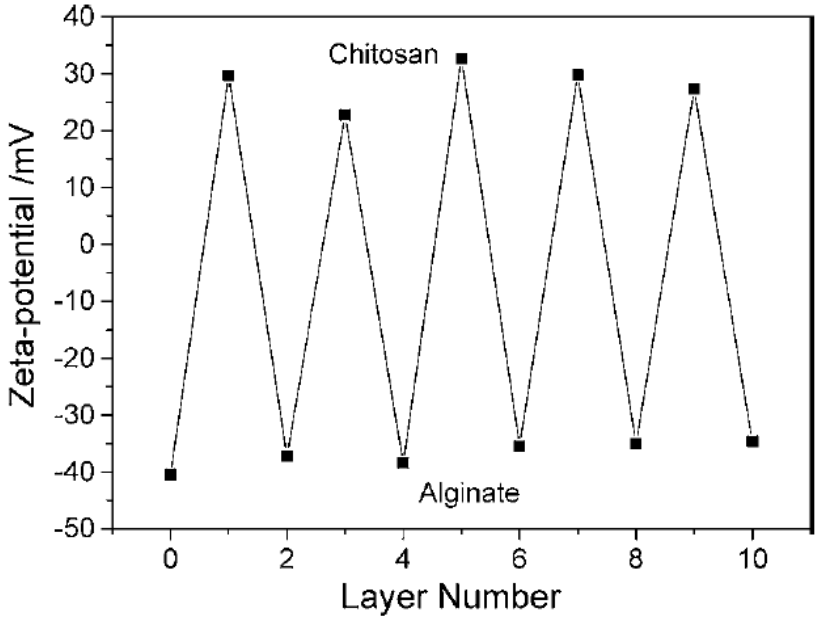


Fig. 3.3 Graph of zeta-potential of CHI and ALG depositing on PS particles [113]

The instrument used in this project to measure the zeta-potential of was the Zeta Potential Utilizing Phase Analysis Light Scattering (ZetaPALs) from the Brookhaven Instruments Corporation (Fig. 3.4). The general procedure for determining the zeta-potential of a sample is as follows:

- First, the measuring electrode was rinsed with deionised water and air dried.

- Then 1.5 ml of the sample was put into the measuring cuvette and the air-dried electrode was tightly plugged into the cuvette. The 1.5 ml liquid could totally cover the surface of the electrode.
- Afterwards, the whole system (the cuvette and the electrode were carefully put into the measuring slot inside the machine).
- All the measuring conditions were set to the default condition and if there was no specific situation, the measuring medium was chosen as water. Each measuring cycle lasts for about one minute 5 cycles were recorded for each measurement, the zeta-potential then being taken as the average of these five measurements.
- Each Layer-by-Layer adsorption process was duplicated in this project and thus the zeta-potential of each layer was measured twice to see whether the two results shared same trends and had similar value (Same trend means the two results were both positive or negative and similar value means that there was no big variance (within ±10 mV). If there were large variations then the experiment was repeated a further time). For all zeta-potential measurements, no added electrolyte was required as the adsorption process occurred in moderately concentrated sodium chloride solutions (typically 0.1 mol/L).



Fig. 3.4 The machine (ZetaPALs) used to measure the Zeta-potential of the nanoparticles

To make the measurement process clearer, a typical example of the zeta-potential results is given in Table 3.1 and Table 3.2 for two independent experiments for the adsorption of chitosan and dextran sulphate onto 95 nm silica particles.

Table 3.1 The zeta-potential of each polyelectrolyte layer coated on 95 nm silica particles (CHI/DS 0.1 M NaCl) (First measurement)

Number of Layers	Zeta-potential (mV)
0	-38 ±3
1	+28 ±4
2	-32 ±3
3	+58 ±5
4	-26 ±2
5	+51 ±4
6	-30 ±3
7	+53 ±5
8	-25 ±3
9	+56 ±4

Table 3.2 The zeta-potential of each polyelectrolyte layer coated on 95 nm silica particles (CHI/DS 0.1 M NaCl) (Second measurement)

Number of Layers	Zeta-potential (mV)
0	-34 ±4
1	+29 ±1
2	-37 ±3
3	+57 ±3
4	-30 ±4
5	+53 ±2
6	-28 ±2
7	+51 ±5
8	-29 ±2
9	+50 ±3

In tables 3.1 and 3.2, it can be clearly seen that considering the standard error, the zeta-potential measurements of each polyelectrolyte layer lies in the variation zone (±10 mV) that we set before the experiment. Therefore, the result of the first experiment was taken and reported. All the zeta-potential measurements followed this standard process.

3.2 Dynamic Light Scattering

Dynamic light scattering (DLS) (also known as Quasi-elastic Light Scattering, or Photon Correlation Spectroscopy) is a technique used to measure the size and size

distribution of small particles in suspension or polymers in solution [191-193]. The advantages of the DLS measurement are obvious, such as short measuring duration, automatic measurement and no extensive experience needed. Thus, DLS as a routine measurement of particle size distribution is now being widely used [194].

The basic principle of DLS is described as below: When a small particle is hit by light, as long as the particle is small enough compared with the wavelength of light, the light would scatter in all directions. When the light source turns to a laser which is coherent and monochromatic, a time-dependent fluctuation could be observed in the scattering intensity [195]. These fluctuations are caused by the Brownian motion of the small particle/molecule in solutions. Also the intensity of the fluctuation is at a rate affected by the particle size, as smaller particles in the same time span would move farther and faster. The dynamic information (e.g. the diffusion coefficient) could be derived from the autocorrelation of the intensity records [196] and with the Stokes–Einstein equation [197] (Equation 3.2), the particle size may be calculated [195, 198]. The particle size obtained here is called hydrodynamic diameter, because the size from this technique not only includes the exact size of the particles but also any structure attached to the particles [191].

Equation 3.2 $$D_h=\frac{Tk_B}{3\pi\eta D}$$

Where D_h is the hydrodynamic diameter of the particles; T is the temperature in Kelvin degree (in this thesis, it was set as 298 K); k_B is the Boltzmann constant; η is the viscosity of the medium; D is the diffusion coefficient [195].

The instrument used in this project was the 90Plus Size Analyzer from Brookhaven Instruments. Before the test, 0.05 ml of the sample was diluted with deionised water to

a total volume of 0.5 ml. Then, 0.1 ml of the diluted sample was added into a 3 ml acrylic square cuvette, and then the total volume made up by deionised water to 2.5 ml. The cuvette was then placed into the instrument to measure the size distribution of the nanoparticles. As it was the case for the zeta-potential measurement, all the measuring conditions were set as default and generally the measuring medium was chosen as water. Each measuring cycle lasts for about one minute and five cycles were recorded for each measurement and the particle size was taken as the average of five readings. Each sample was tested twice and if there was no obvious difference (less than 5%) between the two tests, the result from the first measurement was selected as the average particle size.

3.3 Electron Microscope

Electron microscopes (EM) are scientific instruments that use a beam of highly energetic electrons to examine objects on a very fine scale [199]. Due to the big difference of the wavelength between electron and visible light, the EM, compared with optical microscopes, has much higher resolution (down to 50 pm [200]) and much greater magnification (up to 10^7) [201]. Therefore, electron microscopes are widely used to observe biological, organic and inorganic samples. There are several types of electron microscopes, including scanning electron microscope (SEM), reflection electron microscope (REM), transmission electron microscope (TEM), scanning transmission electron microscope (STEM), low-voltage electron microscope (LVEM) et al [199]. In this thesis, SEM and TEM were the two main characterisation methods to observe the nanocapsules obtained from the experiments. In the following paragraphs, details of these two methods including theory and sample preparation are discussed.

3.3.1 Scanning Electron Microscope

The scanning electron microscope (SEM) is a type of electron microscope utilising the interaction of emitted electrons and atoms of a sample to collect information of the topography and other properties of the samples surface [202]. Due to the manner in which the image is created, SEM images have a characteristic appearance and are useful for judging the surface structure and topology of the sample [199, 203]. Fig. 3.5 shows the general inner structure of an SEM.

In a typical SEM firstly, electrons are thermionically emitted and are accelerated towards an anode. The electrons can be emitted either, from a metallic cathode (tungsten or lanthanum hexaboride LaB_6) or, via field emission. After being focused by a series of (magnetic) lenses and passing through pairs of scanning coils which makes the beam raster scan over the sample. When the electron beam strikes the surface of the sample, the primary electron beam effectively spreads and interacts with the sample and fills a teardrop-shaped volume, known as the interaction volume, extending 100 nm to 5 μm depths into the surface. Interactions in this region lead to the subsequent emission of electrons which are then detected by special detectors to produce an image of the sample surface and displayed on a computer monitor [204, 205].

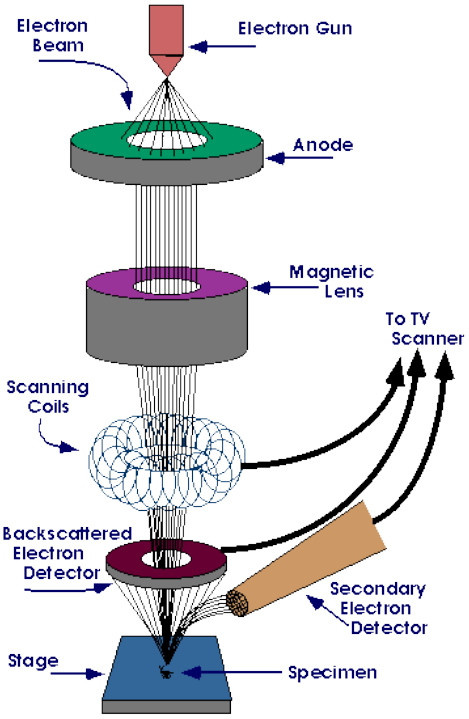


Fig. 3.5 Graph of the inner structure of a SEM [206]

In this projest, a LEO Gemini 1525 SEM (shown in Fig. 3.6) was used to analyse the nanoparticles coated with polyelectrolytes and hollow capsules derived from the core removal process. The samples for SEM test were prepared as followings.

- Firstly, the samples of coated particles were diluted approximately 10 times with deionised water; the hollow capsule samples were used as they were after the core removal process.
- The samples were then dropped onto the pre-polished SEM aluminium stub and the drops were dried in a petri dish at room temperature for at least 24 hrs.
- The dried samples were coated with a layer of gold or chrome at the presence of argon in a special coating machine (Peltier Cooled High Resolution Sputter Coater K575X, EMITECH). This coated process lasted for one and half minutes.
- The pre-coated samples were placed in the SEM and observed under electron beams from 1 kV to 5 kV.

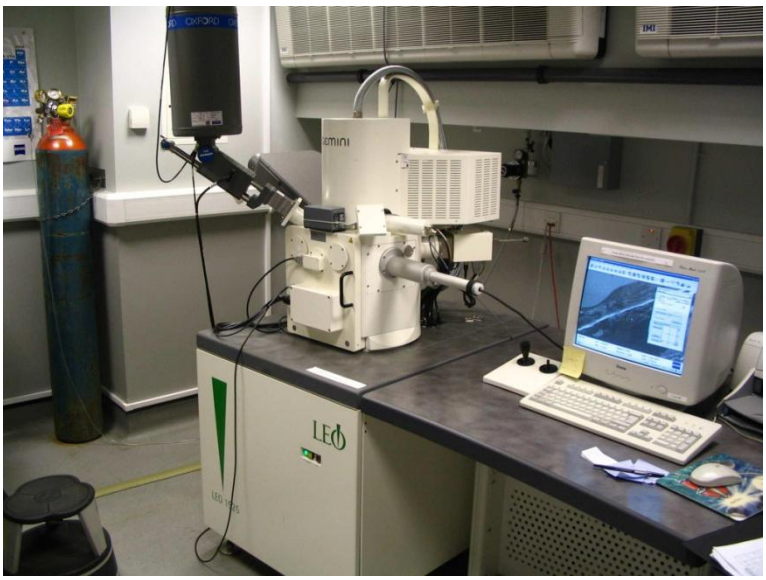


Fig. 3.6 Leo 1525 Gemini Field Emission Gun SEM

3.3.2 Transmission Electron Microscope

Transmission electron microscope (TEM) is an imaging technique in which a beam of electrons interacts with a sample when it passes through and an image of the sample could be generated by the interactions [207, 208].

The basic components of TEM are similar to those of SEM as both contain an electron gun, lens to focus the electron beam, and coils to deflect the beam. Only with a much more powerful electron gun and much thinner samples, the electron beam in a TEM can transmit through the sample, which makes a TEM works much like a slide projector. A projector shines a beam of light through (transmits) the slide (the specimen holder), as the light passes through, it is affected by the structures and objects on the slide. These effects result in only certain parts of the light beam being transmitted through certain parts of the slide. This transmitted beam is then projected onto the viewing screen, forming an enlarged image of the slide [207, 209].

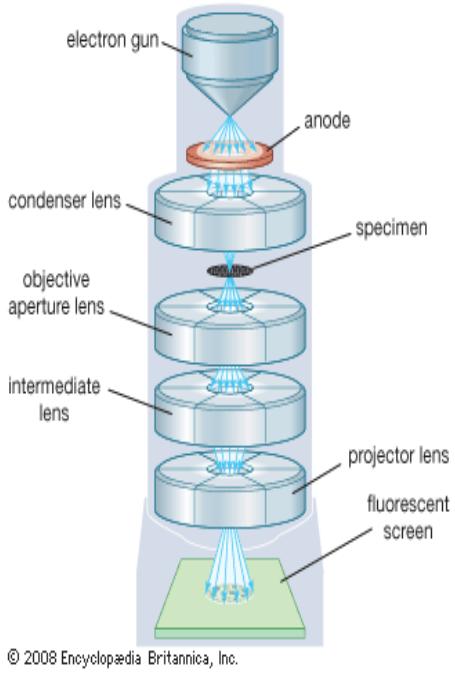


Fig. 3.7 Graph of working principle of TEM [210]

For all the experiments in this thesis, the TEM machine used was a JEOL 2010 TEM (shown in Fig. 3.8), fitted with Oxford Instruments ISIS EDS (energy dispersive X-ray 200kV) system. To prepare the samples for the TEM test, all the samples were diluted 100 fold with deionised water and the diluted samples were dropped onto the TEM sample holder (200 mash copper grid form Agar Scientific Inc.). The samples were dried under an air drier at a temperature of around 35 ^{o}C.

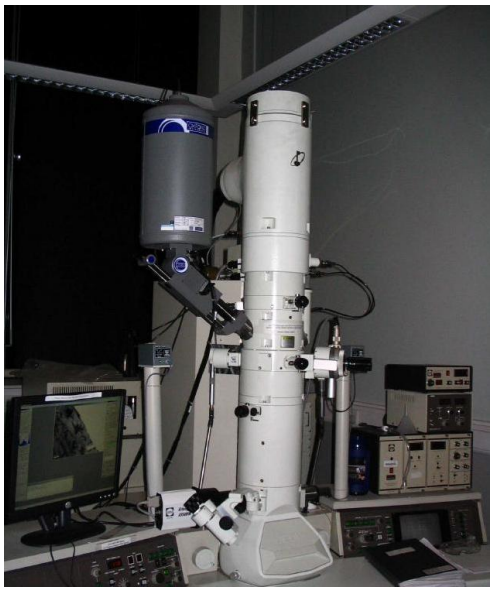


Fig. 3.8 JEOL 2010 TEM

3.4 Disc Centrifuge

As a complementary method of particle size measurement, the Disc Centrifuge was used in this project to measure the size distribution of gold nanoparticles. The reason for using this technique was because it could measure nanoparticles as small as 2 nm, which is suitable for the size range of the gold nanoparticles prepared for functionalising the nanocapsules. The basic principle of the Disc Centrifuge is illustrated in Fig. 3.9.

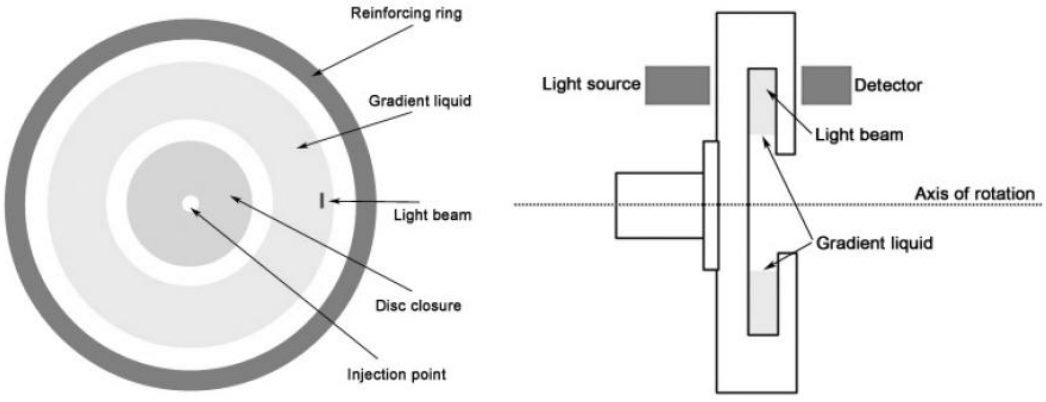


Fig. 3.9 Illustration of principle of the Disc Centrifuge [211]

As is shown in the Fig. 3.9, the particle suspension is injected into the centre of a rotating disc such that the particles move by a centrifugal force towards the outside of the disc. As it was described by Stokes (Stokes' law), the velocity of the particles is in direct proportion to the square of the particles' diameters [212, 213]. By the light beam shone through the disc, the velocities of all the particles is detected and the size distribution of the particles could also be deduced [214].

In this project, 0.05 ml gold nanoparticles suspension was injected directed into Disc Centrifuge after the preparation and the spin speed was set at the maximum of 20,000 rpm. The sample was tested twice and the average of the two readings was taken.

3.5 X-ray Powder Diffraction

X-rays were discovered in 1895 by W. C. Rœntgen and their wavelength is within the range of 0.1 to 10 nm. This range lies between gamma rays and UV rays [215]. There are many applications of X-rays, such as X-ray crystallography, X-ray radiography and X-ray fluorescence spectrometry [216]. In this thesis, the application of X-ray on crystallography will be discussed and X-ray powder diffraction (XRD) as a main technique in this category was employed in this project to characterise the magnetite particles prepared for functionalising the nanocapsules.

X-ray powder diffraction is a technique used to identify and analyse crystalline materials, such as minerals, ceramics, and other chemical compounds [216] and it was independently discovered by Debye (1916), Scherrer (1917) and Hull (1917) [217]. Thus, it is widely used in geology, chemistry, material science and biology [218].

As Fig. 3.10 shows, there are 3 main parts of a diffractometer: the X-ray tube, the sample holder and the detector. The X-rays are generated by a cathode in the X-ray tube. The X-ray is then filtered and concentrated to obtain monochromatic radiation. When the incident X-ray shines on the sample, the ray will interact with the sample and if the conditions described by the Bragg's Law (Equation 3.3) are met, the interaction would provide constructive interference and a diffracted ray is detected. Therefore, as can be seen in Fig. 3.10, following Bragg's Law, if the angle between incident ray and the lattice surface is θ, then the angle between the diffracted ray and incident ray remains as 2θ [219]. The detector in the diffractometer would move through a range (normally 5 to 70 degrees) to collect all the possible 2θ diffraction information, due to the random orientation of the lattices [218]. Then all the information is recorded and a diffraction pattern is observed.

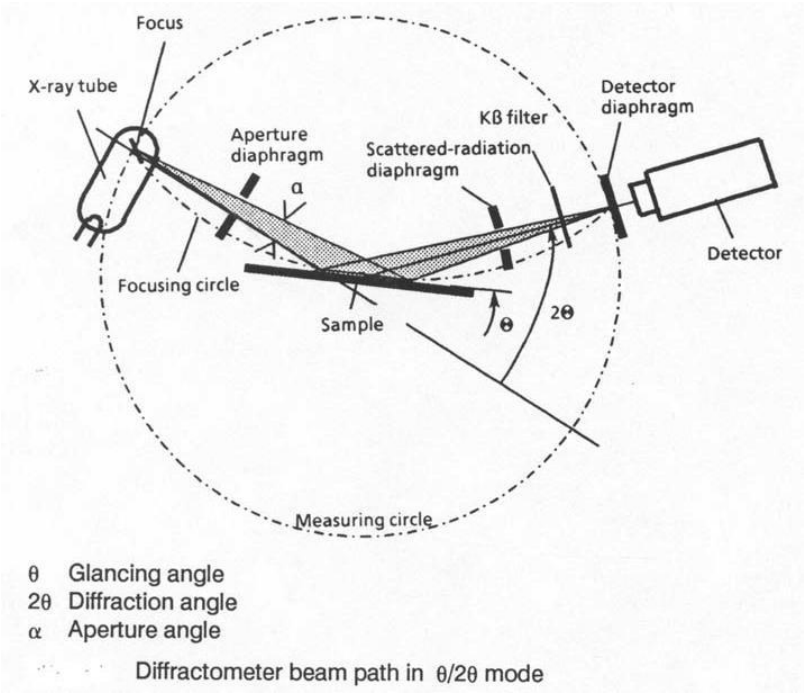


Fig. 3.10 The diagram of the principle of the X-ray powder diffractometer [216]

Equation 3.3 $n\lambda=2d\sin\theta$

Where n is an integer, λ is the wavelength of the incident X-ray, d is distance between the atom layers in the lattice, θ is the angle between incident ray and the lattice surface.

Because each material has its unique arrangement of atoms, each material produces a unique diffraction pattern. The structure of the crystal can be calculated and refined a priori, but generally is obtained by comparing the pattern with the standard pattern data bases, such as the Cambridge Structural Database (CSD) or the International Centre for Diffraction Data's Powder Diffraction File (ICDD-PDF) [219]. Generally, the diffraction patterns for crystalline materials present a series sharp peaks whereas broader peaks could be observed for amorphous materials [219].

The crystallite domains of the materials could be calculated [220] from the Sherrer equation (Equation 3.4) , and when this domain is less than 100 nm, it corresponds approximately to the actual average size of the particles [221]. Therefore, XRD data could be used to estimate the average size of nanoparticles. In this thesis, the mean size of magnetite nanoparticles was calculated by the XRD diffraction pattern of the particles [222] and the size distribution of the nanoparticles was further confirmed by TEM.

Equation 3.4 $\tau=K\lambda/(\beta\cos\theta)$

Where τ is the size of the crystalline domain; λ is the wavelength of the X-ray; β is the width at half maximum intensity of the peak; θ is the angle between incident ray and the lattice surface [223]; K is a shape factor which for magnetite, is normally set as 0.9 [222].

For this experiment, due to the sample size being around 10 nm, no further grinding was needed. Therefore, the sample suspension was dried in the fume cupboard for 48 hrs and 100 mg of the dried powder was placed into the sample holder as the specimen for the XRD analysis. The X-ray diffractometer used was a Philips PW1700 instrument (Fig. 3.11) which was operated at 40 kV and 40 mA. The diffraction pattern was compared with the database of ICDD-PDF.

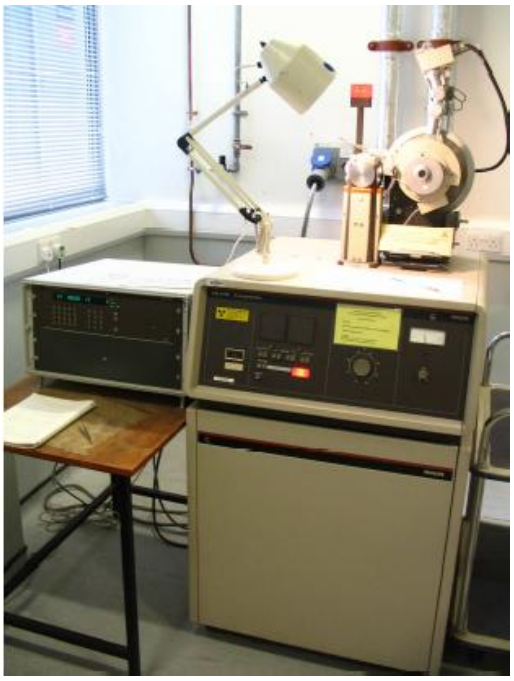


Fig. 3.11 The Philips PW1700 X-ray diffractometer

Chapter 4 Nanocapsules Based on Silica Core Templates

4.1 Materials

The core template used in this section was silica nanoparticles which were prepared in our laboratory; the methodology will be discussed in the following section. The biodegradable polysaccharides were cationic chitosan of low molecular weight and anionic dextran sulphate. Chitosan (CHI) (50,000-190,000 Da, 75-85% deacetylated, pKa 6-7) was purchased from Sigma-Aldrich and Dextran sulphate (DS) sodium salt from Leuconostoc spp. (approximate 10,000 Da) was obtained from Sigma-Aldrich. Other chemicals involved in this experiment include: Ethanol (CH_3CH_2OH, 96% v/v, BDH), Ammonium Hydroxide Solution (NH_4OH, 28-30% NH_3 content, Sigma-Aldrich), Tetraethylorthosilicate ($Si(OC_2H_5)_4$ or TEOS, 98%, Sigma-Aldrich), Sodium Chloride (≥ 99.5%, Sigma). Hydrofluoric acid and Ammonium fluoride, used in the core removal process were obtained from Aldrich. The Visking dialysis tubing (diameter 38.1 mm, MWCO-12-14000 Da) used here was obtained from the Medicell International Ltd. All water used in the experiment was deionised. All the materials used in this experiment were used without further purification.

Safety note: During the core removal process, HF was used. Because HF is highly toxic, the core removal process was carried out in a fume cupboard. Double layer gloves and safety goggles were worn and another person was asked to stand by during the process in case of any emergency.

4.2 Methodology

4.2.1 Synthesis of Silica Nanoparticles

There are two important advantages of using silica nanoparticles as a core material to prepare biocompatible nanocapsules. The first one is the size of the particles. By using different methods, the particle size could be confined within the range between 96 nm to 250 nm. As it was mentioned in the literature review, there are many advantages to use nano-scale drug delivery system, so the size range is a key point of the whole project. The second advantage is that as an inorganic template, the silica cores could be removed completely by etching with HF and there is barely any core material residue left in those capsules.

To prepare the silica nanoparticles, the method first introduced by Werner Stöber et al. [224] was used in this work. First, 1.6 ml of NH_4OH and 50 ml of ethanol were thoroughly mixed together, and then 4 ml of TEOS was added into the solution. Initially the reaction time was varied (between 4-24 hr). However it was determined that at least 8 hr was required to produce mono-modal dispersions (see section 4.3.1.1). Thus, in this experiment, the system was left in the fume cupboard and stirred at a speed of 300 rpm overnight. NH_4OH is a catalyst in this system, and the amount of NH_4OH will affect the size of the silica particles. So in this experiment the amount of TEOS and Ethanol were fixed and 1.4 ml 1.6 ml, 2.0 ml, 2.4 ml, 2.8 ml and 3.2 ml of NH_4OH were employed to make the silica particles ranging from 96 nm to 250 nm.

After the reaction ended, the whole solution was transferred into the dialysis tubing (both ends were tied up) and dialysed against deionised water (2 L in a beaker) for at least two weeks, during which the deionised water was changed at least once every day (see Fig. 4.1). After the dialysis, the total volume of the particle suspension was slightly

different from the original one (due to the empty space left during the tying of the dialysis tubing) and the volume was about 5-10% (by estimation) larger than the original volume. Therefore, the concentrations of the silica nanoparticles were measured and calculated after the dialysis process.



Fig. 4.1 Diagram of the dialysis process

After dialysis, the silica suspensions were collected from the dialysis tubes and stored in wide neck glass bottles. 10 ml of the silica particles prepared from the methods (1.4 ml NH_4OH/4 ml TEOS, 1.6 ml NH_4OH/4 ml TEOS, 1.8 ml NH_4OH/4 ml TEOS) were dried in the oven at a temperature of 100℃ for 48 hr to measure the weight percent of the silica suspensions. The weight percent of all three suspensions was close to 1.2% (the weight of silica nanoparticles versus the weight of the particle suspension), compared to a theoretical weight percentage of the silica particles of around 2.3%.

4.2.2 Polyelectrolyte Preparation Process

Both the low molecular weight Chitosan (CHI) and Dextran sulphate sodium salt (DS) were dissolved in 0.1 M of NaCl solution at a concentration of 1 mg/ml; note that because of the screening effect, the concentration of NaCl will affect the electrical double layer thickness of each poly-electrolyte layer [113].. However, CHI could only be dissolved in acidic conditions so the CHI solution was also adjusted to pH 3 by HCl. The pH value of the DS solution was 6.5. All the measurements of the pH value in this thesis were carried out on a Fisher Accumet pH Meter 15 and each measurement was repeated to ensure the accuracy of the data (difference within 0.1).

4.2.3 Layer-by-layer Self Assembly Process

In this process, all of the materials including the silica particles and polyelectrolyte solution were prepared as described in the previous sections. Ionic polysaccharides were adsorbed onto the silica particle surface via the Layer-by-Layer method. Since the silica particles were negatively charged, the first layer of polyelectrolyte was CHI. The first layer was deposited with addition of 2 ml CHI solution (1 mg/ml) solution and 1 ml deionised water into 1 ml silica particles (1.2 wt%). The pH value of the mixture was determined to be 3.3, and it was incubated for 1 hr under gentle shaking. After that, the excess polymer was removed by two repeat cycles: centrifugation (3000 g, 4 min)/ re-dispersed in 2 ml of deionised water. The second layer followed the same procedure of the first layer but DS replaced CHI. By repeating this process, 9 layers of polyelectrolyte were deposited on the silica particles. The deposition of each layer was monitored by zeta-potential measurements.

Although in this process no accurate determination of the excess polyelectrolytes in the solution was made, the two centrifugation and re-dispersion cycles would

approximately remove more than 99% of the excess polyelectrolytes. Because after each centrifugation, the particle residue plus solution remaining would be no more than 0.2 ml and that means in the two washing cycles the remaining 0.2 ml liquid from the original solution would be diluted 100 times. Since the original residue was 10% of the total amount, in that case after the centrifugation/re-dispersion process the final particle suspension only contained about 1% of the polyelectrolyte from the last layer, which could be ignored.

4.2.4 Core Removal Process

Hollow nanocapsules were prepared by dissolving the silica cores in the HF/ NH_4F buffer solution (2 M HF/8 M NH_4F), this process was performed in polycarbonate tubes as the HF would dissolve glass as well as silica. The coated particles were dissolved in the HF/ NH_4F solution for 2 hr (volume ratio 1:1). Then, the solution was centrifuged at 9400 g for 6 min. After that, the residual was rinsed, centrifuged and re-dispersed in water to thoroughly remove the buffer solution.

Dissolving the silica core was simulated by dissolving silica particles directly. 1 ml of the HF/ NH_4F buffer solution and 1 ml of silica particles were mixed together, and kept for 2 hr. The solution, which contains silicon ions was analysed by inductively coupled plasma - optical emission spectrometer (ICP-OES), to ensure dissolution.

4.3 Results and Discussions

4.3.1 Sizes of Silica Particles

4.3.1.1 The Reaction Time of TEOS Hydrolysis

Judging from the final particles sizes distribution it was found that 8 hr is the minimum time for the TEOS hydrolysis reaction and that 20 hours was a more suitable time to allow the reaction to proceed. If the reaction ran for less than 8 hr, a bimodal particle-size was found, as is shown in the Fig. 4.2.

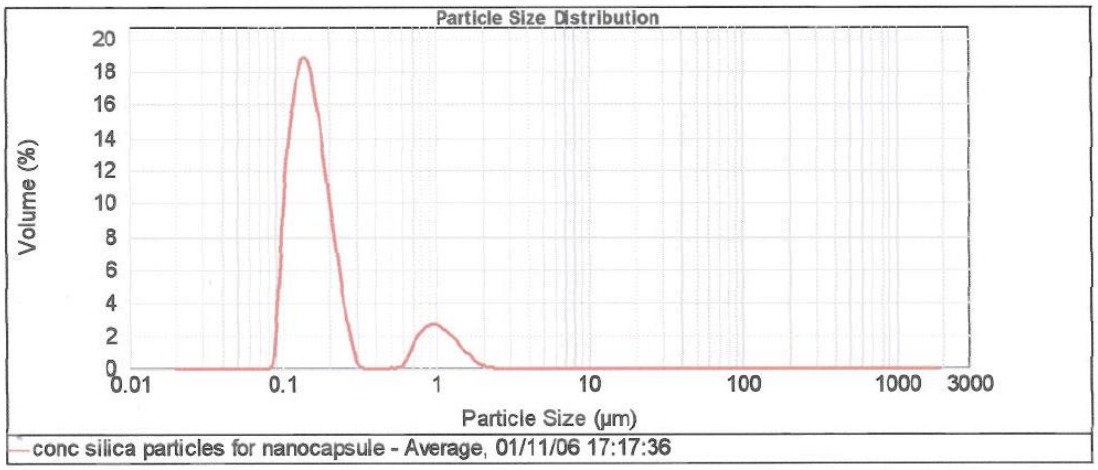


Fig. 4.2 Particles size distribution of the silica particles from the method: 50 ml Ethanol 4 ml TEOS and 2.4 ml NH_4OH with reaction time of 4 hr.

From Fig. 4.2, it can be seen that as well as particles in the size range 100-300 nm, a batch of larger particles (around 10 vol% of the total amount) with a size diameter of round 1 μm was prepared during the process as well. Compared with this dispersion, the particles made from the reaction which lasted overnight (at least 20 hr) produced a mono-dispersed distribution (Fig. 4.3).

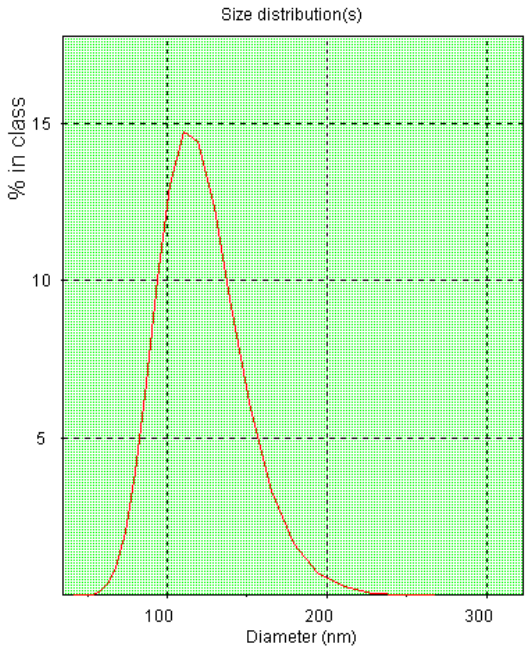


Fig. 4.3 Particle size distribution of the silica particles with the method of 2.4 ml NH_4OH.

4.3.1.2 The Effect of the Catalyst (NH_4OH)

Ammonium hydroxide is the catalyst in this reaction and will affect the size of the silica particles [224]. Therefore in this experiment, different amounts of NH_4OH were used to obtain different sizes of silica particles. In this experiment 6 different amounts of NH_4OH were used to prepare silica nanoparticles with different sizes. The results are given in Table 4.1.

Table 4.1 Silica particles prepared with different amounts of NH_4OH

Amounts of NH_4OH(ml/50 ml Ethanol)	Particle sizes(nm)
1.4	96 ±14
1.6	114 ±12
2.0	154 ±10
2.4	200 ±25
2.8	224 ±34
3.2	252 ±38

As can be seen in Table 4.1, the effect of increasing the NH_4OH concentration is to increase the particle size.

4.3.1.3 SEM Results of Particles Derived from Different Methods

After the measurement of all the size distributions of the silica particles, all the samples (few drops of each sample) were dried out on aluminium stubs and coated with a layer of chromium. SEM tests to see the morphological properties of the silica nanoparticles are shown in Fig. 4.4 - Fig. 4.8.

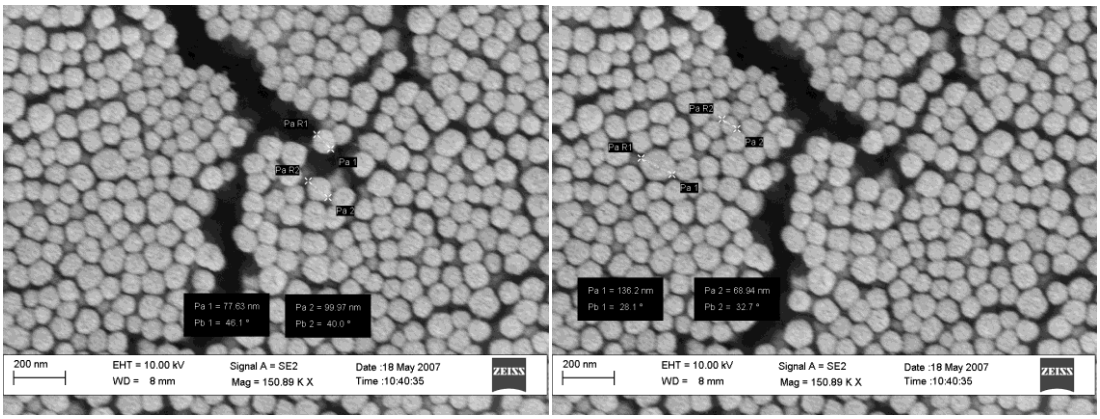


Fig. 4.4 SEM micrographs of the silica particles from the method: 1.4 ml NH_4OH/4 ml TEOS

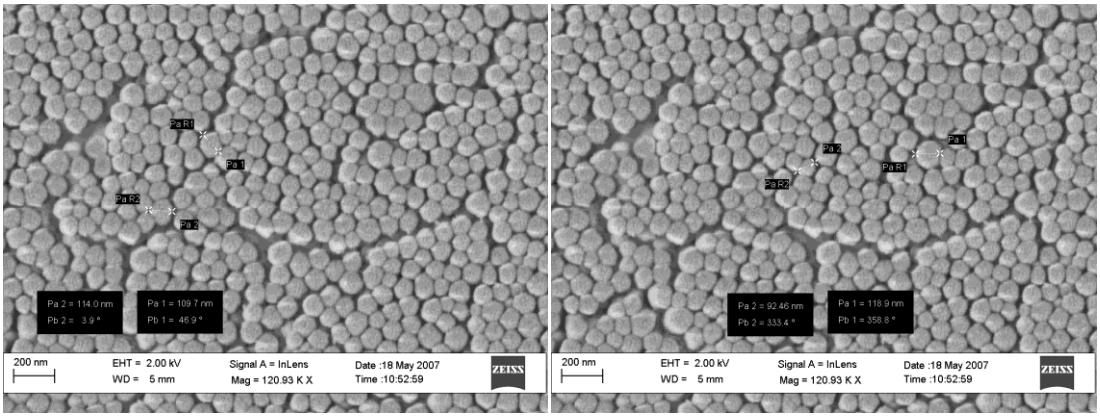


Fig. 4.5 SEM micrographs of the silica particles from the method: 1.6 ml NH_4OH/4 ml TEOS

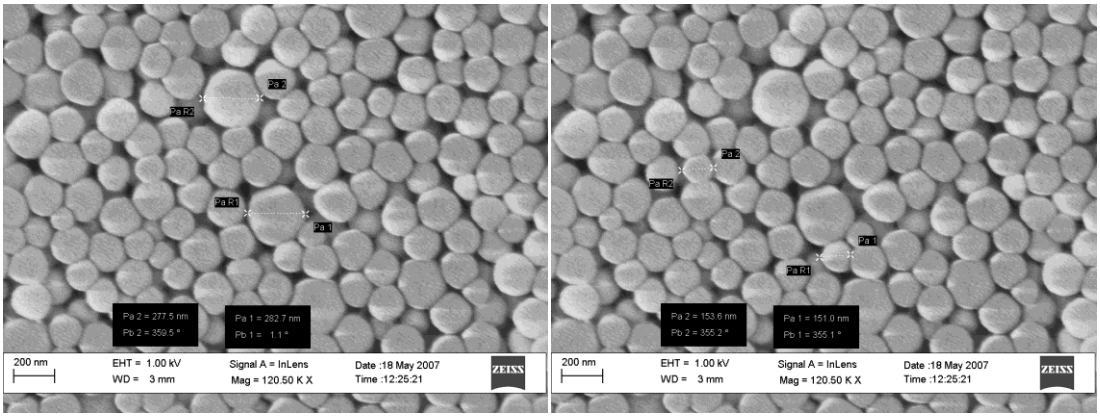


Fig. 4.6 SEM micrographs of the silica particles from the method: 2.4 ml NH_4OH/4 ml TEOS

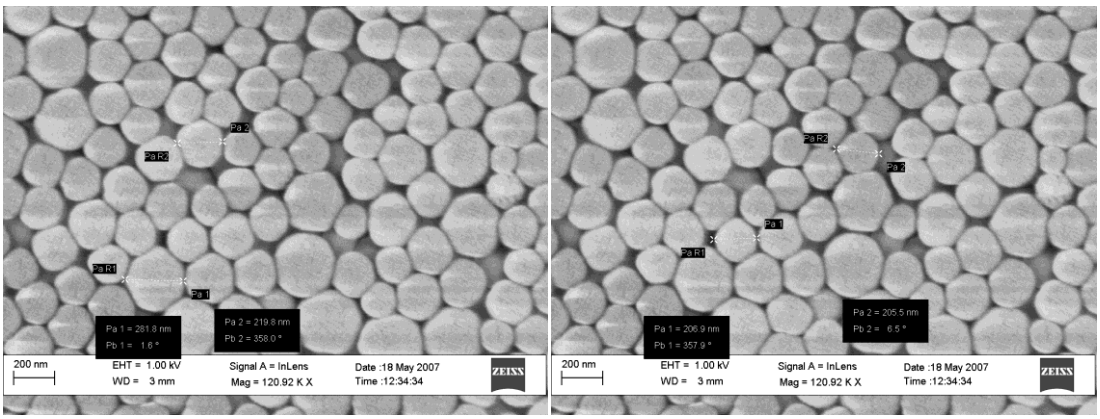


Fig. 4.7 SEM micrographs of the silica particles from the method: 2.8 ml NH_4OH/4 ml TEOS

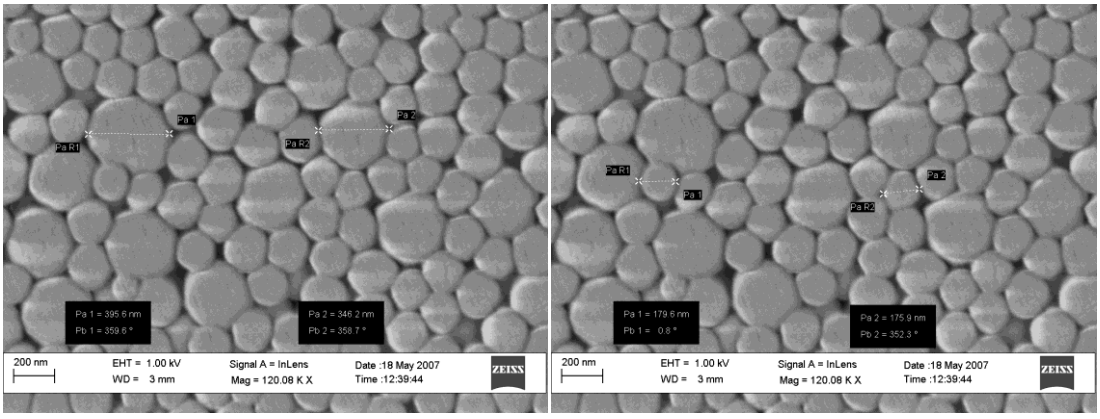


Fig. 4.8 SEM micrographs of the silica particles from the method: 3.2 ml NH_4OH/4 ml TEOS

From the above figures, the shape and size distributions of the silica particles are clearly demonstrated. From the micrographs, it can be seen that the silica particles are tightly arranged and formed multi-layer silica clusters. The fact that the particles appear to be in layers suggest s that the particles are not aggregated but formed these layers on drying. From the micrographs, it also could be seen that the higher the NH_4OH concentration used the broader the size distribution of the silica particles. This situation might be because at high NH_4OH concentration the TEOS/ethanol/NH_4OH mixture was not stirred fast enough. However, due to the limitation of the experimental equipment, it was very hard to keep this system running at very high stirring speeds without any spillage. Because we are trying to build a therapeutic delivery system into

the human body, as it was mentioned in the literature, particles of smaller size would be preferred, therefore, silica particles (from the methods: 1.4, 1.6 ml NH_4OH/4 ml TEOS) were adopted as core templates for the polyelectrolyte self-assembly experiments.

4.3.2 Polyelectrolyte Assembly Process

4.3.2.1 Salt Concentration in Polyelectrolyte Solution

Different salt concentrations were used in this experiment to analyse the affect of salt concentration on each polymer layer. Four salt concentrations: 0.5 M, 0.3 M, 0.1 M, 0.01 M NaCl were used in these experiments, and the rest of the method kept the same. The difference for each layer deposited under different salt concentrations could also be monitored by zeta-potential measurement and the results are shown in Table 4.2.

Table 4.2 Zeta-potential of the 1st layer under different NaCl concentration

Salt concentration	Zeta-potential of the 1st layer(mV)
0.5 M	$+21 \pm 3$
0.3M	$+23 \pm 3$
0.1M	$+28 \pm 4$
0.01M	$+35 \pm 5$

The data in Table 4.2 shows that the higher the salt concentration, the lower the layer zeta-potential. That is mainly because the ions from the salt will screen the charges on the layer surface. So that is why with higher salt concentration, the thickness of the polyelectrolyte layers is larger [225]. However, in this experiment, 0.1 M NaCl was chosen as the salt concentration for the polyelectrolyte solution. That is because after deposition, it was found very hard to re-disperse the samples at salt concentrations of

0.3 M and 0.5 M and some aggregation was observed at the bottom of the centrifuge tubes (see Fig. 4.9); for a sodium chloride concentration of 0.01 M, the polyelectrolyte layers formed at this concentration would probably be too thin, which would reduce the strength of the nanocapsules. Therefore a concentration of 0.1 M NaCl was used.

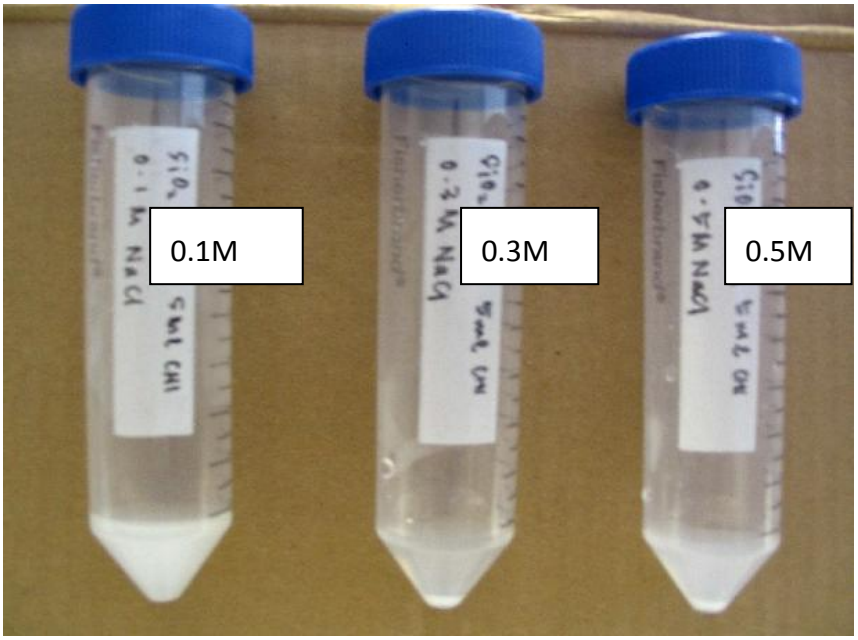


Fig. 4.9 The first layer (CHI) deposition at different salt concentration (from left to right 0.1 M, 0.3 M, 0.5 M)

4.3.2.2 Deposition Time

The time for polyelectrolyte layer deposition was also investigated. The times: 15 min, 30 min, 1hr and overnight were evaluated. The results of the zeta-potential of the 1st layer deposition at different deposition time are shown in Table 4.3. All the depositions were carried out at conditions of particle suspension: de-ionised water: polyelectrolyte solution 1:1:2 and a salt concentration is 0.1 M.

Table 4.3 The zeta-potential of the 1st polyelectrolyte layer at different deposition time span

Deposition Time	Zeta-potential of the 1st layer(mV)
15min	$+26 \pm 3$
30min	$+24 \pm 3$
1hr	$+28 \pm 3$
Over 12hr	$+31 \pm 4$

From Table 4.3, within error (around 3 mV) no obvious difference could be observed in the 4 zeta-potentials. All the values would be sufficient for the next polyelectrolyte layer deposition. Therefore, in this experiment 1hr was used as the deposition time for each polyelectrolyte layer.

All the deposition time and salt concentration tests were carried out on silica cores (95 nm). Because the size difference is within 20 nm and zeta-potential difference is within 10 mV, these conditions were also applied for the silica particles of 114 nm.

4.3.2.3 Layer-by-layer Self-assembly Process

Silica particles with a size of 95 nm and 114 nm were used as core templates in this experiment and 9 layers of biocompatible polyelectrolyte layers were coated onto the two samples. The zeta-potential of each deposition layer was measured to monitor the status of each deposition. The zeta-potential results are shown in Fig. 4.10 and Fig. 4.11 (The values of the zeta potential are listed in appendix Table A.1 and Table A.2 respectively).

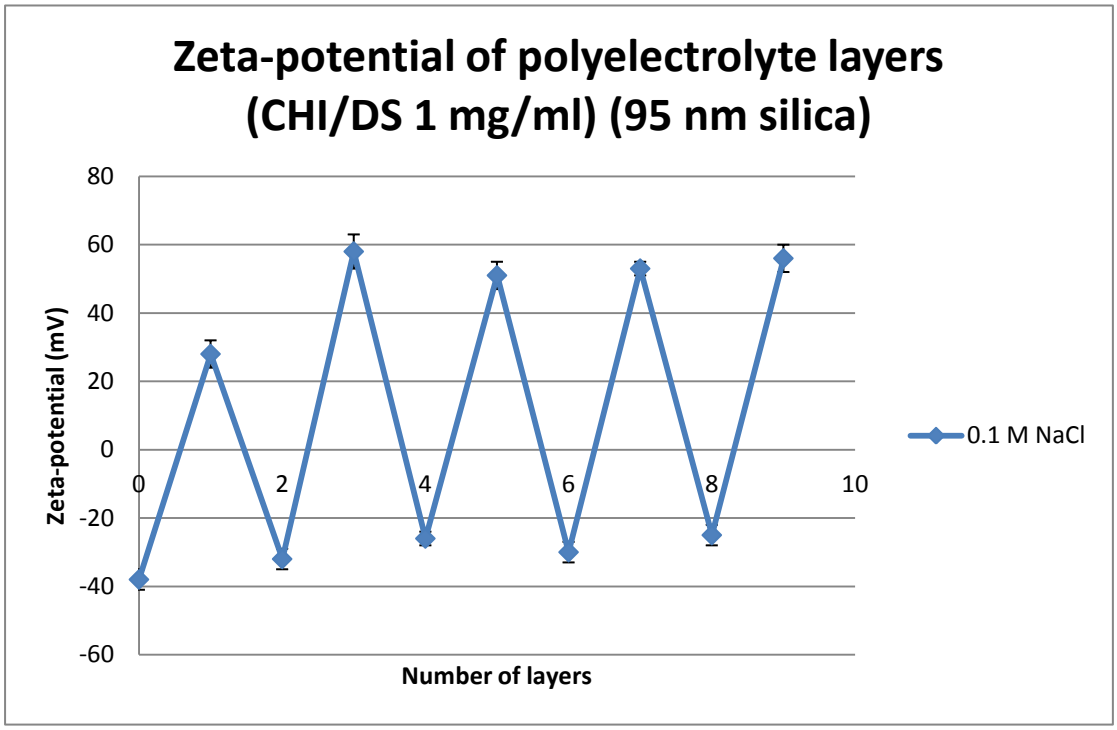


Fig. 4.10 The zeta-potential of each polyelectrolyte layer coated on 95 nm silica particles (CHI/DS)

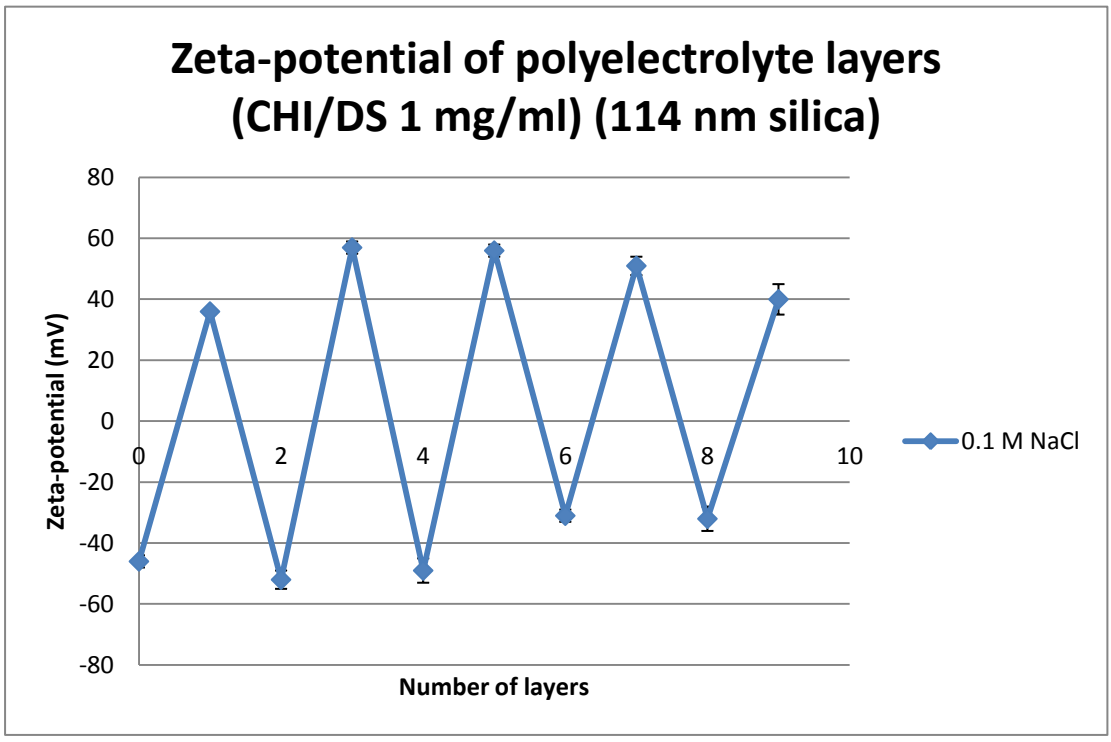


Fig. 4.11 The zeta-potential of each polyelectrolyte layer coated on 114 nm silica particles (CHI/DS)

From both graphs, the shift of the zeta-potential negative/positive/negative confirmed the deposition of each layer. The zeta-potential of the bare silica is around -40 mV and for the layers of CHI and DS, it lies between 40 to 60 mV (except the first layer) and -30 to -50 mV respectively. It can be seen in both Fig. 4.10 and Fig. 4.11 that the zeta-potential of the first layer is lower than the other odd layers. The reason for this situation is likely to be the level of adsorption of the first layer is slightly less than the other layers, as the first layer the chitosan adsorbs onto the sluice directly, whilst in all other cases the chitosan adsorbs onto the dextran sulphate layers.

After coated 9-layer polyelectrolytes, the coated silica samples were also examined using the SEM tests (Fig. 4.12, Fig. 4.13) to compare with bare nanoparticles.

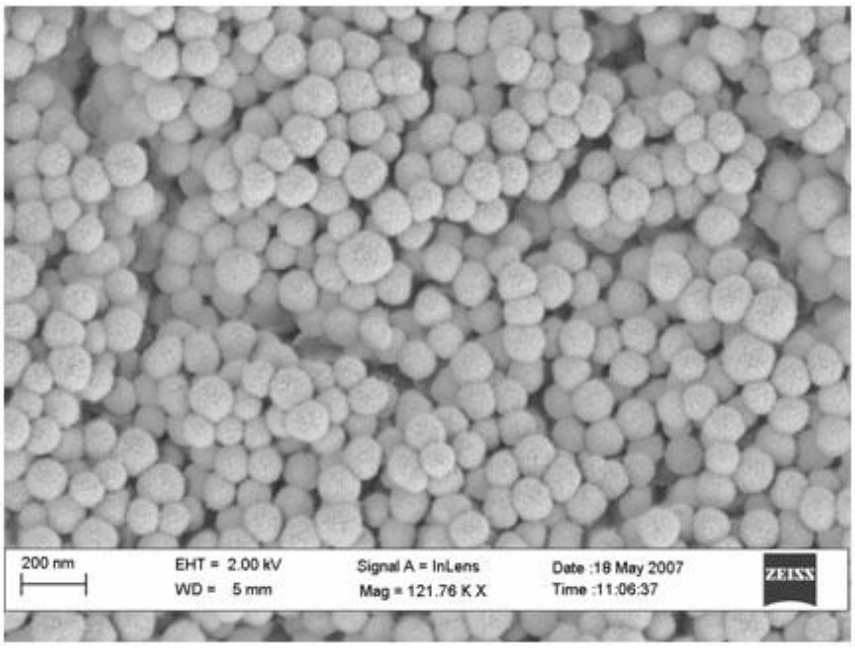


Fig. 4.12 SEM micrograph of silica nanoparticles 95 nm (from 1.4 ml NH_4OH/4 ml TEOS system) coated with 9 layers polyelectrolyte with a sequence: CHI/DS/CHI.

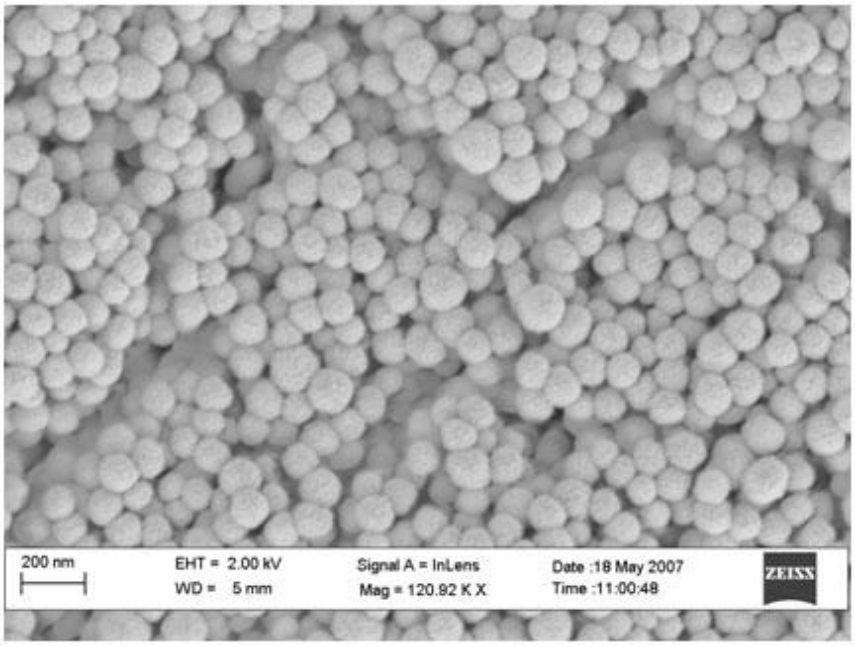


Fig. 4.13 SEM micrograph of silica nanoparticles 114 nm (from 1.6 ml NH_4OH/4 ml TEOS system) coated with 9 layers polyelectrolyte with a sequence: CHI/DS/CHI.

From Fig. 4.12 and Fig. 4.13, it is clearly seen the difference between the original (Fig. 4.4, Fig. 4.5) and the 9-layer coated silica nanoparticles. After 9-layer coating, Instead of being smooth, the surface of the particles became fluffy, this is likely to be due to the adsorbed polyelectrolyte layers.

4.3.3 Core Removal Process

To obtain the hollow capsules, the core materials should be removed after the fabrication of the nanocapsules. Since silica particles could be dissolved in HF, an HF/ NH_4F (2 M/8 M) buffer solution was adopted to try to control the dissolution process. Because for each layer deposition, some silica particles will be lost during the centrifugation process, it is hard to analyze the silica dissolving after the silica cores dissolved. Therefore, a simulation of dissolving the silica particles was employed to ensure the correct dissolution conditions were adopted. The original silica particle

solution contains 1.196 wt% of silica particles. The density of the solution is 1000 kg/m^3, so 1g of the solution contains 0.01196 g silica particles. The silica suspension was mixed with 1 ml HF/NH_4F buffer solution and the solution was kept in the fume cupboard for 2 hr. After dissolution, the mixture was diluted 10000 times and analysed in the ICP-OES. The data showed that over 90% of the silica (more than 90% of the silica present as an ion type in the solution) was dissolved. Therefore this condition was used to dissolve the core templates from the nanocapsules, the nanocapsules were then recovered and observed with both an SEM and TEM.

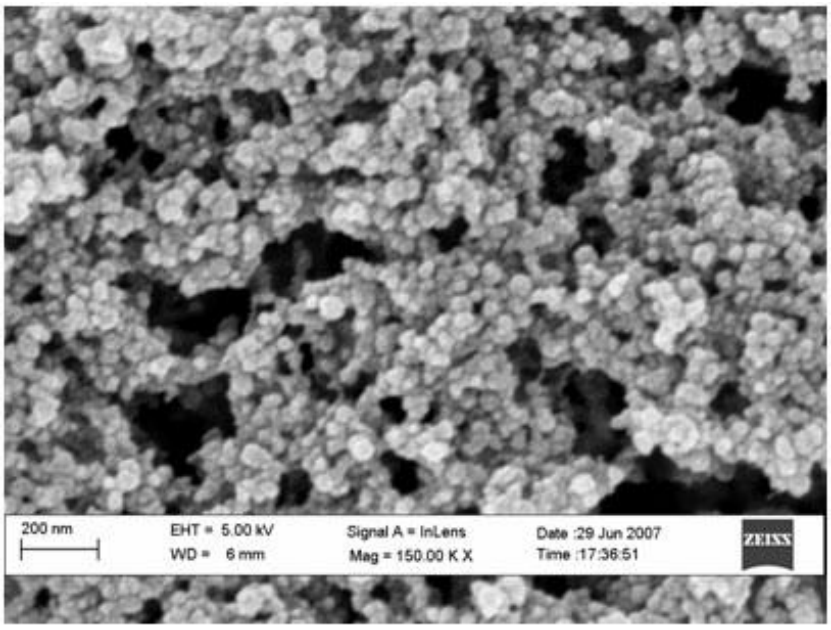


Fig. 4.14 SEM micrograph of nanocapsules consisted of CHI and DS, based on silica nanoparticles 95 nm (from 1.4 ml NH_4OH/4 ml TEOS system)

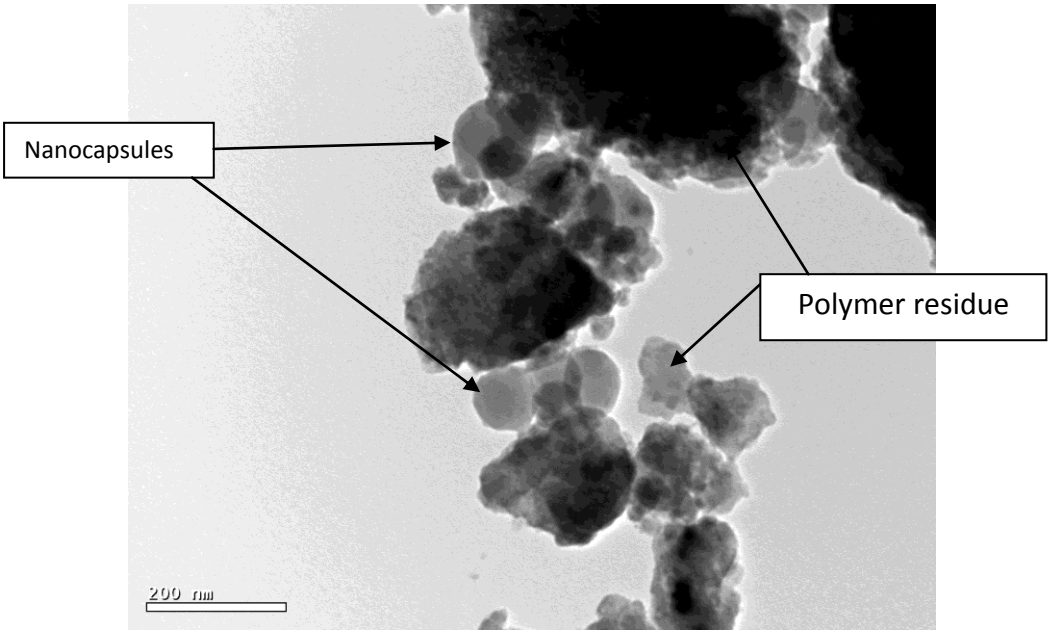


Fig. 4.15 TEM micrograph of nanocapsules consisted of CHI and DS, based on silica nanoparticles 95 nm (from 1.4 ml NH_4OH/4 ml TEOS system)

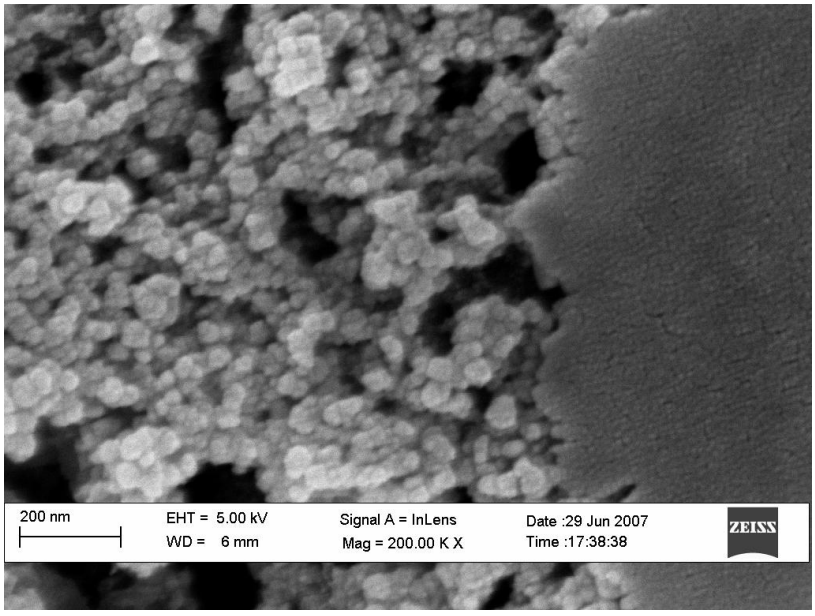


Fig. 4.16 SEM micrograph of nanocapsules consisted of CHI and DS, based on silica nanoparticles 114 nm (from 1.6 ml NH_4OH/4 ml TEOS system)

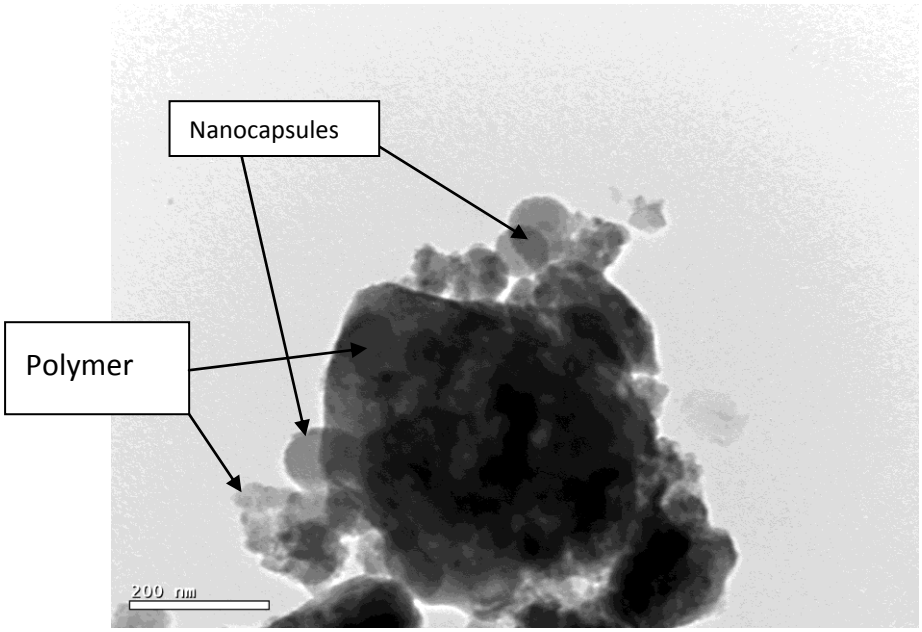


Fig. 4.17 TEM micrograph of nanocapsules consisted of CHI and DS, based on silica nanoparticles 114 nm (from 1.6 ml NH_4OH/4 ml TEOS system)

From Fig. 4.14 and Fig. 4.16, the particles cluster after the core removal process can be observed. Compared with Fig. 4.12 and Fig. 4.13, the nanocapsules arrayed in Fig. 4.14 and Fig. 4.16 appear aggregated. This may be due to the collapsing of some of the nanocapsules during the core removal process, and those polymer residuals attached to the rest nanocapsules to form the clusters in the SEM micrographs. The structure of polymer residuals attaching to the nanocapsules can also be seen in Fig. 4.15 and Fig. 4.17. From Fig. 4.15 and Fig. 4.17, many collapsed nanocapsules were found. Some of them aggregated together and formed a very thick layer of polyelectrolytes (the dark areas in both graphs), whereas the others formed very thin layer (probably single or double layers) of polyelectrolytes (the grey amorphous areas in both graphs). There are also some grey spherical areas in both pictures and they have similar contrast as the thin amorphous polyelectrolyte layer, which indicates they are also only composed of polyelectrolytes. The spherical shape and the contrast demonstrate that those spherical grey areas are intact hollow capsules (spotted in Fig. 4.15, Fig. 4.17). In Fig. 4.15 and Fig. 4.17, it can be observed that, except the ones at the edge of the dark area, which is the polymer residue, there are also many nanocapsules lying under the polymer residue.

Thus nanocapsules can be prepared by this method. However, because the HF is a very strong acid, many nanocapsules were broken during the core-removal process. It was very hard to separate the collapsed nanocapsules from the intact ones, so this result might not meet our needs for the further research. In addition HF is a dangerous acid and if such capsules are being contemplated for medical usage the use of HF is, to say the least, questionable. Therefore in the next Chapter the results for nanocapsules prepared using organic core templates will be presented and discussed.

4.4 Conclusion

In this Chapter the process of preparing nanocapsules derived from silica nanoparticles (size of 95 nm and 114 nm) was discussed. Silica nanoparticles were obtained via the hydrolysis of the alkoxysilane (TEOS) in a saturated alcoholic ammonia solution. In the reaction, the NH_4OH was the catalyst and the amount of NH_4OH confined the size of the silica nanoparticles. In this experiment, silica nanoparticles sizing from 95 nm to 250 nm were prepared by varying the amount of NH_4OH. Because the system was designed for drug delivery, two types of silica nanoparticles (95 nm and 114 nm) were chosen as the core templates and the Layer-by-Layer self-assembly method was applied to the silica cores with two oppositely charged polyelectrolytes: Chitosan and Dextran sulphate. The proper deposition time and salt concentration in the polyelectrolyte solution were also discussed. After the LbL process, the core-shell structures comprised of silica core templates and 9 layers of polyelectrolyte were finally obtained. Eventually, these two batches of coated silica nanoparticles were dissolved in the HF/NH_4F buffer solution and nanocapsules were acquired from both batches. However, due to the strong erosion of the HF, some of the nanocapsules collapsed during the core removal process, the productivity was relatively lower than expectation. This might be due to the very small size of the core templates can result in thin and weak nanocapsules which could not survive from the erosion. Also the extreme toxicity of the HF could be a serious problem when applying the nanocapsules for drug delivery purpose.

Therefore, in the following Chapters, a new core template: polystyrene nanoparticles, was employed.

Chapter 5 Nanocapsules Based on Large Polystyrene Core Templates

5.1 Materials

The chemicals involved in this experiment were: Styrene monomer (99%, Sigma Aldrich), potassium persulphate (Sigma Aldrich), poly(sodium 4-styrenesulfonate) (PSS) (70000 Da, Sigma Aldrich), Poly (diallydimethylammonium chloride) (PDADMAC) (20 wt% in water, 100,000-200,000 Da, Sigma-Aldrich) and Sodium Chloride (99.5% Sigma Aldrich), Chitosan (CHI) (50,000-190,000Da, 75-85% deacetylated, pKa 6-7), Dextran Sulfate Sodium Salt (DS) (approximate 10,000 Da, from Sigma-Aldrich), Laponite (Rockwood additives), Tetrahydrofuran (THF, ≥99%, Aldrich). All water used was deionised. Two Visking dialysis tubings (diameter 38.1 mm and 6.3 mm, MWCO-12-14000 Daltons) used here were obtained from the Medicell International Ltd.

Because of safety considerations, all the experiments which employed styrene monomer in this thesis were carried out in fume cupboard. For the operators, safety goggles and double layer gloves were worn and a colleague was asked to stand by in the lab in case of any emergency.

5.2 Methodology

5.2.1 Synthesis of Polystyrene Nanoparticles

The polymerization of styrene, to prepare mono-dispersed polystyrene particles followed the method described by Goodwin et al. [226-228]. The experimental procedure is described below. Initially, because there is 10-15 ppm of inhibitor 4-tert butylcatechol (an inhibitor for the polymerisation of styrene) contained in the styrene supplied, the inhibitor was removed by flushing the styrene monomer at atmospheric pressure through an inhibitor removal column (obtained from Sigma-Aldrich Chemicals, Enzyme Commission Number 215-691-6, MDL number MFCD00081548) (Fig. 5.1). The styrene after this stage was kept in the fridge at 4 ℃ for further use. The dispersion polymerisation took place in a 1L 3-neck round-bottom flask, an electric stirrer was placed in the middle inlet while the other 2 inlets were connected with a N_2 supply and a reflux condenser respectively (Fig. 5.2).

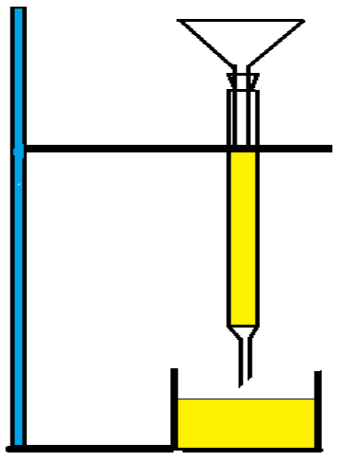


Fig. 5.1 Inhibitor removal column

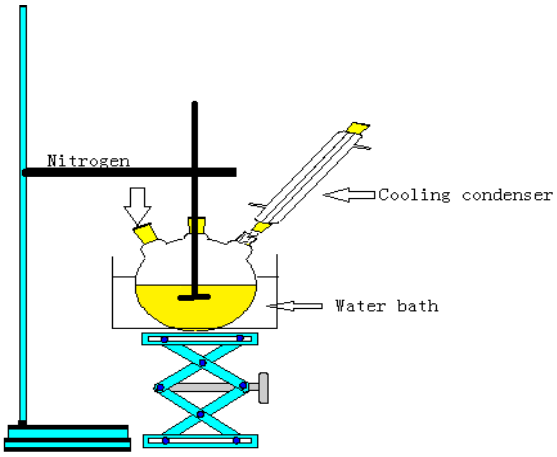


Fig. 5.2 3-neck Round-bottom reactor for polymerization

The whole system was confined to 600 ml. Firstly 0.48 mol (55 ml) styrene monomer and 0.47 g NaCl were added via the middle inlet into the flask, in the meantime, the deionised water was also added to make a system total volume of 500 ml. The N_2 valve was kept open when adding all the chemicals to quickly displace any oxygen from this system which would inhibit the polymerisation. The flask was immersed in a water bath set to 80 ℃. The stirrer was then fixed into the middle inlet of the flask and the solution was stirred at 350 rpm for 1hr to make sure all the reactants were properly mixed and to ensure the flask and its contents reached 80 ℃. Then 100 ml of an initiator solution (an aqueous potassium persulphate solution at a concentration of 1.332×10^{-2} mol/L) was added into the system. The stirrer speed was maintained at 350 rpm for a further 2 hr and then reduced to 130 rpm. Also after 2 hours the N_2 flow rate was reduced to a minimum to reduce any water evaporation from the flask. Finally the whole system was wrapped up with foil to minimise any water evaporation from the water bath which may occur overnight. The reaction lasted for 24 hr.

After the reaction had finished, the clear solution had become milky. The polystyrene particle suspension was cooled down to room temperature and decanted through a funnel, which was loaded with glass wool to remove any large lumps of polystyrene

from the liquid. The filtered suspension was then dialysed to remove any unreacted styrene monomer, NaCl, initiator and surfactant. The dialysis lasted for 4 weeks, and fresh deionised water was changed every 24 hr. Due to the empty space left while tying the tube up process, the final volume of the particle suspension was slightly different from the original reaction volume, which could be 5-10% larger by estimation. After the dialysis, the particle suspension was tested and the concentration of the polystyrene nanoparticles was found to be 2.5 wt%.

5.2.2 Layer-by-Layer Self-assembly Process

5.2.2.1 Polyelectrolyte

As well as the chitosan and dextran sulfate sodium salt, two other synthetic polymers were employed: negatively charged poly (sodium 4-styrenesulfonate) (PSS) and positively charged poly (dialyldimethyl ammonium chloride) (PDADMAC). Because polystyrene particles were negatively charged, PSS in the assembly process, acted as the even layers while PDADMAC as the odd layers. The PDADMAC and PSS solution contained: 1 mg/ml polyelectrolyte, 0.1 M NaCl; while the bio-compatible polymer solutions contained: 1 mg/ml polyelectrolyte and 0.1 M NaCl. However, chitosan, it could only be dissolved in an acidic condition, so the CHI solution also adjusted to pH 3 by HCl.

Laponite was used in this experiment as an alternative to a negative polyelectrolyte to strengthen the nanocapsules. Laponite is a synthetic silicate which resembles the natural smectite mineral hectorite, in both structure and composition [229]. Its molecular formula is $Si_8[Mg_{5.5}Li_{0.4}H_{4.0}O_{24.0}]^{0.7-}Na_{0.7}^{0.7+}$. The laponite particles were a commercial product obtained from Rockwood (Princeton, New Jersey), they are disk shaped (Fig. 5.3), approximately 25 nm in diameter and 1 nm thick. The disk itself is

strongly negatively charged on the flat face surfaces and has a weak positively charged on the edge (Fig. 5.3).

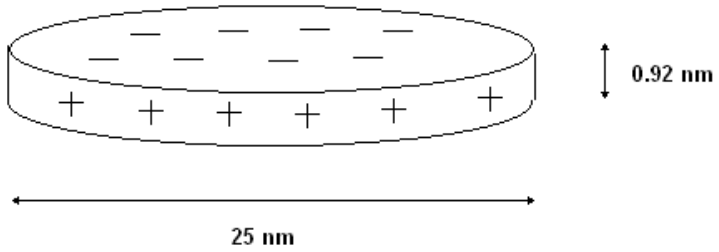


Fig. 5.3 Geometry of Laponite disk [230].

In water, the laponite will exist as particle suspension. Under different salt and laponite concentration this suspension will demonstrate quite different properties (Fig. 5.4) [231, 232].

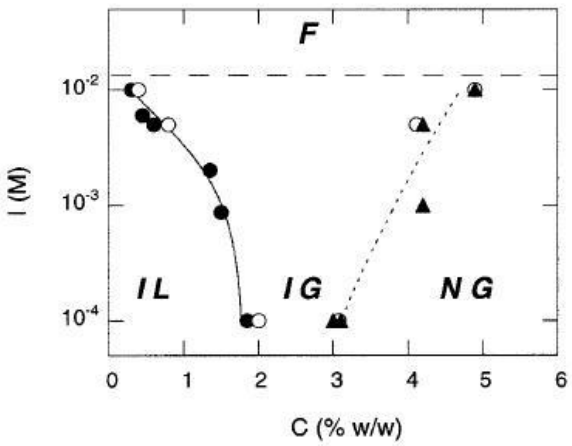


Fig. 5.4 Phase Diagram of Laponite suspensions [232]

F: Flocculation; IL: Isotropic Liquid; IG: Isotropic Gel; NG: Nematic Gel

(●)rheological data, (○) osmometric data, (▲) birefringence data

From Fig. 5.4, it can be seen that there are 4 distinct regions: F, where Flocculation

occurs; IL, where dispersion exist as an isotropic liquid; IG, where the dispersion exist as an isotropic gel; NG, where dispersion exist as a nematic gel. For the purpose of this research, it is clear that the laponite suspension should be kept within the IL region, in which the fluid exhibits Newtonian behaviour and the laponite disks are randomly dispersed in the suspension without any flocculation. In this experiment, the laponite particles (powder) were dispersed (by 2 min ultra-sonication) in deionised water and the concentration of the suspension was 10 mg/ml.

5.2.2.2 Layer-by-Layer Self-assembly

5.2.2.2.1 Nanocapsules Assembled with Synthetic Polyelectrolyte Only

Initially, the polystyrene particles with size range around 480 nm were used as core templates. For the first layer, 10 ml of 1 mg/ml PDADMAC solution, which contains 0.1 M NaCl, was added into the 5 ml polystyrene suspension (2.5%wt) with 10 ml deionised water. After 1 hr gentle shaking, the sample was centrifuged in an accuSpinTM 400 (obtained from Fisher Scientific).in a series of steps to separate the excess polymers from the coated particles: 3000 g for 5 minutes, 5472 g for 6 minutes, 8425 g for 8 minutes, and 8425 g for another 13 minutes. The reason why several centrifugation steps were applied here was to gather the particles with different size ranges at different centrifugal forces, so that aggregation can be avoided; this ensured that the re-dispersion time was shorter and the effect was better than a one-step separation method where high speeds and long times were used.

After centrifugation, all the particles were gathered and re-dispersed in 15 ml of deionised water. The re-dispersion was carried out in an ultra-sonic bath to break down the clusters of particles from the centrifugation by intensively shaking the suspension until the particle size fell down to 400-600 nm again. Such a cycle including

centrifugation/washing/re-dispersion was repeated 3 times for each coating layer. The deposition of subsequent PE layers was accomplished by repeating the same procedure.

5.2.2.2.2 Nanocapsules Assembled with Polyelectrolyte and Laponite

5.2.2.2.2.1 Synthetic Polyelectrolyte

Following the same procedure mentioned in the last paragraph, 3 polyelectrolyte (PE) layers which consist of PDADMAC/PSS/PDADMAC were firstly deposited onto the particles. After coating the polystyrene particles with 3 layers of PE layers, a layer of laponite followed by PDADMAC were added. However, it was found that the concentration of the particles was too high for the laponite deposition and the particles readily aggregated easily. Therefore, before coating with laponite, the polystyrene suspension was diluted 5 times to reduce the concentration to 20% of the original. Subsequent separation and re-dispersion cycle also followed the same manner as described above for PE layers. In this way one or more layers of laponite could be added into the walls of the nanocapsules.

5.2.2.2.2.2 Bio-compatible Polyelectrolyte

The nanocapsules based on the 480 nm polystyrene nanoparticles were also prepared with biocompatible polymers, CHI and DS. The deposition procedure of CHI and DS followed the one of PDADMAC layer; because polystyrene particles were negatively charged, the CHI was employed as odd layers while DS, on the even layers.

There was one difference of the capsule preparation procedure between the bio- and synthetic- polymer, which refers to the laponite layers. Instead of putting several layers of laponite, only one layer of laponite was added as the outer layer after the deposition of the polymer layers.

5.2.3 Core Removal

As an organic core template, polystyrene particles can be removed either by calcination or by dissolving in a solvent [1]. In this case however, because the capsule itself was made from organic material, the capsule wall cannot survive the very high temperature of the calcination, thus tetrahydrofuran (THF, ≥99%, Aldrich) was used to dissolve the polystyrene core (THF was used as it is a good solvent for polystyrene and is miscible in all proportions with water). Each of the coated particle suspensions was mixed with twice volume of pure THF, and the mixture was kept sealed in the fume cupboard for 48 hr. After dissolution, in order to remove the THF and polystyrene residue, the solution was dialysed against de-ionised water. The solution of the mixture was moved to dialysis tubing (6.3 mm) and both ends of the tubing were then tied up. The loaded tubing was then placed into a beaker of 1 L deionised water and the water was changed every 12 hr for 7 days.

5.3 Results and Discussion

5.3.1. Polystyrene Core Particles

5.3.1.1 Synthesis without Surfactant

DLS using the 90Plus Size Analyzer determined the particle size distribution to be 483±31 nm. Fig. 5.5 shows SEM micrographs of the particles which confirms this size. Fig. 5.5 also shows that the particles are largely mono dispersed, although there are some much smaller particles visible. A determination of the polystyrene weight percentage was also carried out. 10 ml of the polystyrene suspension was placed in a pre-dried Petri dish and kept in a high temperature oven for 48 hr. The weight of the aqueous suspension and the dried out residue were recorded as 2.5 wt%.

The zeta-potential of the surface of the core particle was also measured by the ZetaPALS. The result showed the zeta-potential of the polystyrene particles is -48±3 mV.

(a) (b)

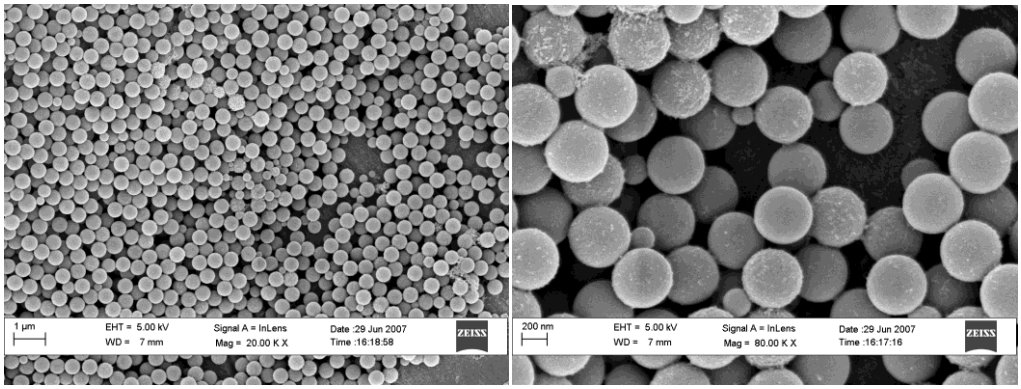


Fig. 5.5 SEM micrographs of the polystyrene particles with different magnifications

5.3.2 Layer-by-Layer Self-assembly

5.3.2.1 Parameters Affected the Experiment

Parameters, such as the salt concentration, the deposition time, were tested and determined in order to optimize the LBL deposition process. In the following sections we will focus on the effect of these parameters.

5.3.2.1.1 The Deposition Time

For the synthetic polymers, the deposition time of the first layer of PDADMAC was examined, and the results are presented in Table 5.1.

Table 5.1 Zeta-potential of the particles after coating 1 mg/ml PDADMAC for different time

Coating time	20 min	24 hr	72 hr
Zeta-potential (mV)	$+46 \pm 2$	$+46 \pm 3$	Aggregated

The results showed that under gentle shaking for 20 min or 24 hr, there was no obvious change of the zeta-potential of the first polyelectrolyte layer. That indicated 20min or more is enough for finishing the polymer layer deposition. However, if this deposition lasted for too long, e.g. 72 hr (Table 5.1), some aggregation was found to occur in the particle suspension. That may be due to the extra polymer causing bridging flocculation or bare patch flocculation [1]. Subsequently, to make sure the polyelectrolyte deposition had finished and the polymer was properly arranged on the surface of the particles, 1 hr was chosen as the time allowed for PDADMAC deposition.

For the bio-compatible polymers CHI + DS, the optimum time had already been determined on silica particles as 1hr. Therefore 1hr was also the time chosen for adsorption of CHI + DS onto polystyrene particles.

5.3.2.1.2 Salt Concentration

The NaCl concentration of the polyelectrolyte solution is also an important factor to affect the properties of each layer. As has been mentioned in the literature review, sodium chloride was introduced into the experiment to reduce the repulsion between polymer molecules. The sodium salt here acted as an agent to screen some of the charges on the surface of the polymer molecules, and decreased the repulsion between the same charged polymers. This effect would increase the polymer deposition and lead to thicker polymer layers. However, higher salt concentration would also result in a

lower zeta-potential of the coated particles. In this experiment, 3 different salt concentrations (0.0 M, 0.1 M and 0.5 M) were tested, based on polymer layers (PDADMAC/DS/PDADMAC) to determine the optimum salt concentration (Fig. 5.6).

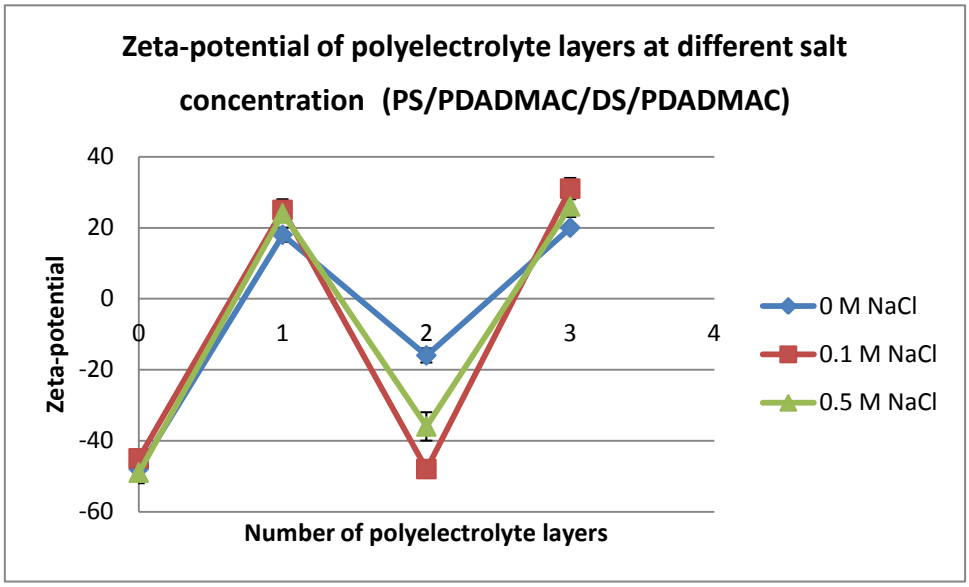


Fig. 5.6 Zeta-potential of the polymer layers (polystyrene/PDADMAC/DS/PDADMAC) at different salt concentration.

The values are given in Appendix Table A.3.

From Fig. 5.6, it can be clearly seen that there is an effect of salt concentration on the zeta-potential of the polymer layers. For the same polymer layer, the value of the zeta-potential follows the order: 0.1 M>0.5 M>0 M; this phenomenon was much more obvious in the second layer which consisted of DS, Therefore, 0.1 M Sodium Chloride was chosen to prepare the polyelectrolyte solution and conduct the adsorption experiments.

5.3.2.2 Preparation of the Nanocapsules

5.3.2.2.1 Synthetic Polymers without Laponite

5.3.2.2.1.1 Fabrication of the Nanocapsules

Zeta-potential measurement was one way to determine each layer's deposition during the preparation process. Fig. 5.7 shows the variation of the zeta-potential of each coating layer of the experiment of 5 bilayers of PDADMAC/PSS depositing onto PS particles (1 mg/ml PE and 0.1 M NaCl). Because each component was charged and the main interaction in this research was an electrostatic interaction, after each layer's deposition, the zeta- potential shifts from the original to the opposite direction. In this graph, as expected, the zeta-potential varied between negative and positive, which confirmed the deposition of each sequential polyelectrolyte layer.

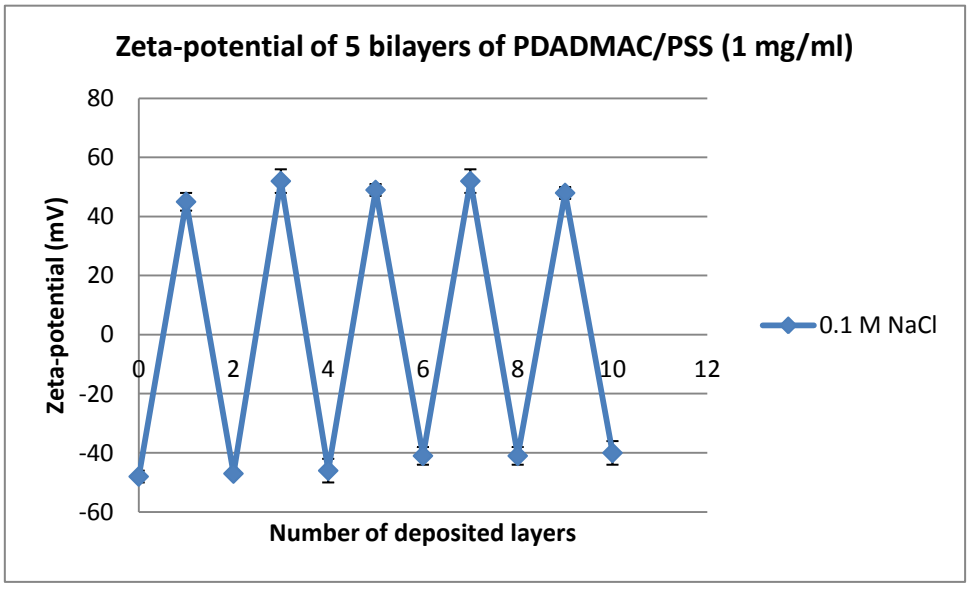


Fig. 5.7 The zeta-potential of the each coating layer ($(PDADAMAC/PSS)_5$ 1 mg/ml PE, 0.1 M NaCl).

The value of each layer's zeta-potential is given in the Appendix Table A.4.

From Fig. 5.7, it can be seen that the absolute values of zeta-potential of odd and even layers are larger than 40 mV, which meant that the deposition of each layer was complete and the coated particles were in a relatively stable state during each coating process. Also it can be found that the absolute value of the zeta-potential was tending to be smaller after each layer-coating. That explained why the coated particles occasionally became aggregated after around 12 layers. The coated particles were also examined under an SEM to monitor the coating and re-dispersion situation.

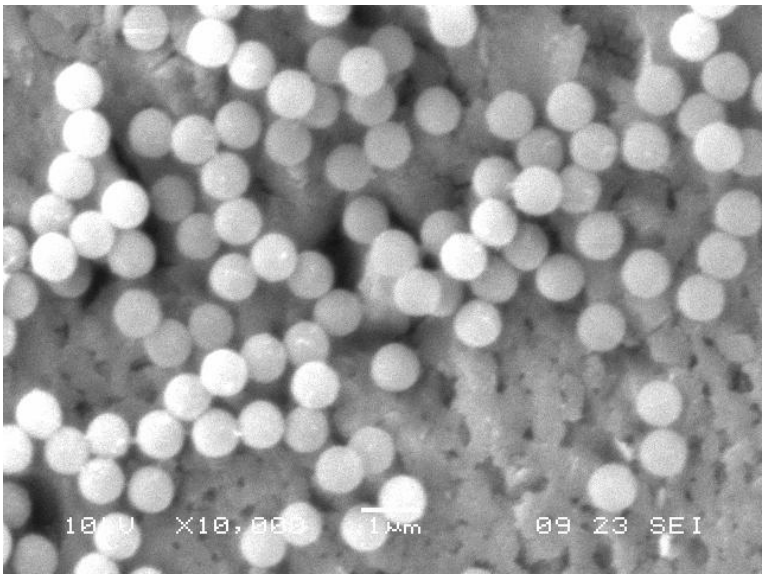
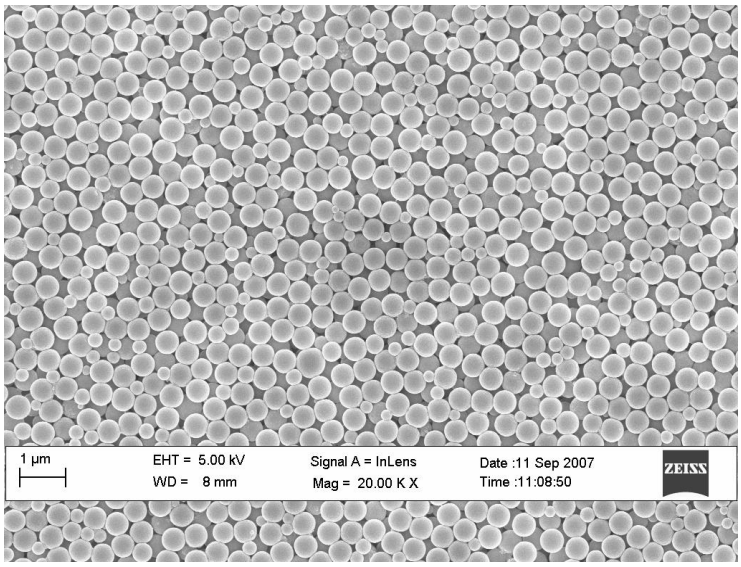


Fig. 5.8 SEM micrograph of 10 layers (5 PDADMAC/PSS bi-layers) coated polystyrene particles

It is clearly demonstrated in Fig. 5.8 that after coating with 10 layers of polymers, the coated particles were still well dispersed in the solution, and exhibited no obvious bulk aggregation. However, from Fig. 5.8, it can be observed that the particles were not as spherical as the original ones (Fig. 5.5) and there were some thread structures around the particles. The change of shape of the particles can be attributed to the fabrication of the 10 layers of polymers, and the thread materials is likely to be some residual polyelectrolyte dried from the solution.

In this project, laponite was also used as a capsule material to strengthen the capsules themselves. However, In order to create a particle surface with homogeneous charge density and to avoid ill-structured polyelectrolyte multilayer assembled, where the film roughness was too high compared with the film thickness [233], it was generally suggested that three layers of polyelectrolyte are required before the deposition of any inorganic nanoparticles such as silica and TiO_2 [104]. As was mentioned in the methodology section, three layers of synthetic polyelectrolyte consisting of PDADMAC/PSS/PDADMAC were deposited before the laponite particles. The SEM micrographs of these pre-deposited particles are illustrated in Fig. 5.9.

(a)



(b)

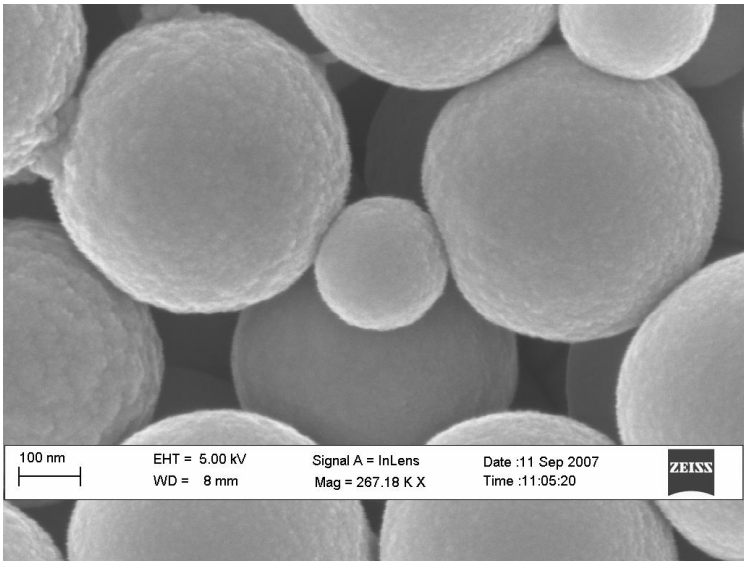


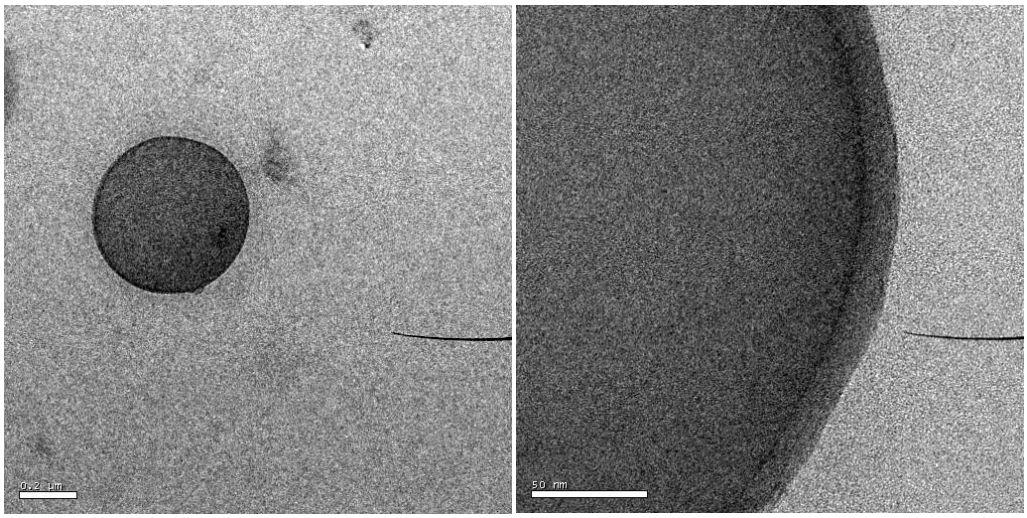
Fig. 5.9 SEM micrographs of different magnifications of particles composed of 3 layers (PDADMAC/PSS/PDADMAC)

From Fig. 5.9, it is clearly seen that compared with the original PS particles (Fig. 5.5), these three layers coated particles are more 'fluffy', but the whole surface of each single particle seems homogeneous, however, these particles still kept within the size range 400-500 nm, as one may expect.

5.3.2.2.1.2 Core Removal

After coating with 10 layers (5 PDADMAC/PSS bi-layers) of synthetic polymers, the coated particles were treated with THF to remove the core material (Fig. 5.10).

(a) (b)



(c)

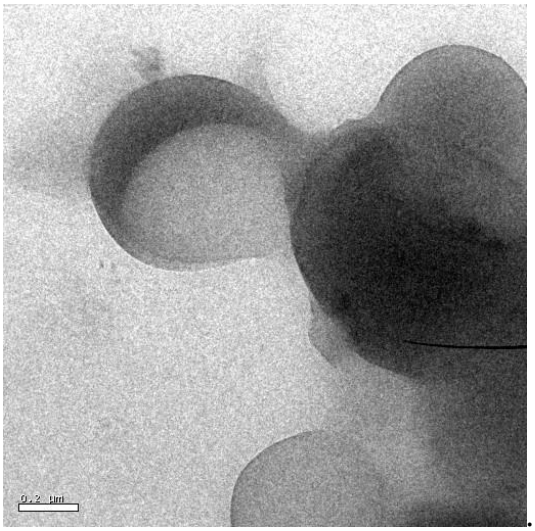


Fig. 5.10 TEM micrographs of the polystyrene particles with 10 layers after 24 hours of core removal

From Fig. 5.10, the result of the core removal process to form nanocapsules can be seen. Fig. 5.10 a and b are micrographs of one single particle shown at different

magnifications. Fig. 5.10 b clearly shows the inner structure of this single capsule. By contrast, it can be clearly seen that the capsule itself has a wall about 10-15 nm thick and the hollow shell structure illustrated the successful removal of the polystyrene particle. Fig. 5.10 c is a cluster nanocapsules. There is a shadow area at the edge of the particle which stands in the middle of the micrograph. This shadow is likely to be formed by some polystyrene residues, however, the other particles compared with this one were relatively monotonic in colour, which illustrates that after the core-removal process, most of the polystyrene were removed from the hollow shell structure. However, it is clearly seen that the cluster of the particles were several nanocapsules overlapped together, and that some of the capsules were collapsed. It is not clear whether the clustering was due to the capsules being flocculated or whether this clustering occurred during the drying of the capsules. The collapsing of the capsules suggests that the nanocapsules were not strong enough to survive as spherical capsules after core removal with THF. This is the main reason why laponite nanoparticles were introduced as a capsule material to prevent the collapsing of the walls of the capsules.

5.3.2.2.2 Synthetic Polymers in Presence of Laponite

5.3.2.2.2.1 The Precursor Polyelectrolyte Film

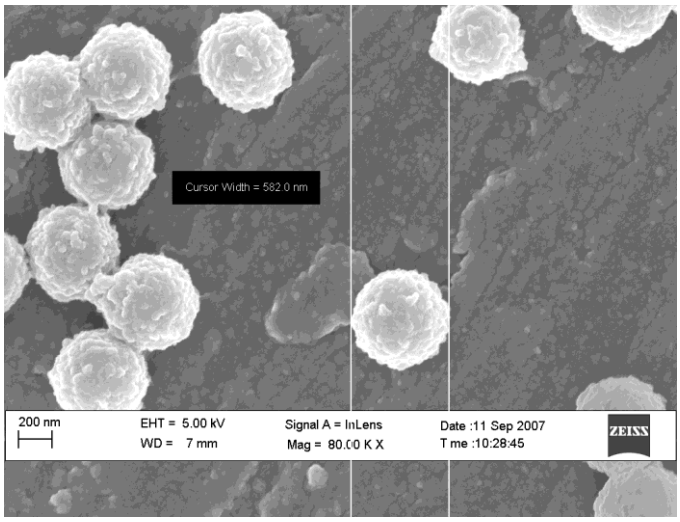
As was described in section 5.3.2.2.1.1**,** the precursor particles (coated with 3 layers of polyelectrolyte) were prepared following the same deposition method used for the nanocapsules consisting of polyelectrolyte only.

5.3.2.2.2.2 Fabrication of the Rest Layers (Laponite /PDADMAC)

After the preparation of the polyelectrolyte precursor films, laponite and PDADMAC were added onto the polystyrene particles respectively. As Caruso et al. (1999) reported, 3 or 4 layers of polyelectrolyte precursors could not only make the particle surfaces uniformly charge to facilitate subsequent deposition of protein or other

alternative materials, but also can change the surface charge (from positive to negative and vice verse) for adsorption of some specific materials [170, 172]. Therefore, for the deposition of the laponite particles (inorganic nanoparticles), 3 layers of PE were used as deposition precursor. Since laponite particles were negatively charged in the water solution, laponite was used to form the even layers while PDADMAC formed the odd layers. Fig. 5.11 demonstrated the SEM micrographs of the 8 (3 laponite layers) and 13 (5 laponite layers) layers coated polystyrene particles.

(a)



(b)

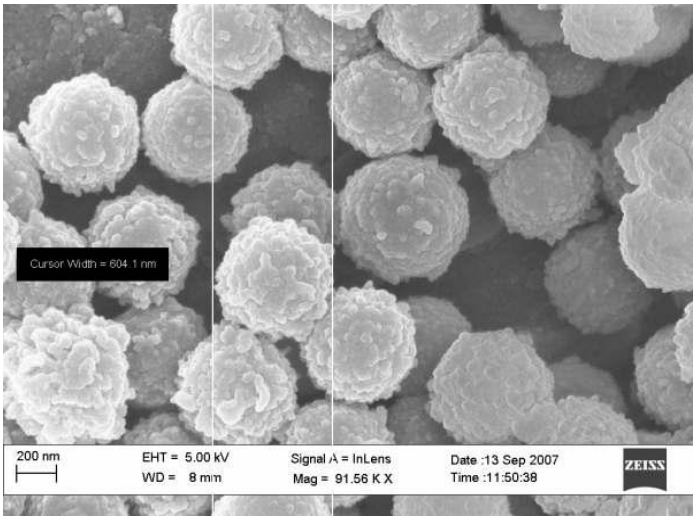


Fig. 5.11 SEM micrographs of the particles composed of (a) 8 coating layers (3 Laponite layers), (b) 13 coating layers (5 Laponite layers)

In Fig. 5.11, it was clear that the surfaces of the 8-layer (a) and 13-layer (b) coated particles are much rougher compared with polyelectrolyte coated ones (Fig. 5.9). Considering the shape of the laponite particles which is disk like, it was not surprising to find such a surface structure. However, there was no obvious difference between the 8-layer sample and the 13-layer sample, which also indicated that the deposition of

Laponite particles introduced the roughness no matter what the outer layer was. From Fig. 5.11, it can be seen the size of 3, 8, and 13-layer sample was increasing steadily from 499 nm to 582 nm and finally reached to 604 nm, clearly demonstrating the deposition of polyelectrolyte and Laponite layers.

Fig. 5.12 showed the shifting of the zeta-potential of each coating layer. As it was mentioned before, the shift of the zeta-potential confirms each layer's deposition.

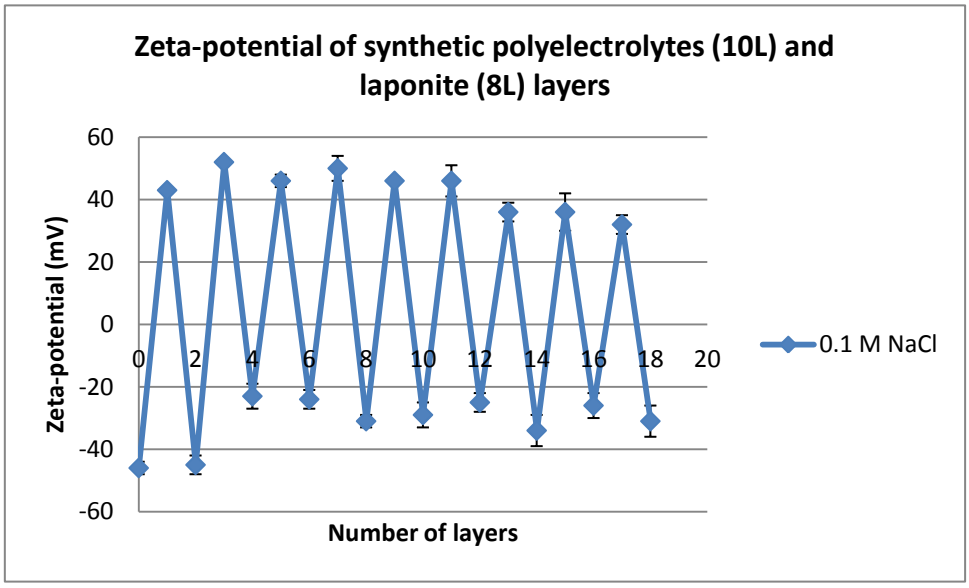


Fig. 5.12 The zeta-potential of the each coating layer (synthetic polyelectrolyte and Laponite).

The value of each layer's zeta-potential is given in the Appendix Table A.5.

From Fig. 5.12, the values of the zeta-potential can be divided by 2 parts. Part I is the region that only contained the 3 layers of precursor PE. The absolute values of these layers (above 40 mV) indicated a proper adsorption. In this part, the zeta-potential of the third layer (52.4 mV) was relatively higher than it of the first layer, which might be because of the reason explained in the section 5.3.2.2.1.1 and 5.3.2.2.2.2. At least 3 layers of PE precursor can provide the particles with a uniformly charged surface [170,

172]. Also in Buron et al. and Dejeu et al.'s works [234, 235] indicated that it is necessary to employ some polyelectrolyte layers as a precursor before laponite or any other alternatives to polyelectrolytes. This precursor can on one hand provided a uniform and smooth surface for the further deposition, and on the other hand can enhance the zeta-potential of the exposed layer and made the next deposition more stable.

Part II shows the process of the alternative deposition of the laponite and PDADMAC layer. Up to the 12th layer, all the zeta-potential were (above 40 mV) for the PDADMAC layers, which were very stable and very similar to the values of the first and third layers. However, compared with the PSS layers, the zeta-potential of the laponite layers were somewhat lower i.e. less negative (-30 mV). This difference was due to the structures of the PSS and Laponite. PSS was fully negatively charged molecules and Laponite was disk-shaped particle and was negatively charged on both flat surfaces and positively charged at the edge. Therefore, it was hard for 2 Laponite particles to pack as close as 2 PSS molecules on a polystyrene particle surface, and so the even layers after the 2^{nd} layer were more weakly charged. Also charge density of laponite particles may be less.

It is noticeable in the second region, after the 12^{th} layer, the values of the PDADMAC layers were decreased (from 45 mV to 35 mV). This might due to the accumulation the laponite layers disrupted the smooth nature of the particles causing roughness and shifting the plane of shear of the zeta-potential from the particle surface. In that case, the PDADMAC layer may also not fully cover the surface, which reduced the absolute value of the zeta-potential, furthermore covered and uncovered areas of different particles would attracted each other and aggregation would occur as was seen after 18 layers (7 layers of Laponite) coating (Fig. 5.13).

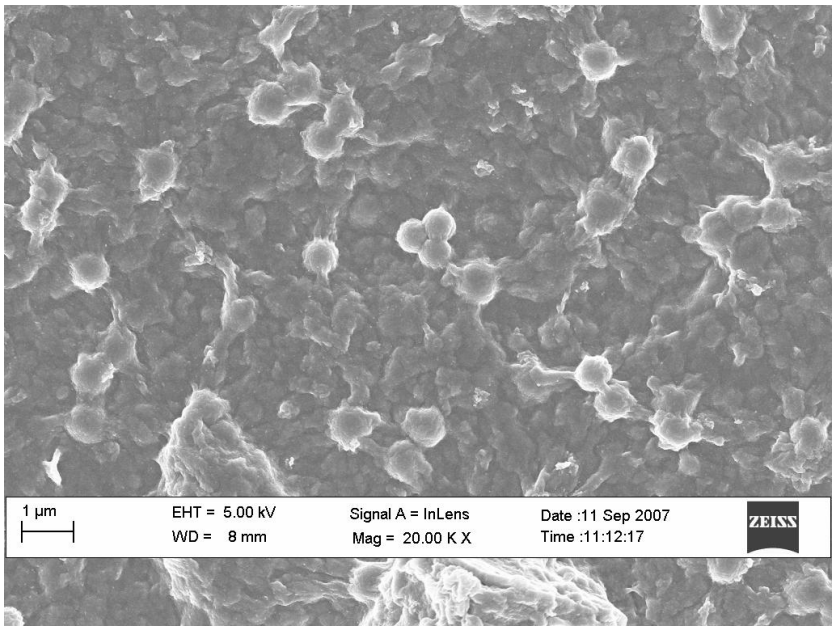
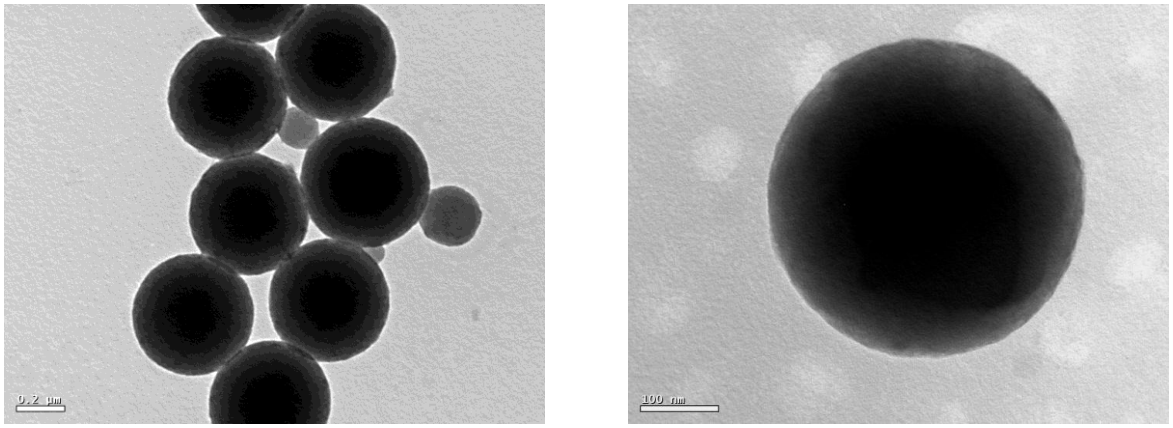


Fig. 5.13 SEM micrographs of the particles coated with 18 layers (PDADMAC/PSS/laponite) (10 PE/8 laponite)

5.3.2.2.2.3 Core Removal

After the layer-by-layer self-assembly process, it was necessary to remove the PS cores. A solvent capable of dissolving PS and which is miscible with water is required. In this case, only THF and 1, 4-Dioxane met the requirement. Since THF is much cheaper, it was employed to remove the polystyrene nanoparticle core. Fig. 5.14 shows the TEM micrographs of before and after the THF treatment of the 5 layers coated polystyrene particles.

(a) (b)



(c) (d)

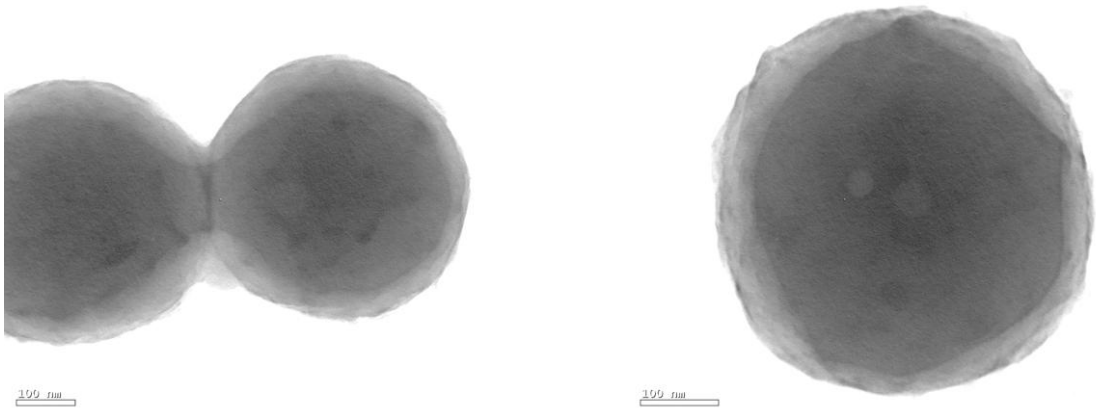
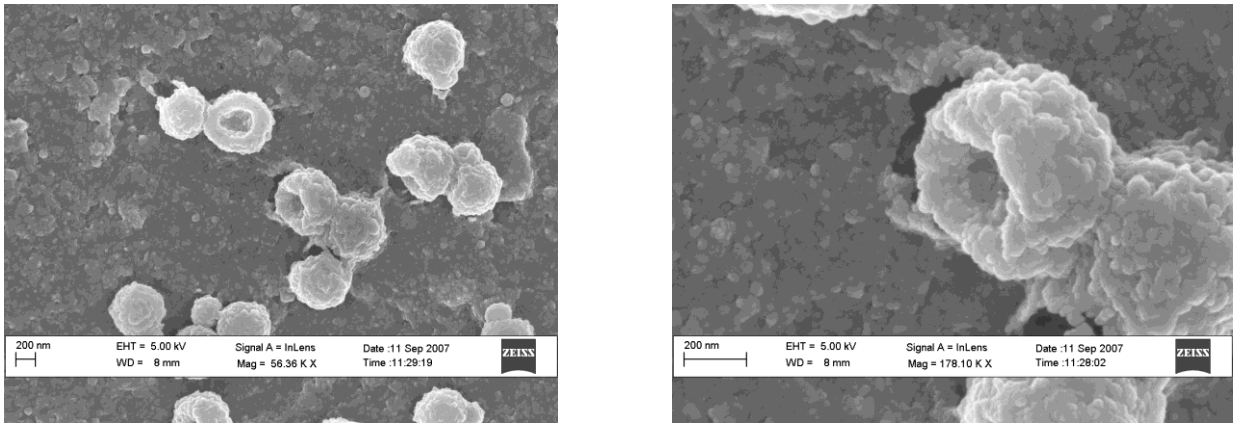


Fig. 5.14 TEM micrographs of nanocapsules consisting of 5 layers of polyelectrolyte and Laponite before (a,b) and after (c,d) the THF dissolving.

The difference between the coated polystyrene particles and the hollow shells after the core removal process can be clearly seen in these transmission electron micrographs (TEM). In Fig. 5.14 a and b, the inner part is darker and represents the solid polystyrene particles and the bright part was the outer layers as here the material is thinner. After the core removal (c, d), the inner part was no long as dark as it was in micrographs a and b. Only a few dark particles can be seen in the micrographs, probably due to some un-removed polystyrene. This situation might be because the polystyrene particles are comprised of high molecular weight polymers which are hard to completely.

(a) (b)



(c) (d)

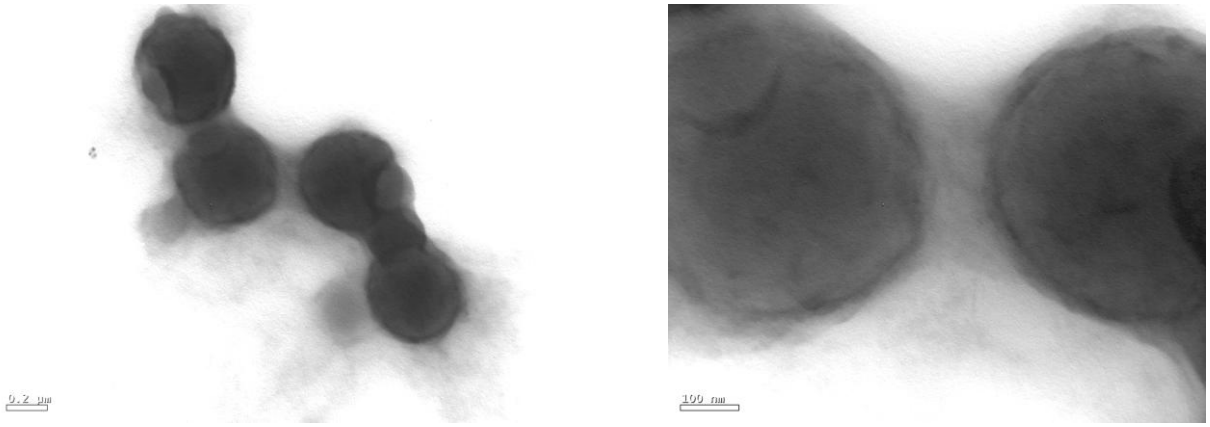


Fig. 5.15 TEM and SEM micrographs nanocapsules consisting of 8 layers (5PE/3Laponite) after the core removal process, (a) (b) SEM and (c) (d) TEM

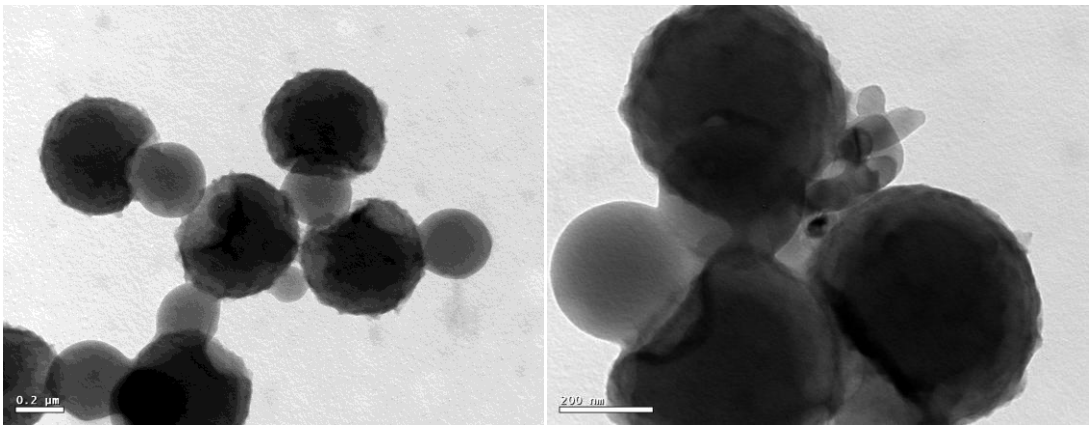
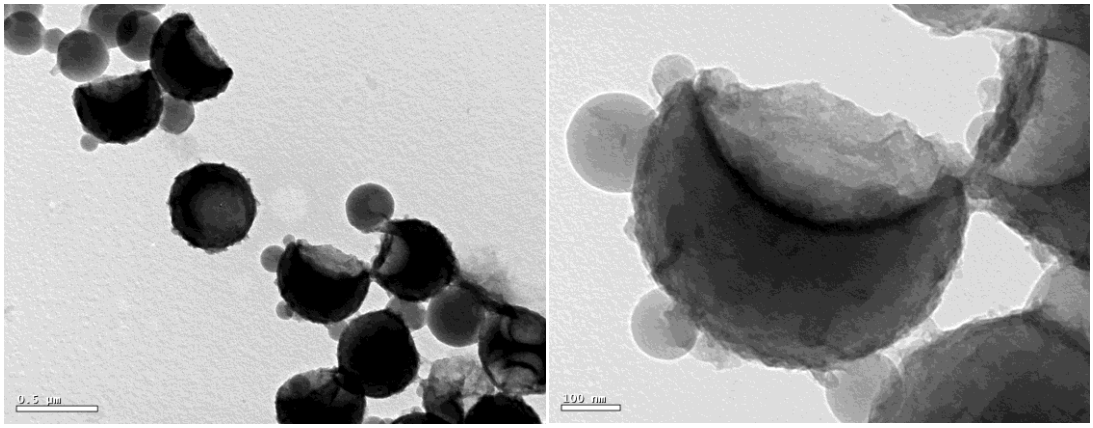


Fig. 5.16 TEM micrographs of the nanocapsules consisting of 9 layers of polyelectrolyte and Laponite (6PE/3Laponite) after the core removal process

(a) (b)



(c) (d)

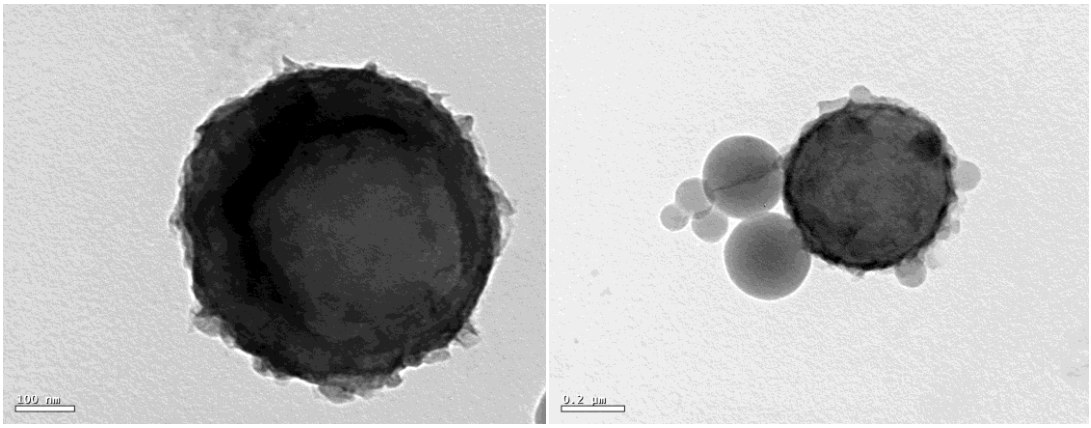
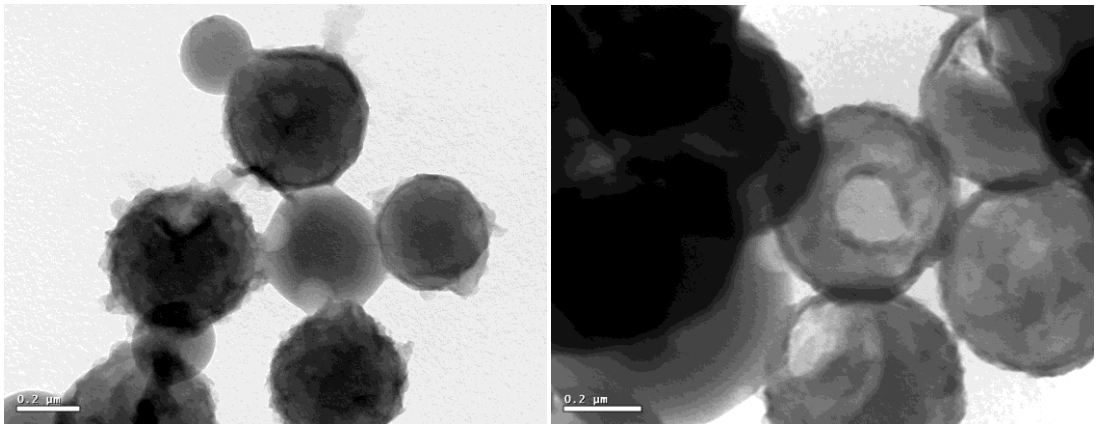


Fig. 5.17 TEM micrographs of the nanocapsules consisting of 12 layers of polyelectrolyte and Laponite (7PE/5Laponite) after the core removal process

(a) (b)



(c)

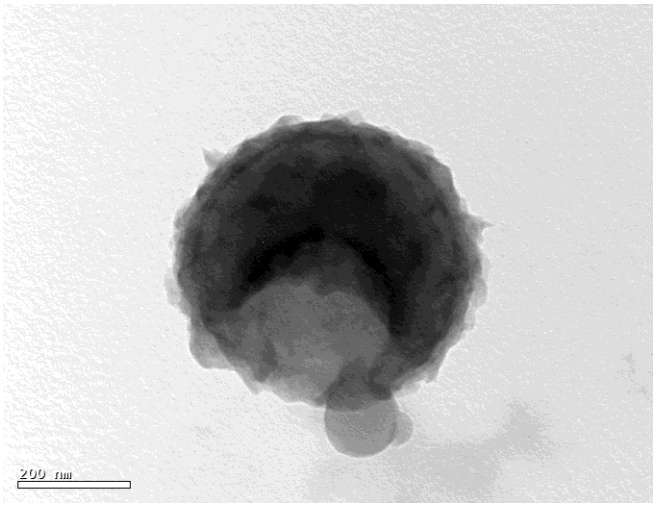


Fig. 5.18 TEM micrographs of nanocapsules consisting of 13 layers of polyelectrolyte and Laponite (8PE/5Laponite) after the core removal process

Fig. 5.15-Fig. 5.18 show micrographs with different number of laponite layers (8, 9, 12 and 13 layers). According to the micrographs, there is no obvious difference between the coated particles terminated with a laponite layer or the ones terminated with a polyelectrolyte layer. This suggests that the component of the outer layer would not affect the structure of the hollow capsules. Another phenomenon can be easily noticed from Fig. 5.15-Fig. 5.18 is that after the core removal treatment, some of the capsules collapsed and formed the "Cup-shape" structure. From the hollow and half-opened

structure, the removal of the polystyrene particles was confirmed. Beside the capsules, some polystyrene particles with much smaller size can be observed. The surface of these particles is smooth which seems there was not much PE or Laponite deposited. There may be two reasons for the appearance of these particles, one is the original particles just with smaller size (due to insufficient mixing, the particles did not have full exposure to the PE or laponite solution) and the other one is after core removal the polystyrene residuals escaped from the capsules. However, compared with Fig. 5.15-Fig. 5.18, fewer particles (the smaller and smoother ones) are observed in Fig. 5.14. During the core removal process, the solvent THF would diffuse through the preformed capsule walls and enter the inside of the nanocapsules. In this process, when accessed the THF the polystyrene particles would swell and become a little larger before dissolution. The swelling action of the polystyrene cores could deform the capsules attached to them. In Fig. 5.14, the capsules were consisting of only one Laponite layer, which makes the capsule themselves are more flexible than the ones in Fig. 5.15-Fig. 5.18 which contain more Laponite layers. In this case, during the swelling of the core templates, the more rigid capsules would possibly collapse more easily and the partially dissolved particles could easily escape to the solution. This also explained the phenomenon that much more cup-shaped hollow capsules were spotted in Fig. 5.15-Fig. 5.18 compared with Fig. 5.14. Also considering the Fig. 5.11, most of the particles presented the fluffy structure, so there was less opportunity for the appearance of the uncovered/incompletely covered polystyrene particles after the LbL coating process. Hence, in this case, the second explanation of the smaller and smoother particles seems more plausible.

Overall, considering all the results and discussion in the core removal section, it may be concluded that the capsules without any laponite layers would be not strong enough to survival the core dissolving process, whereas, as for capsules consisting of several layers of laponite, the thickness and the strength can possibly be a barrier for the small

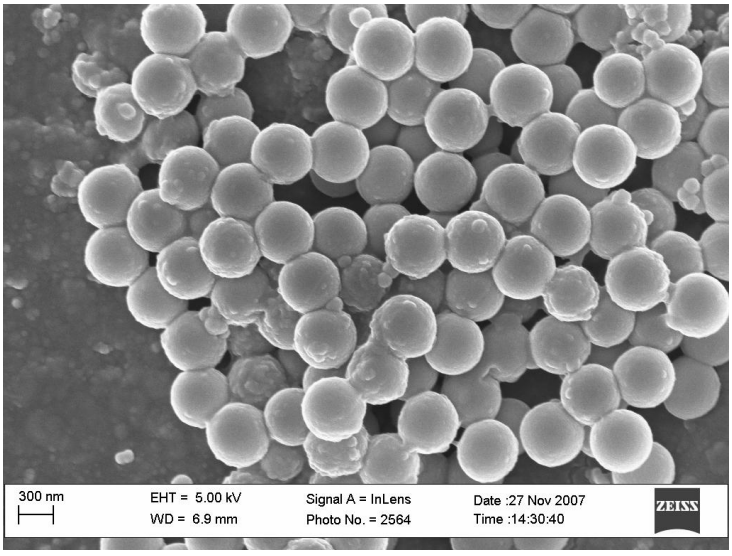
polystyrene particles to diffuse out of the capsules and led the capsule collapsed. So in the following experiments, only one layer of laponite was employed.

5.3.2.2.3 Bio-compatible Polyelectrolyte

5.3.2.2.3.1 Preparation of the Nanocapsules

After the fabrication of the nano-capsules consisting of the bio-compatible polymers, 10 layers (5 CHI/DS bi-layer) of polymer were deposited onto the polystyrene particles (Fig. 5.19). Then these particles were coated with another bi-layer (CHI/Laponite), which made the outer layer of these particles was Laponite (Fig. 5.20).

(a)



(b)

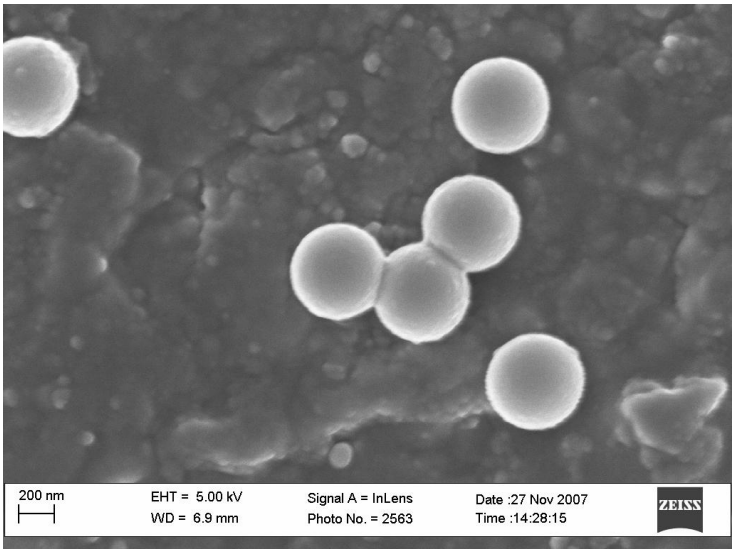
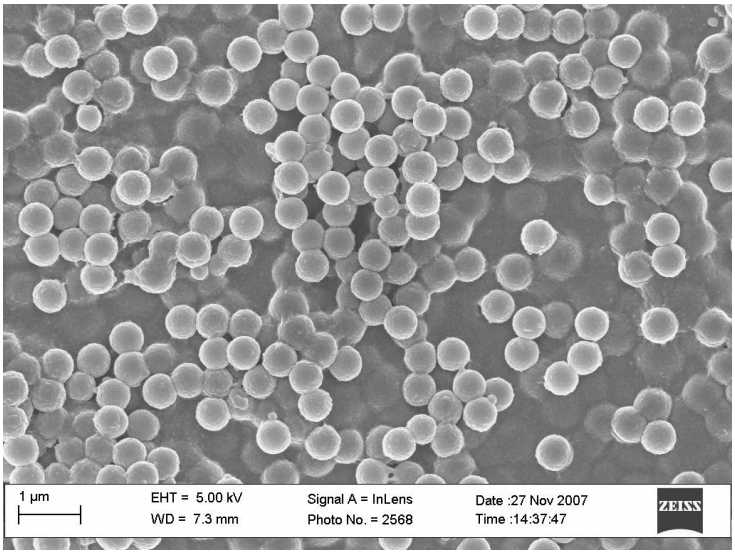


Fig. 5.19 SEM micrographs (at different magnification) of polystyrene particles coated with 10 layers of biocompatible polymers

(a)



(b)

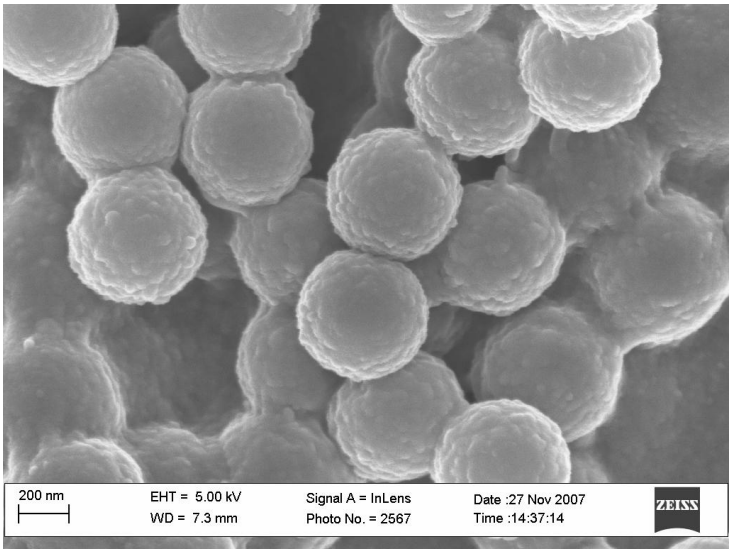


Fig. 5.20 SEM micrographs of polystyrene particles coated with 11 layers of biocompatible polymers and one layer (outer layer) of Laponite particles, a) b) represent different magnifications

From Fig. 5.19 and Fig. 5.20, it can be clearly seen that after the coating process, all the coated particles were well re-dispersed in the suspensions and all the particles shared similar appearance which confirmed all the particles were fairly coated. In Fig. 5.20 the surface of the particles is rougher than it is in Fig. 5.19. This is because the outer layer in Fig. 5.20 is laponite while it is dextran sulphate in Fig. 5.19. Also it can be seen that in Fig. 5.19 there are some small lumps which might be capsule polymer residues attached to some particles, while in Fig. 5.20, they can be barely seen. That phenomenon illustrated that the laponite layer not only strengthened the capsules but also modify the shapes of the coated particles which might support the capsules surviving from the dissolving in THF.

The deposition of the polymers was also confirmed by the zeta-potential measurement of each coating layer (Fig. 5.21).

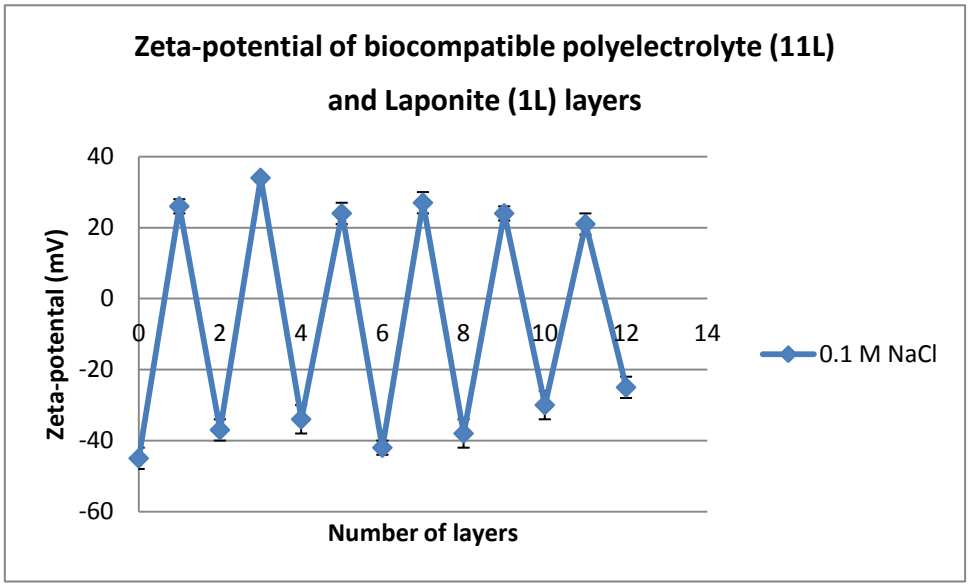


Fig. 5.21 The zeta-potential of the each coating layer (biocompatible polymers and outer layer Laponite).

The value of each layer's zeta-potential is given in the Appendix Table A.6.

Because the original particles and DS were negatively charged, and CHI was positively charged, the value of odd layers should stay positive while for the even layers the value should be negative. From Fig. 5.21, this point had been confirmed. Also from the trend of the zeta-potential, it can be noticed that the more layers coated onto the particles, the closer the zeta-potential was getting closer to zero. This might because there were mutual effects (electrical and steric) between different layers, and those effects can affect the outer layer to be thinner (compared with the former ones) or even not completely covered the whole particle surface, so the absolute value of the zeta-potential was becoming smaller. In that case, it was more complicated for further layer to deposit, and also the lower zeta-potential can result aggregation easily at some stage of the experiment like the centrifugal part. So this experiment, 10-12 layers of biocompatible polymers would be a proper structure for the nano-capsules. It is also noticed that compared with the synthetic polymers the zeta-potential of the biocompatible polymer layers was relatively lower (-40 mV to +30 mV). This can be

explained by the hardness of dissolving the CHI powder to make homogeneous solution.

5.3.2.2.3.2 Core Removal

After the preparation of the nanocapsules, the coated particles were treated with THF to dissolve the polystyrene core templates.

(a) (b)

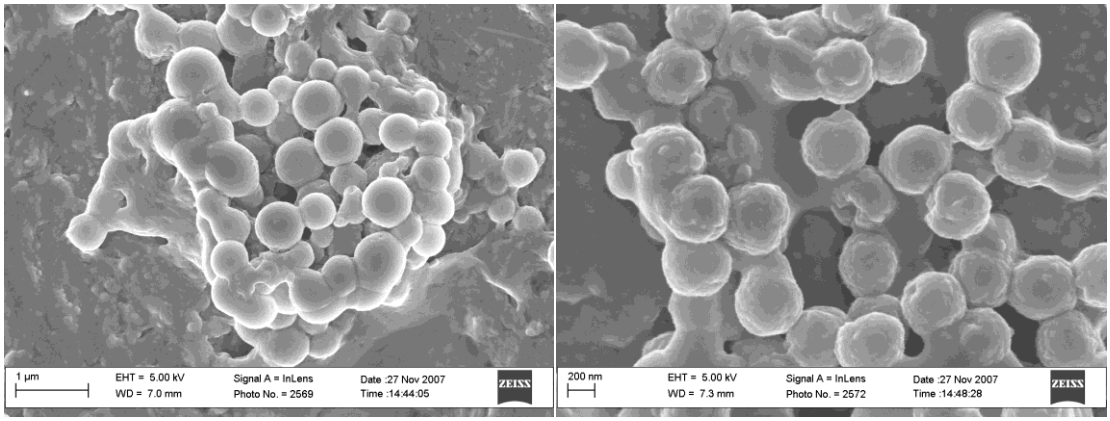


Fig. 5.22 SEM micrographs of coated polystyrene particles after treated with THF. (a) coated with 10 layers(5 bi-layers CHI/DS); (b) coated with 12 layers (5 bi-layers CHI/DS plus bi-layer CHI/Laponite)

The THF dissolving process was the same as that reported earlier, and the dissolution of the polystyrene particles was confirmed by the Fig. 5.10, Fig. 5.14- Fig. 5.18. Compare Fig. 5.22(a) and Fig. 5.22(b), it can be noticed that after dissolving of the polystyrene nanoparticles, the capsules with a layer of laponite survived more than those with only polymer layers. Also compared with the nanocapsules with several layers of laponite, the nanocapsules with only one layer of laponite were more likely to hold the shape and intact after dissolution in THF.

5.4 Conclusion

In this Chapter, the fabrication of nanocapsules based on polystyrene nanoparticles (size around 480 nm) was discussed. Polystyrene nanoparticles were prepared via the polymerization of styrene monomers. The deposition time and salt concentration in the polyelectrolyte solution optimised and discussed. Nanocapsules of different composition were fabricated onto the polystyrene core-templates, including nanocapsules of polyelectrolyte, nanocapsules of polyelectrolyte and several layers of laponite and nanocapsules of polyelectrolyte and one layer of laponite. After the core-removal process, it was found the nanocapsules comprised of only polyelectrolyte were collapsed, due to the insufficient strength of the nanocapsules and nanocapsules of several laponite layers were also collapsed and formed some bowl-shaped hollow capsules, which might because the wall of the capsules is too thick. Finally, the nanocapsules comprised of one layer Laponite and polyelectrolyte was found to be the most regular, such as those nanocapsules consisting of 5 CHI/DS bi-layers plus one CHI/Laponite bi-layer were obtained after the core-removal process.

Chapter 6 Nanocapsules Based on Small Polystyrene Core Templates

In Chapter 5, the preparation of nanocapsules based on submicron polystyrene particles has been discussed, however, due to the size issue we had discussed in the literature review that nanocapsules which are smaller than 200 nm would be preferable for the therapeutics delivery system, therefore, in this Chapter, we would investigate the preparation of nanocapsules based on polystyrene particles (less than 200 nm) and some further functionalisation of these nanocapsules.

In this Chapter, firstly the synthesis of the polystyrene particles (around 130 nm) is discussed. Then, the preparation of nanocapsules consisting of biocompatible polyelectrolytes (CHI/DS) and laponite is demonstrated. Finally, the fabrication of the nanocapsules functionalised by gold/magnetite particles is also discussed.

6.1 Materials

The chemicals involved in this experiment were: Sodium Chloride (99.5% Sigma Aldrich), Chitosan (CHI) (50,000-190,000Da, Aldrich), Dextran Sulfate Sodium Salt (DS) (approximate 10,000Da, Sigma), laponite (Rockwood additives), Tetrahydrofuran (THF, ≥99%, Aldrich), Hydrogen Tetrachloroaureate (III) Trihydrate ($HAuCl_4$, 99.99%, Acros Organics), Tetrakis(hydroxymethyl)phosphonium Chloride (THPC, 80% in water, Fluka), Sodium hydroxide (NaOH, semiconductor grade, Aldrich), Iron (II) chloride tetrahydrate ($FeCl_2 \cdot 4H_2O$, 99%, Sigma-Aldrich), Iron (III) chloride hexahydrate ($FeCl_3 \cdot 6H_2O$, BDH), Sodium Oleate ($C_{17}H_{33}COONa$, BDH). All water used was deionised. The visking dialysis tubing (MWCO-12-14000 Daltons, diameter 38.1 mm and 6.3 mm) used here was obtained from the Medicell International Ltd.

6.2 Methodology

6.2.1 Synthesis of Polystyrene Nanoparticles

The procedure of preparing size around 100 nm polystyrene nanoparticles followed the same basic styrene polymerization procedure described in Chapter 5 section 5.2.1 with only a few changes to the method. Firstly, the reaction volume was enlarged to 2 L. Secondly, except for adding the deionised water, styrene monomer and NaCl, sodium dodecylbenzene sulphonate (SDBS) as a surfactant was also added into the system. It is well known [236] that the addition of surfactant reduces the particle size of PS particles. Therefore, in this case, 1650 ml water, 100 ml styrene monomer and 2.5 g sodium dodecylbenzene sulphonate was initially added into the flask. Then, after vigorous stirring, the initiator solution (2.5 g potassium persulphate in 250 ml water) was added to make this reaction take place and the total volume reached to 2 L. Thirdly, the temperature of the water bath was raised from 80 ^{O}C to 85 ^{O}C.

6.2.2 Fabrication of Nanocapsules via Layer-by-Layer Self-assembly Method

6.2.2.1 Preparation of the Polyelectrolyte Solutions

Biocompatible polyelectrolytes: CHI and DS were employed in this experiment to prepare nanocapsules based on polystyrene nanoparticles. The concentration of the polyelectrolyte solution is 1 mg/ml in 0.1 M NaCl solution. For CHI, the solution was also adjusted to pH 3 by HCl. Laponite was also used in this experiment as a layer material to strengthen the capsules. The laponite particles were dispersed in de-ionized water with a concentration of 10 mg/ml.

6.2.2.2 Preparation of the Nanocapsules

Two types of nanocapsules have been prepared in this experiment. One of them consisted of 10 layers of biocompatible polyelectrolyte (CHI/DS), whereas the other contained 9 layer of biocompatible polyelectrolyte (CHI/DS) and one layer of laponite.

The methodology was as follows: 5 ml of polystyrene particles (1.8 wt%) was mixed with 10 ml 1 mg/ml of CHI (dissolved in 0.1 M NaCl solution) and 10 ml de-ionized water. Then the mixture was gently shaken for 60 min before 2 centrifugation-redispersion cycles (the particle suspension was centrifuged at 3000 g and 5472 g for 5 min, and finally 8425 g for 15 min) applied. Then all residue obtained from the centrifugation process were re-dispersed in 15 ml de-ionized water. The rest of the layers (except the laponite layer) were added in the same way.

For the second type of nanocapsules, laponite was used as the fourth layer. For the deposition of the laponite layer, the 3-layer coated particle suspension was diluted to 20% of the original concentration. Then to 5 ml of the diluted sample was added of 5 ml 10 mg/ml laponite and 20 ml de-ionized water. The coating and wash cycle was as same as described above for the first layer. After the laponite layer, further layers were added in the same way.

6.2.2.3 Functionalizing the Coated Polystyrene Nanoparticles

In this section, two inorganic nanoparticles were introduced to add possible functionality to the coated polystyrene nanoparticles and subsequent nanocapsules. One of them was gold nanoparticles and the other one was magnetite nanoparticles.

6.2.2.3.1 Preparation of Gold Nanoparticles

The gold nanoparticles were prepared by the THPC method introduced by Duff et al [237]. The method was to reduce $HAuCl_4$ by using the reducing agent tetrakis(hydroxymethyl)phosphonium chloride (THPC). The method was as follows:

- Firstly, 2 ml of 25 mM $HAuCl_4$ solution was prepared and stored (dark-aged) for 3-4 days (Fig. 6.1).
- 1.2 ml THPC (80% aqueous) was then added into 100 ml of de-ionized water.
- 1 ml of this solution was mixed with 0.5 ml of 0.1 M NaOH solution and de-ionized water was added to fix the volume to 50 ml.
- Finally, 50 ml of this solution was mixed with the dark-aged $HAuCl_4$, and the dark brown gold nanoparticle suspension was obtained (Fig. 6.2).

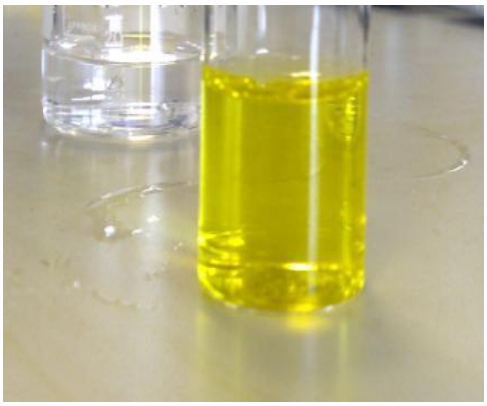


Fig. 6.1 Dark-aged HAuCl4 solution



Fig. 6.2 Gold nanoparticle suspension

6.2.2.3.2 Preparation of Magnetic Nanoparticles

The method used in this experiment to produce magnetic nanoparticles was that introduced by Sun et al [222].

- Firstly, 1.99 g (0.01 mol) of $FeCl_2 \cdot H_2O$ and 5.41 g (0.02 mol) of $FeCl_3 \cdot 6H_2O$ were dissolved in 50 ml of de-ionized water.
- Then the mixture was stirred vigorously and 1.5 M NaOH solution was added to adjust the pH to 11. The solution was kept vigorously stirred for another 60 min to ensure complete crystallization. The whole system, during the experiment, was kept in a water bath of 50℃, whilst adding the NaOH solution, it was noticed the colour of the solution changed from light brown to dark brown and finally to black which indicated the formation of the magnetite particles.
- The particle suspension was centrifuged and the particles were then re-dispersed in the same volume of de-ionized water.

The experiment was then modified and 3v% of 0.1M sodium oleate was added into the Fe solution as a surfactant to produce better-dispersed Magnetic particles. This surfactant was added before the addition of the NaOH solution.

6.2.2.3.3 Functionalisation of Polyelectrolyte Coated Polystyrene Nanoparticles with Gold and Magnetic Nanoparticles

The gold particles were negatively charged in the suspension, so they were used as an even layer of the nanocapsules. Due to the presence of sodium oleate, the magnetite particles were positively charged and were used as an odd layer of the nanocapsules.

In this experiment, 10 ml of magnetic particles were mixed with 25 ml of 10-layer coated polystyrene nanoparticles (9 layers of biocompatible polyelectrolyte and 1 layer of laponite) suspension. Then the mixture was gently shaken for 1hr and the excess magnetic particles were removed by 2 centrifugation-re-dispersion cycles. The gold particles were added when the polystyrene particles were coated with 8-layers of biocompatible polyelectrolyte and one layer of laponite, and the coating procedure followed the one outlined above for the magnetite.

6.2.2.3.4 Core Removal

After all the coating processes, the coated particles were dissolved in THF to remove the polystyrene core templates. Each of the coated particle suspensions was mixed with twice the volume of pure THF, and the mixture was kept sealed in a fume cupboard for 48 hrs. After dissolution, in order to get remove the THF and polystyrene residue, the solution was decanted into the dialysis tubings (diameter 6.3 mm and both ends tied up after loading) and the loaded tubing was placed in deionised water. The deionised water was changed every 12 hr for 7 days.

6.3 Results and Discussion

6.3.1 Polystyrene Nanoparticles Synthesized with Surfactant

In this experiment, polystyrene particles with size range lower than 200 nm were made by the polymerization of styrene monomers Both a CPS disc centrifuge (experimental details in Chapter 3) and dynamic light scattering were utilised to investigate the size distribution of these nanoparticles. From Fig. 6.1 and Fig. 6.2, it is clearly demonstrated that the majority of the polystyrene particles from this synthetic method shared an average particle size around 130 ±30 nm

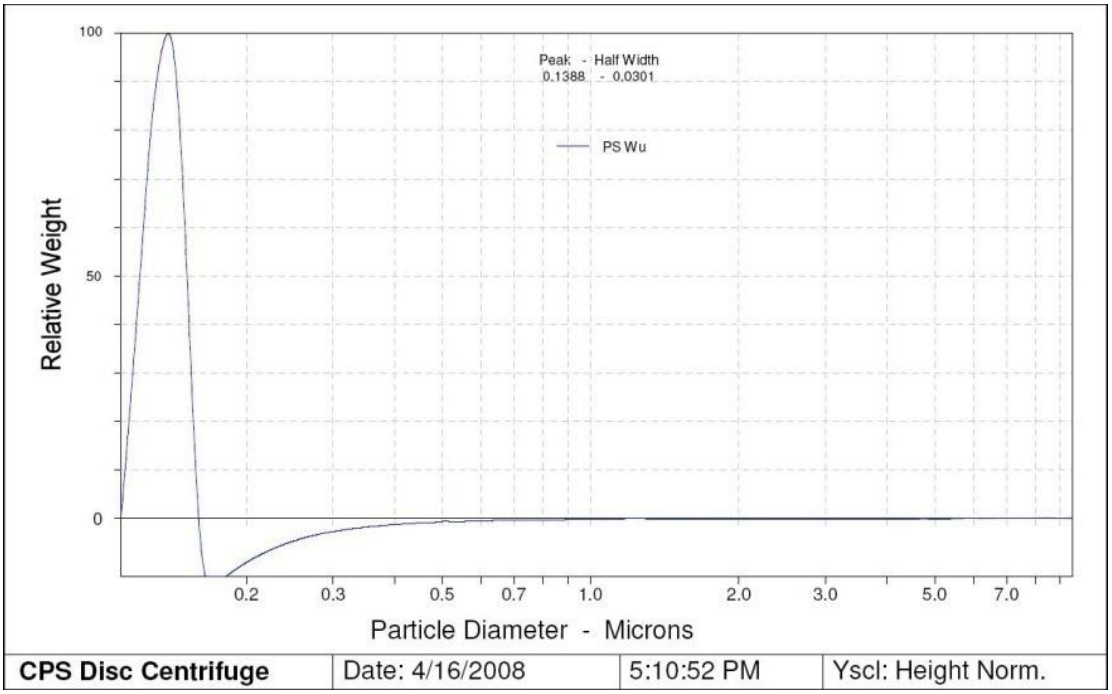


Fig. 6.1 Result from CPS disc centrifuge analysis: polystyrene nanoparticles (synthesized by polymerization of styrene monomers with the presence of SDBS) size distribution

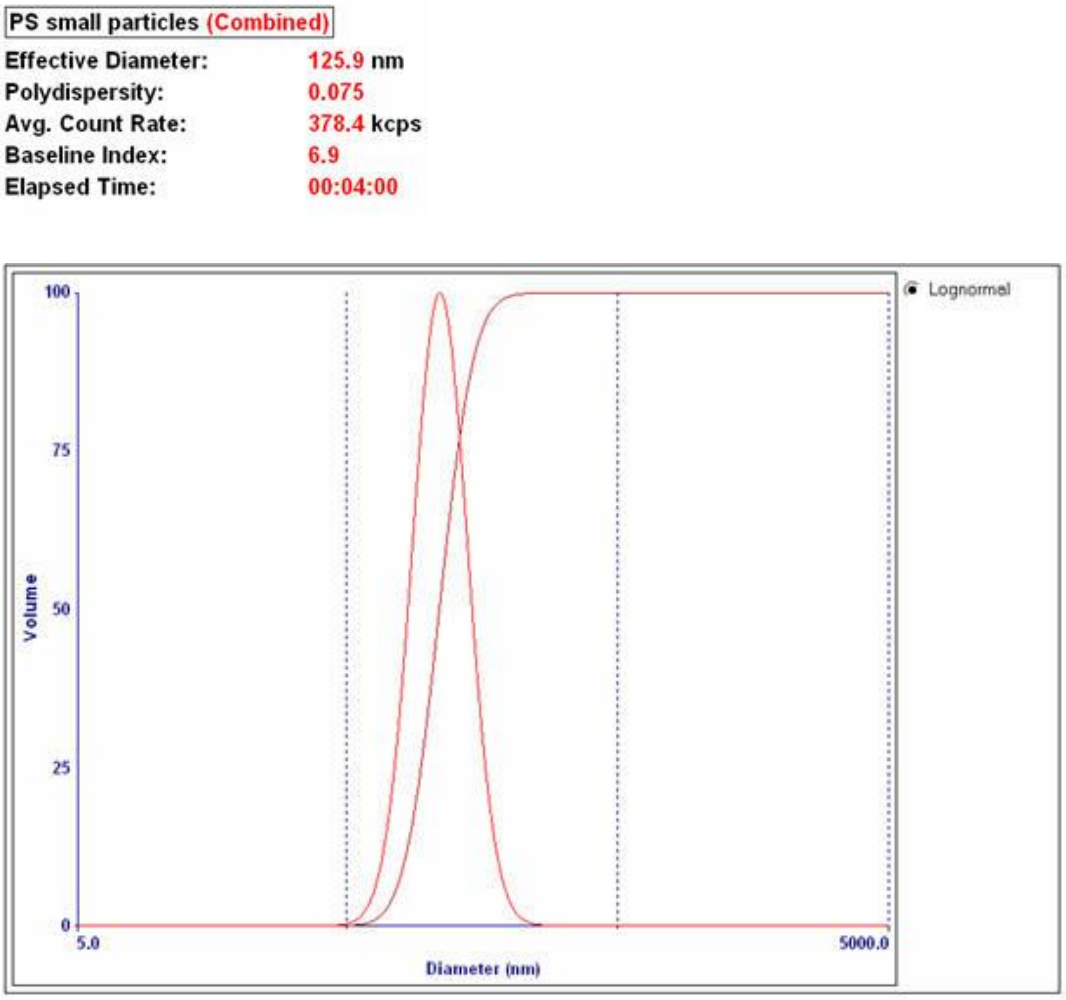


Fig. 6.2 Result from dynamic light scattering analysis: polystyrene nanoparticles (synthesized by polymerization of styrene monomers with the presence of SDBS) size distribution

SEM was also employed in this characterization section to further investigate the shape, surface and size distribution of the polystyrene nanoparticles (130 nm) (Fig. 6.3).

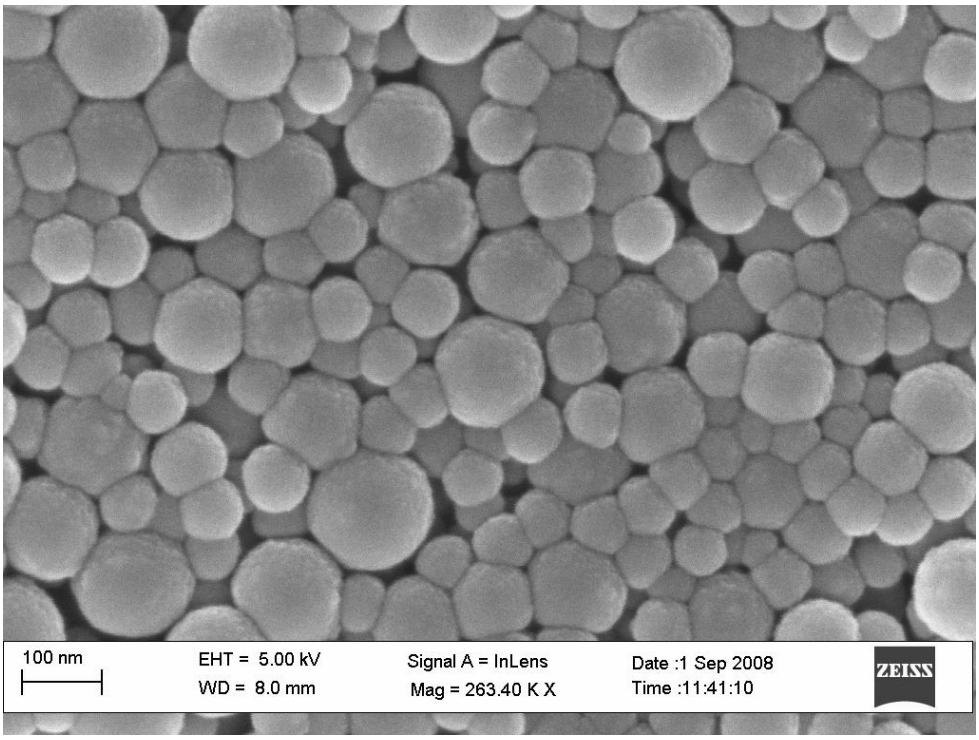


Fig. 6.3 SEM micrograph of polystyrene particles prepared by polymerization of styrene monomers with the presence of surfactant SDBS

Compared with the polystyrene particles with larger size (Chapter 5 Fig. 5.5), these polystyrene particles were more poly-dispersed and also seem softer, as drying forces seem to have deformed the particles. This is likely to be due to the SDBS plasticizing the polystyrene. For the purpose of using these particles as a template, however, this is immaterial. Likewise the wider size distribution did not make the suspension inappropriate for use as a LBL template; indeed in many respects a polydispersed template has the advantage of investigating the behaviour of a variety of different particle sizes in just one experiment.

6.3.2 Nanocapsules Consisting of Polyelectrolyte and Laponite

6.3.2.1 Salt Concentration of the Polyelectrolyte Solution

Before coating with the polyelectrolyte, 3 different sodium chloride concentrations (0.1 mol/ml, 0.5 mol/ml and 1.0 mol/ml) were tested for the first layer deposition. It was found that for 0.5 mol/ml and 1.0 mol/ml, the coated polystyrene particles were hard to re-disperse and a few aggregates were found in the suspension. This aggregation may be due to the relatively small particle size compared to the layer thickness and that the capsules entangled together during centrifugation. Therefore, in this experiment, 0.1 M NaCl was used to prepare the polyelectrolyte solutions.

6.3.2.2 Biocompatible Polyelectrolyte

There were 2 types of nanocapsules prepared in this section: with or without laponite layer. For the nanocapsules without the laponite layer, 10 layers of biocompatible polyelectrolyte were added onto the polystyrene nanoparticles. While the ones with laponite layer were prepared in the same way, only the fourth layer was changed from DS to laponite. Fig. 6.4 and Fig. 6.5 show the zeta-potential of each layer of the 2 samples.

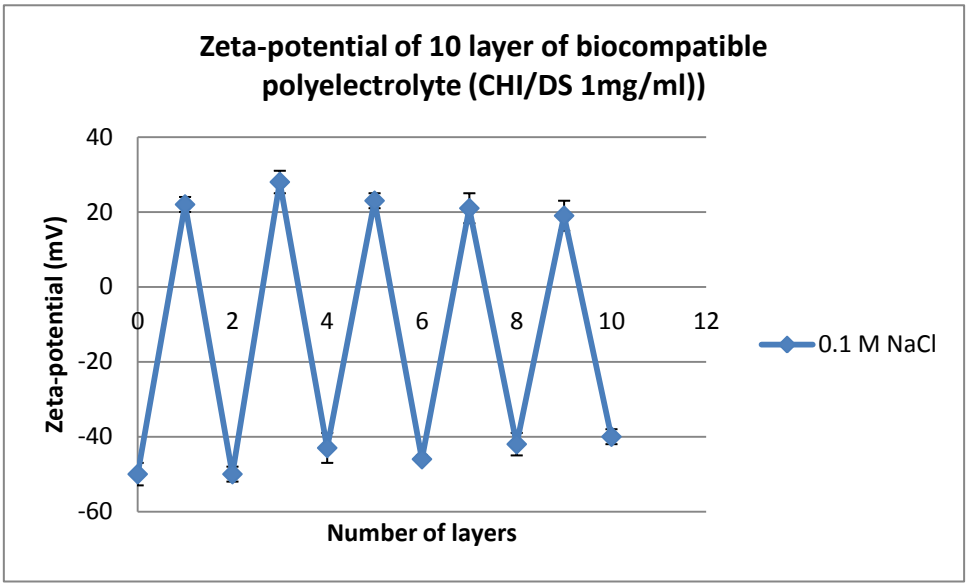


Fig. 6.4 Zeta-potential of layers of nanocapsules consisting of 10 layers biocompatible polyelectrolyte ($(CHI/DS)_5$);The values are given in the appendix Table A.7.

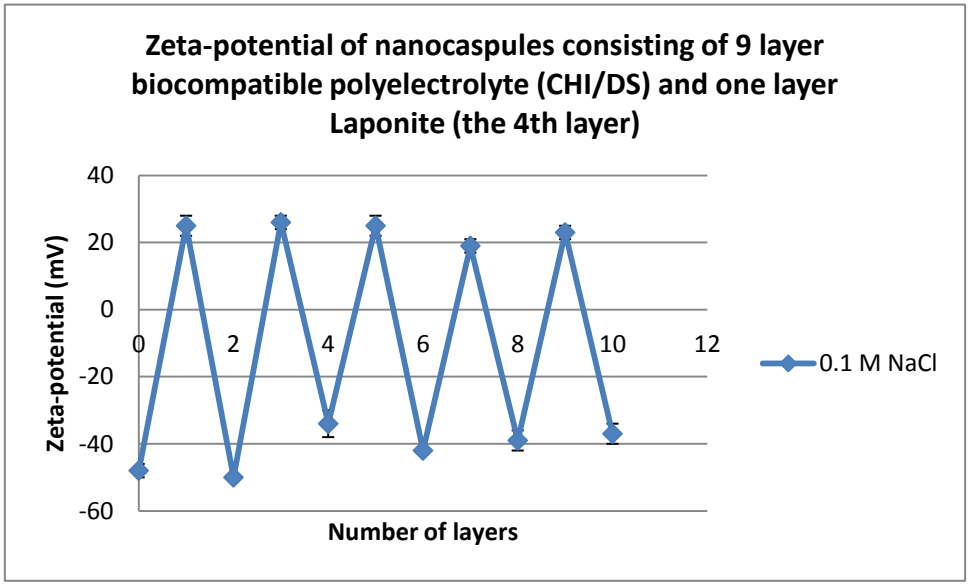


Fig. 6.5 Zeta-potential of layers of nanocapsules consisting of 9-layer of biocompatible polyelectrolyte (CHI/DS) and laponite (the 4^{th} layer); The values are given in the appendix Table A.8.

From Fig. 6.4 and Fig. 6.5, the deposition of each polyelectrolyte layer was confirmed by the changes of the zeta-potential. It can be noticed in both graphs, that the zeta-potential decreased during the Layer-by-layer deposition process. It is also been

noticed the zeta-potential (absolute value) of the laponite layer (4th in Fig. 6.5) is lower than the corresponding layer in Fig. 6.4. This may be due to either the steric effect leading to less deposition of laponite nanoparticles compared to DS, or due to he lower zeta potential of laponite.

After the coating process was complete, the 2 samples were observed under SEM and the micrographs of the coated particles are shown in Fig. 6.6 and Fig. 6.7.

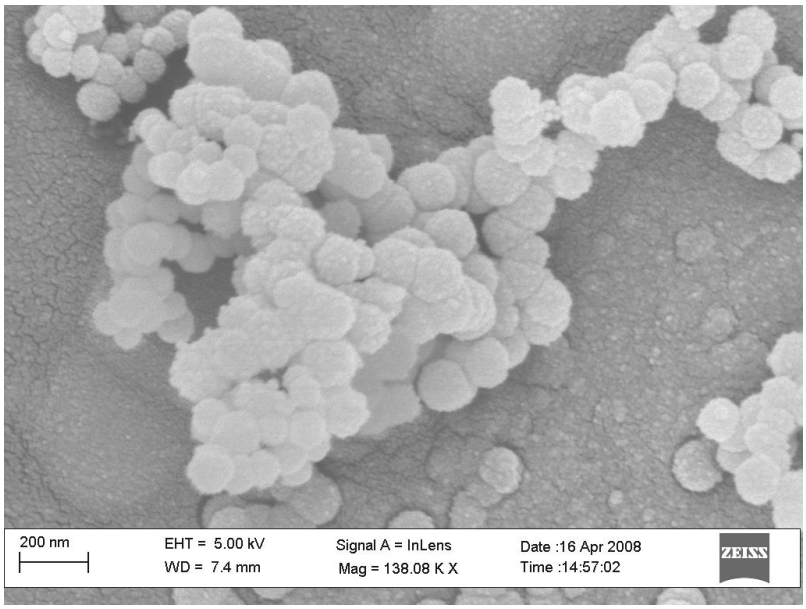


Fig. 6.6 SEM micrograph of polystyrene particles coated with 10 layers of biocompatible polyelectrolyte

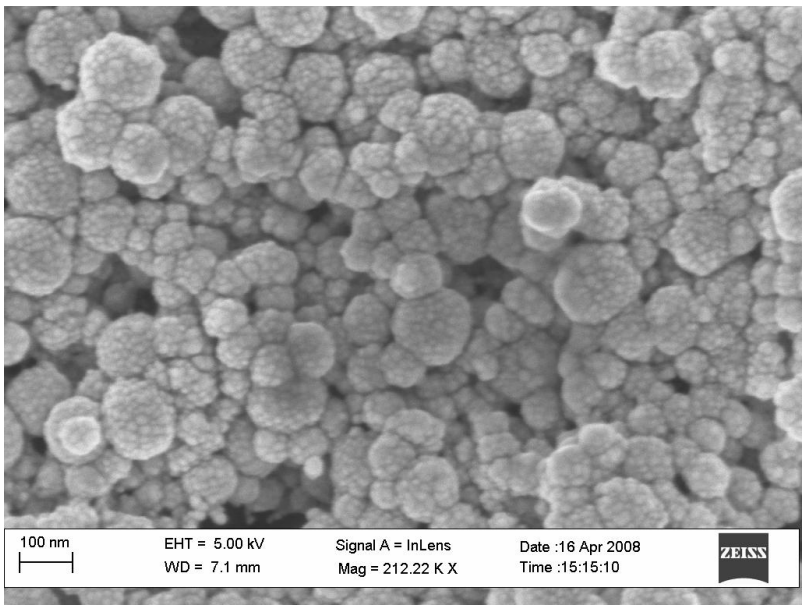


Fig. 6.7 SEM micrograph of polystyrene particles coated with 10 layers of biocompatible polyelectrolyte and where the 4th layer is laponite

From Fig. 6.6 and Fig. 6.7, no obvious difference can be found from the 2 pictures. The roughness of each particle surface seems similar and all the particles attached together and formed clusters of particles. The appearance of the clusters may be because the density of the particles is relatively large and after dried, the coated particles cannot stay flat in the surface and formed this kind of particle clusters. The similar roughness can be explained by the 6 more added polyelectrolyte layers can possibly smooth out the rough surface of the laponite layer and gave the particles a similar appearance of the particles coated with only polyelectrolyte. However, although the roughness of both samples seems similar, it is still rougher compared with the original polystyrene particles, which is further evidence of the formation of relatively thick polyelectrolyte layers

6.3.2.3 Core Removal

After being coated with polyelectrolyte and laponite layers, the 2 samples (prepared in the last section) were dissolved in THF (volume ratio1:2) to remove the polystyrene core templates.

For the particles coated with 10 layers of biocompatible polyelectrolyte, only a few of nanocapsules were found after the core removal process (Fig. 6.8).

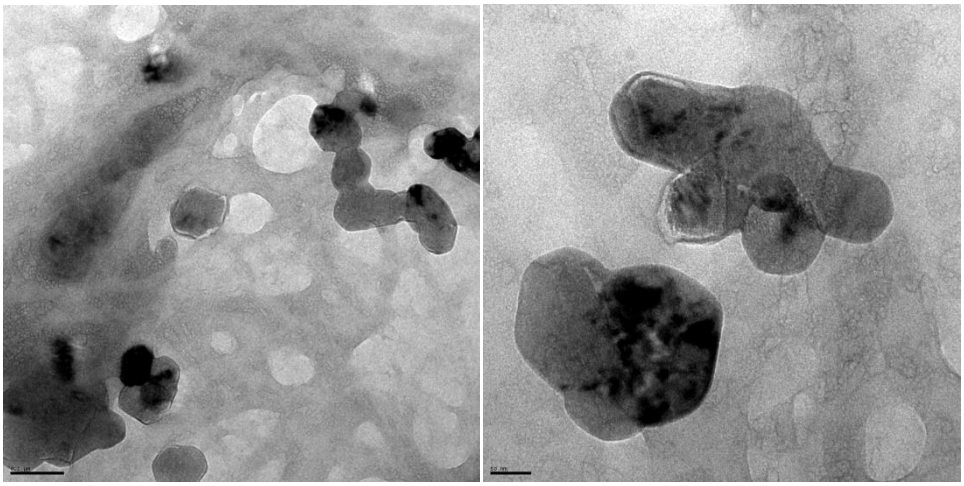


Fig. 6.8 TEM micrographs of nanocapsules derived from 10-layer coated polystyrene nanoparticles of different magnification (no laponite attendance), the size of the left scale bar is 200 nm and the size of the right scale bar is 50 nm

From Fig. 6.8 the nanocapsules obtained from the core removal process can be clearly observed. The capsules were light grey in colour and the black areas in some of the nanocapsules can possibly be the residue of the polystyrene particles. It can also be noticed that the shape of the nanocapsules was not spherical anymore and more like a deflated balloon. The change of the shape indicated the change inside of the capsules (core removed). Because there was no laponite layer of the capsule, and without the support of the core template, the capsule itself would possibly change its form from spherical to irregular.

After core removal, the nanocapsules derived from the polystyrene particles coated with 9 layer of polyelectrolyte and 1 layer of laponite were also observed under TEM (Fig. 6.9). Many more capsules were now visible

(a) (b)

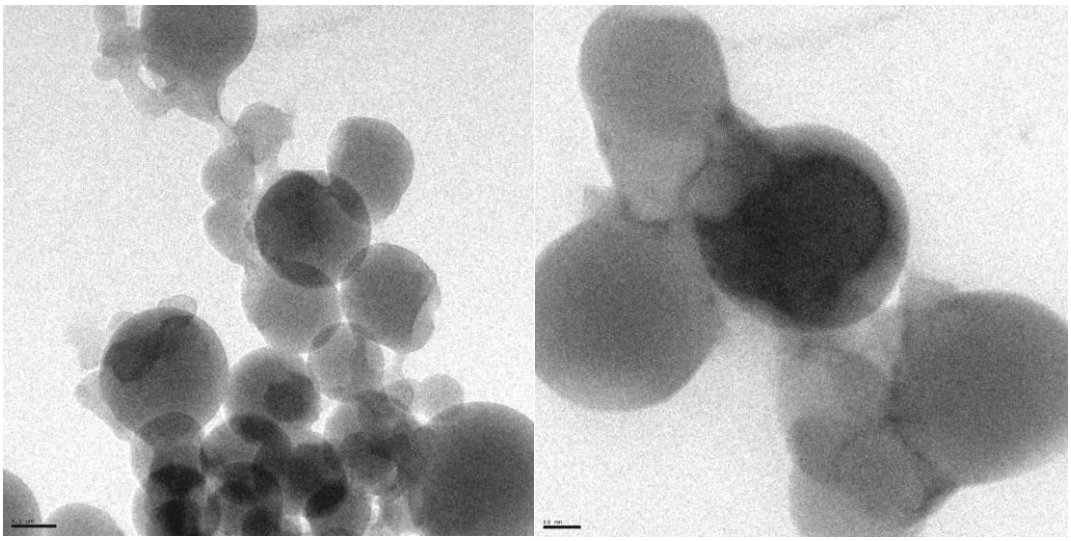


Fig. 6.9 TEM micrographs of nanocapsules derived from 10-layer coated polystyrene nanoparticles of different magnifications (the 4th layer is laponite), the size of the left scale bar is 100 nm, and the size of the right scale bar is 50 nm

From Fig. 6.9 b, it can be clearly seen that an incompletely removed polystyrene particles was surrounded by several nanocapsules obtained from the core removal process. The dark area in the middle of the picture is the un-removed polystyrene particle, and there are 3 empty nanocapsules around it. In Fig. 6.9 a, more nanocapsules obtained from the core removal process can be observed. Although there were some of the nanocapsules collapsed or formed the cup-shape nanoparticles, most of the nanocapsules survived from the THF erosion and kept their spherical shape. Compared with the nanocapsules without laponite layer, it can be noticed that the productivity of the nanocapsules with one layer of laponite is relatively higher. Therefore only the particles coated with 9-layer of polyelectrolyte and 1 layer of laponite were used in the functionalization with gold and magnetic nanoparticles.

6.3.3 Functionalization of the Nanocapsules

Coating with some inorganic particles would change the property of the nanocapsules. In this experiment, gold and magnetite particles were prepared and added onto the coated polystyrene nanoparticles to make the nanocapsules sensitive to infrared (in the case of gold nanoparticles enabling the particles to be heated by near IR radiation) and easy to locate and visualise the nanocapsules (in the case of magnetic particles) during the drug delivery process.

6.3.3.1 Gold Nanoparticles Deposition

6.3.3.1.1 Characterization of the Gold Nanoparticles

The gold nanoparticles used in this experiment were prepared by reducing $HAuCl_4$ with a reducing agent tetrakis(hydroxymethyl)phosphonium chloride (THPC). The gold nanoparticles were characterized by Zeta meter, TEM and CPS disc centrifuge.

The zeta-potential of the gold nanoparticles was -29±2 mV which indicates the gold nanoparticles should be used as an even layer of the nanocapsules. The data obtained from CPS disc centrifuge showed the size range of the gold nanoparticles was between 4-10 nm. The TEM picture of the gold nanoparticles is shown in Fig. 6.10.

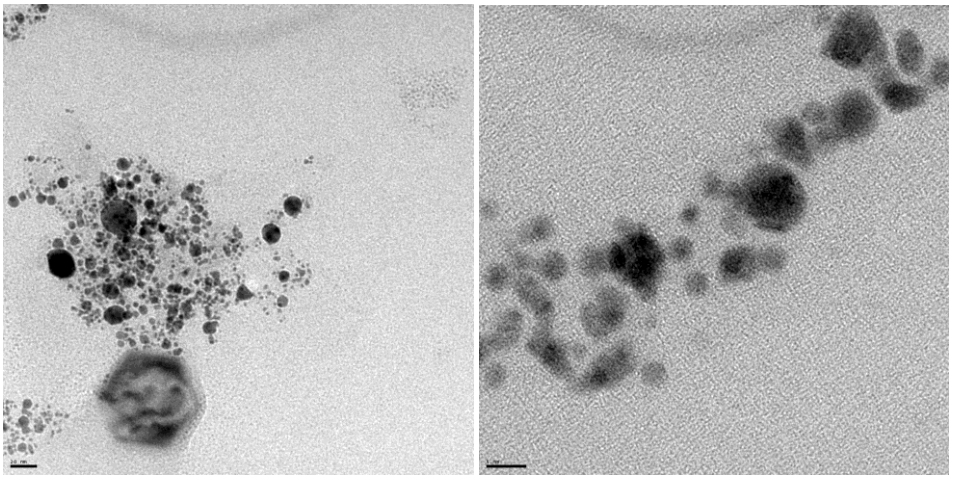


Fig. 6.10 TEM micrographs with different magnifications of gold nanoparticles; the scale bar of the left micrograph is 20 nm and it is 5 nm for the right one

From the TEM pictures in Fig. 6.10, the size distribution of the gold nanoparticles can be roughly observed. Except for a few large particles, most of the particles were under 10 nm. Compared with the diameter of the polystyrene nanoparticles, the size of the gold nanoparticles is small making them suitable as an alternative to an anionic polyelectrolyte and so have the particle to be used to deposit a monolayer onto the core particle.

6.3.3.1.2 Deposition of Gold Nanoparticles

Due to the negative charge, the particles were added onto the 9-layer coated polystyrene particles. The zeta-potential of the particles changed from 23 ± 2 mV to -15 ± 3 mV, which indicated the deposition of the gold nanoparticles. The TEM picture of gold coated polystyrene nanoparticles, coated with 8 polyelectrolyte layers and one laponite layer (4^{th} layer), is shown in Fig. 6.11.

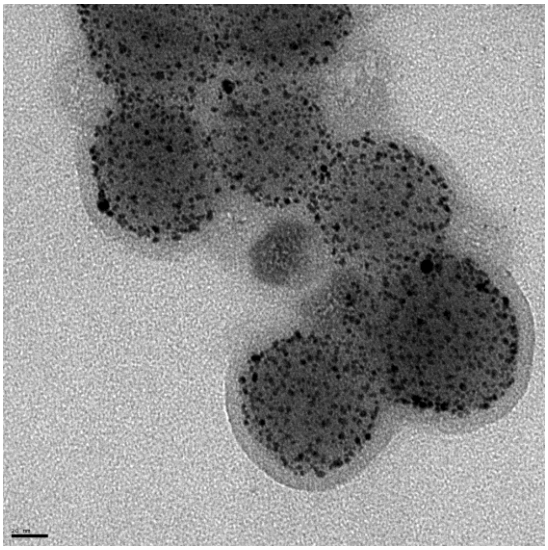


Fig. 6.11 TEM micrograph of polystyrene particles (8 layers polyelectrolyte and the 4th layer is laponite) coated with gold nanoparticles, the scale bar in the graph is 20 nm

In Fig. 6.11, a thin and fine layer of gold was observed on the polystyrene nanoparticles. However, it can be noticed that the coverage of the gold layer is not very high compared with the polyelectrolyte. That can explain the low zeta-potential (absolute value) of the gold coated nanoparticles.

After core-removal process, the gold coated nanocapsules can be seen from Fig. 6.12.

(a) (b)

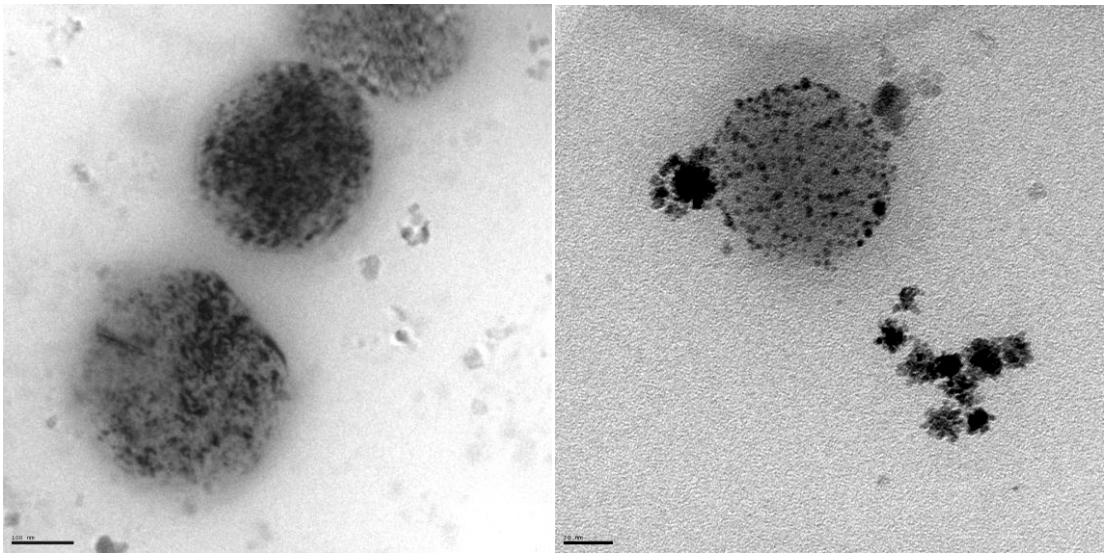


Fig. 6.12 TEM micrographs of nanocapsules (after dissolving by THF for 48 hr) of 8-layer polyelectrolyte (CHI/DS), one layer laponite (4th layer) and the outer layer is gold, the scale bar in the left graph is 100 nm and the scale bar is 20 nm in the right graph

The nanocapsules coated with gold nanoparticles can be observed in Fig. 6.12. Compared with particles in Fig. 6.11, the shape of the nanocapsules (after core removed) and the coverage of the gold particles did not change significantly.

6.3.3.2 Magnetic Nanoparticles Deposition

6.3.3.2.1 Characterization of the Magnetic Nanoparticles

Magnetic Property

The magnetic property of the magnetic particles was assessed directly by the method illustrated in Fig. 6.13.

From the difference between Fig. 6.13 a and b, the attraction of the magnetic particles to the magnetic stirrer can be clearly noticed, demonstrating the magnetic properties of the particles. The nanocapsules coated with the magnetic particles have the

potential to be traced and directed in the human body using magnetic resonance imaging, and so could be used for targeting purposes.

(a) (b)

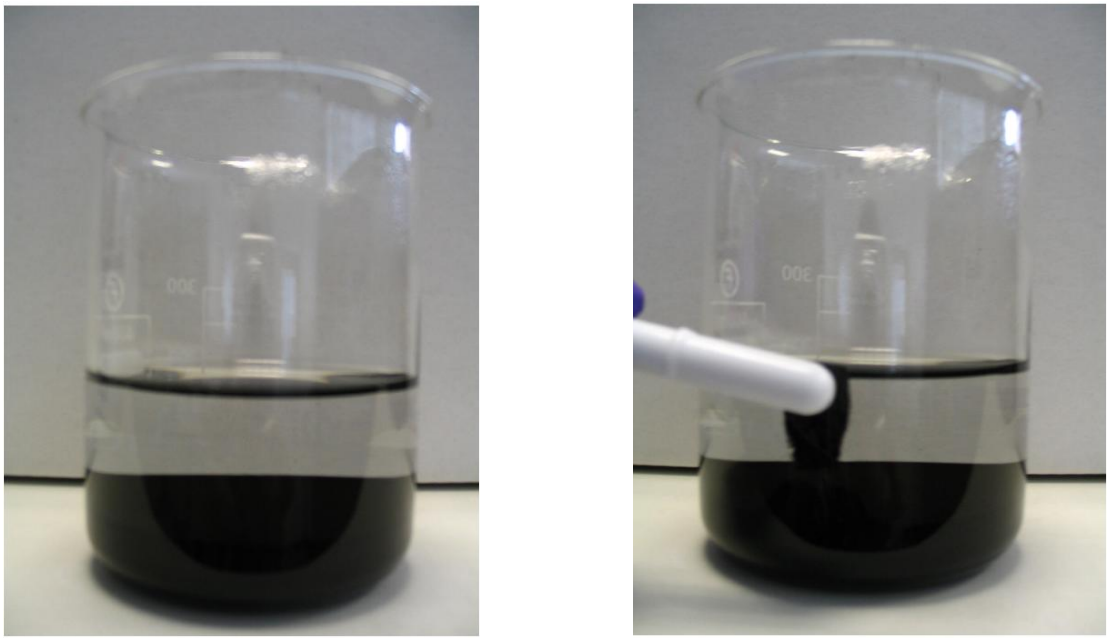


Fig. 6.13 The test of the magnetic property of the magnetite nanoparticles. (a) The magnetic particle suspension; (b) The magnetic particle suspension stimulated by a permanent magnetic stirrer.

Zeta-potential

Since the Layer-by-layer method employed in this experiment is based on electrostatic force, the zeta-potential of the particles is another important property of the magnetic particles. The zeta potential of the particles produced with sodium oleate was +31 ±3 mV and it was -27 ±2 mV of the ones without sodium oleate.

XRD Analysis

The two samples were also analysed by XRD analysis (Fig. 6.14).

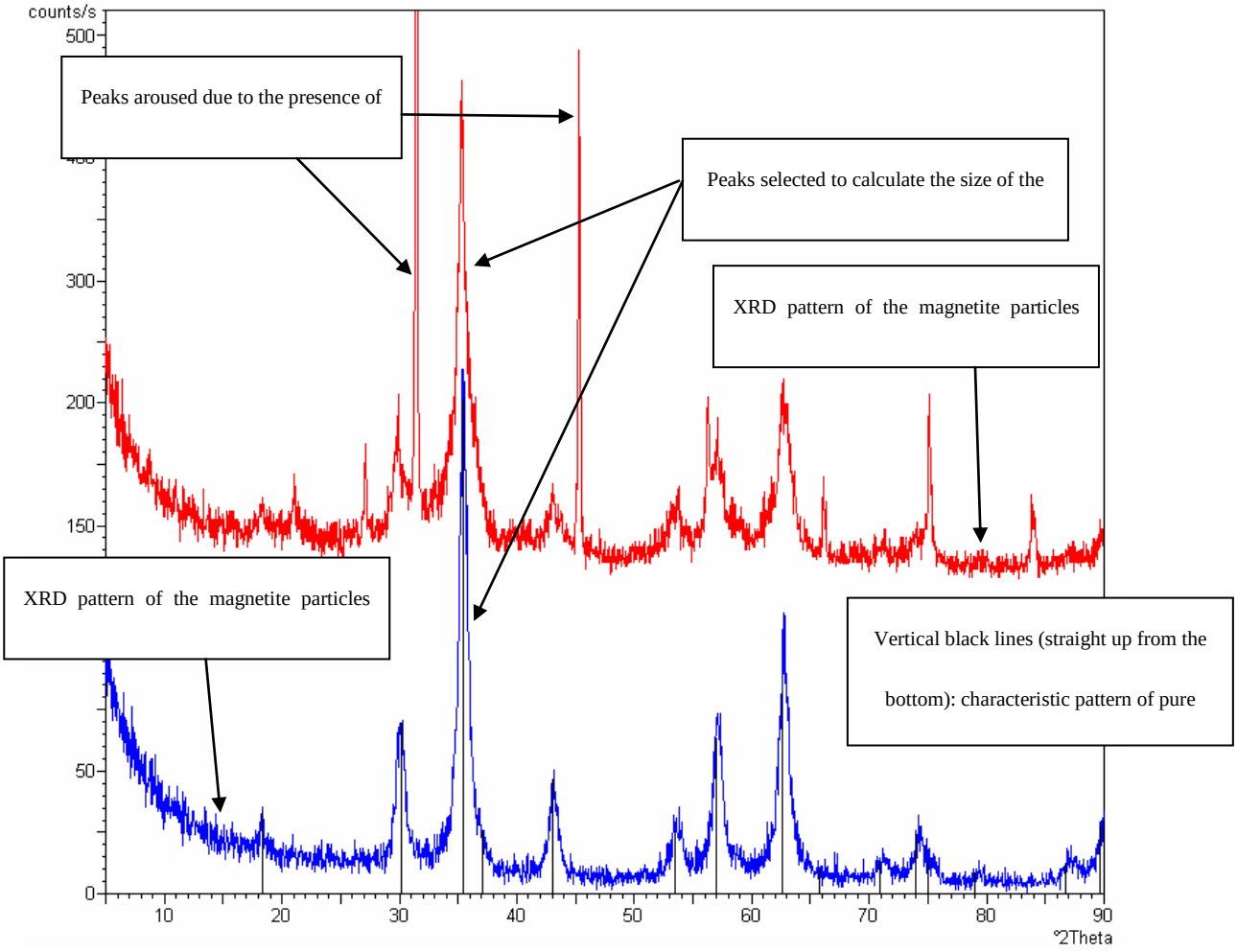


Fig. 6.14 The XRD patterns of magnetic particles with or without sodium oleate. (Blue line: without sodium oleate; red line: with sodium oleate; the straight vertical black line: pure magnetitie)

From Fig. 6.14, the XRD patterns of the 2 magnetic particles (Blue and red patterns) are roughly coincident to that of that pure magnetite (the vertical black lines at the bottom of the graph) (ICDD No. 19-0629), which confirmed the preparation of the magnetite particles in this project. Comparison between these two patterns shows that the diffraction pattern of the magnetite particles prepared without sodium oleate is more similar to the pattern of the pure magnetite, whereas for the magnetite particles prepared with sodium oleate, two characteristic peaks at about 31^{o} and 45^{o} was observed in Fig. 6.14 (spotted on the red pattern). According to the XRD data provided by the technician, who assisted in taking these patterns, those two peaks are characteristic peaks of sodium which was probably introduced by sodium oleate.

Compared with the XRD pattern of the magnetite nanoparticles prepared by Sun et al. [222] (Fig. 6.15), it could be noticed that the two patterns obtained in this experiment are very similar to the result of Sun et al.

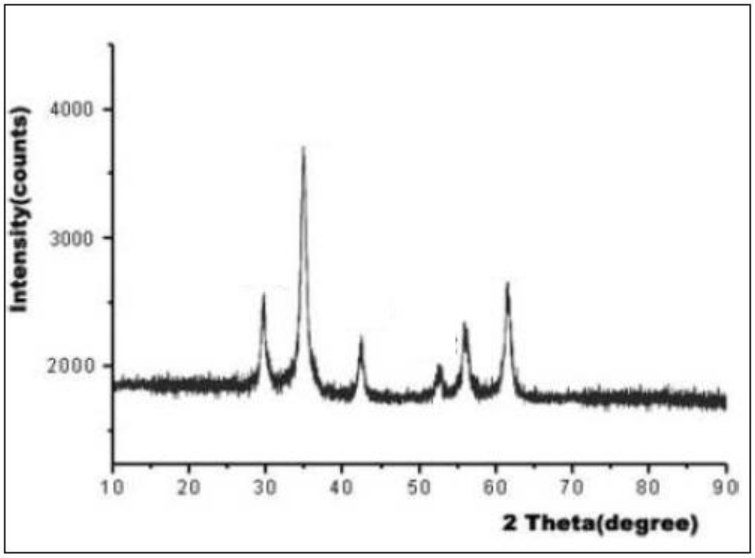


Fig. 6.15 The XRD pattern of the magnetite prepared by Sun et al. [222]

As reported in the Chapter 3 section 3.5, when the crystallite domains of the materials are less than 100 nm, this domain could correspond to the real size of the particles and the size of the domain could be estimated based on the wave length of X-ray and half the maximum intensity in radians [223]. Therefore, by the Scherrer equation (Equation 6. 1), the mean particle diameter of the 2 samples can be estimated (Table 6.1).

Equation 6. 1 $$\tau = \frac{K\lambda}{\beta cos\theta}$$

where K is the shape factor (0.9 was taken here), λ is the x-ray wavelength of the X-rays, β is the line broadening at half the maximum intensity (FWHM) in radians (in this case, the characteristic peaks (30^{O}-40^{O}) of magnetite particles were picked), and θ is the

Bragg angle; τ is the mean size of the ordered (crystalline) domains, which may be smaller or equal to the grain size [238, 239].

Table 6.1 Estimation results of the particle average size of the magnetite particles

	With sodium oleate	**Without sodium oleate**
β(radians)	0.01438	0.01436
2θ (^{o})	35.54	35.48
τ (nm)	10.0	9.6

For the unknown particles, the typical value of dimensionless shape factor K of the crystalline domains (τ) is 0.9 [238, 239], therefore the size of the magnetite particles with sodium oleate is about 11.1 nm and the ones without sodium oleate is about 10.7 nm.

TEM Analysis

The 2 batches of magnetic nanoparticles were both observed under the TEM. And the TEM pictures are shown in Fig. 6.16.

(a) (b)

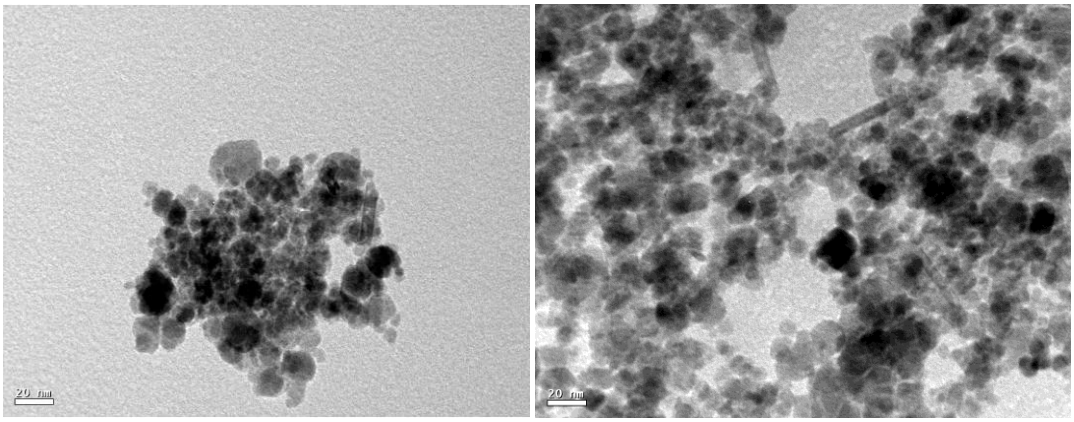


Fig. 6.16 The TEM micrographs of the magnetic nanoparticles (a) prepared with sodium oleate (b) prepared without sodium oleate

From Fig. 6.16, the shape and size of the magnetic particles can be easily observed. The particles demonstrated in the TEM pictures are from several nanometers to almost 20 nm. This size range corresponds to the mean diameter (around 10 nm) calculated from the XRD pattern. Although there is no obvious difference found between these two samples, there are some needle-like particles in Fig. 6.16 (b), which makes the magnetic particles prepared with sodium oleate a better option for the nanocapsules preparation. In theory, the presence of the sodium oleate (as a surfactant) would help to form magnetic particles with a narrower size distribution, therefore, the magnetite particles prepared with sodium oleate was used as a layer material for the nanocapsules fabricated on the polystyrene particles.

6.3.3.2.2 Deposition of the Magnetite Nanoparticles

Due to the positive charge of the magnetite nanoparticles, the particles were mixed with the 10-layer sample (9 layers of biocompatible polyelectrolytes and 1 layer of laponite) to prepare the functionalise nanocapsules. After the coating and centrifuge cycle, the zeta-potential of the coated polystyrene nanoparticles shifted from -37±3 mV to +4±2 mV. The zeta-potential was not very high for the LBL self-assembly

method. The reason of the low zeta-potential value can be explained by the TEM pictures of the coated particles (Fig. 6.17).

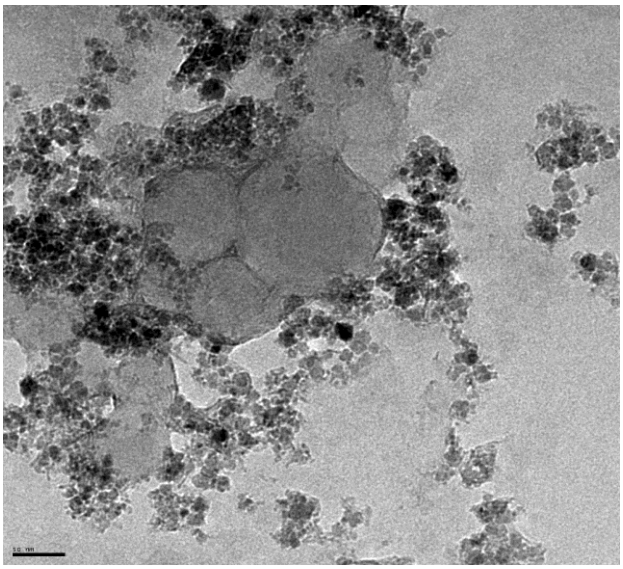


Fig. 6.17 TEM micrographs of 10-layer coated polystyrene sample coated with one layer of magnetite nanoparticles (prepared with sodium oleate), the scale bar is 50 nm

From Fig. 6.17, it can be clearly seen that the deposition of the magnetic nanoparticle layer was incomplete. There was only about 10-20% of the polystyrene particle surface covered by the magnetic nanoparticles. The reason for such a low coverage may be explained by the magnetic property of those nanoparticles. Due to the magnetic property, the magnetite nanoparticles formed some micro-aggregates in the suspension those micro-aggregates were not easily fully re-dispersed. Therefore, after the coating process, only those micro-aggregates and a few single particles attached to the surface of the polystyrene nanoparticles. Furthermore, such a low coverage led the zeta-potential having a very low level, which was close to 0. However, despite the low coverage, the magnetic particles attached onto the polystyrene particle surface can still provide a weak magnetic property. And if the external magnetic field (for example, in an MRI scanner) is strong enough, those nanocapsules could be monitored or directed inside the human body.

After the-core removal process, the nanocapsules coated with magnetic nanoparticles was analysed by TEM. The TEM pictures of the nanocapsules are shown in Fig. 6.18.

(a) (b)

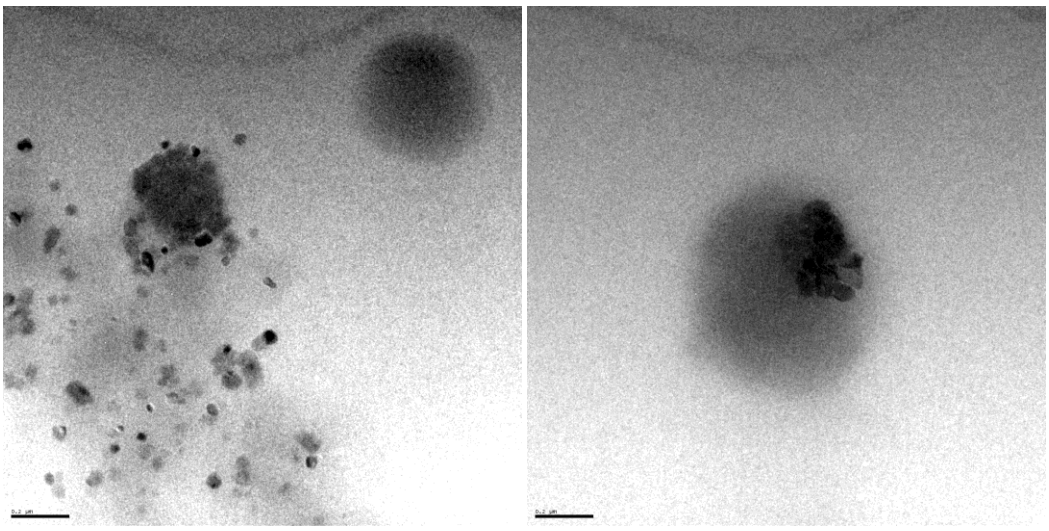


Fig. 6.18 TEM micrographs of nanocapsules consisting of 9-layer polyelectrolyte, one layer of laponite and one layer of magnetic nanoparticles, the scale bar in both graphs is 200 nm

From Fig. 6.18, only a few of nanocapsules were found after the core removal process. There may be 2 reasons to explain the disappearance of the nanocapsules. The first one is that after coated with magnetic particles the property of the nanocapsules were slightly changed and not strong enough to survive from the THF erosion. The other one is that after the core removal, the population density of the nanocapsules was much less than before and due to the little amount of sample used in the TEM analysis, the concentration of the nanocapsules did not represent the whole system. However, some nanocapsules can still be observed. In the Fig. 6.18 (a), a capsule attached with a cluster of magnetic particles can be seen and the shape of the nanocapsule did not change obviously. In Fig. 6.18 (b), there are 2 nanocapsules. One of them was coated with magnetic nanoparticles and the coverage is higher than the one in Fig. 6.18 (a), however, the shape of the capsule became irregular after the core-removal. There are

no obvious magnetite particles coated on the other nanocapsule, but the capsule remained spherical after the core removal process.

6.4 Conclusion

As a follow on from Chapter 5, in this Chapter, the polystyrene nanoparticles with smaller size (130 nm) were employed as core templates. The preparation of the polystyrene particles was almost the same as it was in Chapter 4 except for the adition of the surfactant sodium dodecylbenzene sulphonate (SDBS), to reduce the particl size. Following the same Layer-by-Layer process used in the Chapter 4, two different core-shell structures were obtained. The first one was 5 bi-layer of polyelectrolyte: CHI/DS; while the other one was roughly the same composition only that the 4^{th} layer was replaced by laponite. After dissolving in THF, the results showed that the capsules with a layer of laponite were mechanically more robust as most of the particles survived the dissolution of the polystyrene core by THF. Therefore, the core-shell structure with a layer of laponite was chosen for further modification in this Chapter. Two inorganic particles: gold and magnetite particles were prepared in this experiment; the gold particles had a size range of 4-10 nm; while the size was around 10 nm for the magnetite particles. Both inorganic particles were utilised as the outer layer to deposit onto the polystyrene particles which were already coated with polyelectrolytes and laponite: 8 layers of polyelectrolyte: CHI/DS and one layer of laponite for gold particles and 9 layers of polyelectrolyte: CHI/DS and one layer of laponite for magnetite particles. It was found that the coverage of the gold nanoparticles was higher and more even than that of the magnetite particles. That might be due to the gold particles were relatively smaller and had more regular shape than the magnetite particles. Finally, after the core-removal process, nanocapsules both covered with gold or magnetite particles were attempted to be fabricated. The gold coated nanoparticles were particularly well formed.

Chapter 7 Nanocapsules Consisting of Proteins and Polyelectrolyte

Multiple protein layers attached to solid surfaces have been broadly used in the areas of isolation, localisation and diagnostics in biotechnology [172]. Therefore, in this Chapter, the preparation of nanocapsules consisting of polyelectrolyte (pre-coating) and proteins will be discussed. The first part describes the preparation of nanocapsules with protein walls that were built on polystyrene core-templates and the second concerns the preparation of insulin nanoparticles and coating polyelectrolyte and protein layers onto those particles.

7.1 Nanocapsules Consisting of Proteins via Polystyrene Nanoparticles

7.1.1 Materials

The chemicals involved in this experiment were: Poly(diallydimethylammonium chloride) (PDADMAC) (20 wt% in water, Sigma Aldrich), Sodium Chloride (99.5% Sigma Aldrich), Dextran Sulfate Sodium Salt (DS) (Sigma), Tetrahydrofuran (THF), ≥99%, Aldrich), Bovine Serum Albumin (BSA) (≥98% (agarose gel electrophoresis), lyophilized powder, CAS Number 9048-46-8, molecular weight 66 kDa, Sigma-Aldrich), Lysozyme (from chicken egg white, dialyzed, lyophilized powder, 100000 U/mg, mol wt 14.3 kDa, CAS Number 12650-88-3, EC Number 235-747-3, Sigma-Aldrich), Buffer solution of pH 7.4 (Sigma-Aldrich), Buffer solution of pH 9.2 (BDH Chemicals Ltd.), Buffer solution of pH 10 (BDH Chemicals Ltd.), Polystyrene particles 480 nm (Prepared in Chapter 5), all water used was de-ionised water.

7.1.2 Methodology

7.1.2.1 Preparation of Polyelectrolyte Solutions and Protein Solutions

The polyelectrolyte solutions employed here were PDADMAC and DS. The reason why PDADAMAC was chosen over CHI is because PDADMAC can provide a relatively high value zeta-potential which was better for the protein layers to add on, and did not need to be acidified to become soluble. The PDADMAC and DS solution contained: 1 mg/ml polyelectrolyte, 0.1 M NaCl.

Two protein solutions: BSA and lysozyme were used here to make layers of the nanocapsules. The concentration of BSA solution is 2 mg/ml and for lysozyme solution, it is 4 mg/ml. All the proteins were dissolved in the pH 7.4 buffer solution. The pH measurement was described in Chapter 4 section 4.2.2: and each measurement of sample's pH was repeated one time to ensure the accuracy of the data (difference not larger than 0.1).

Bovine Serum Albumin (BSA) is a blood serum protein which has numerous applications including ELISAs (Enzyme-Linked Immunosorbent Assay), immunoblots, and immunohistochemistry [240]. The amino acid sequence of BSA is known and it is known to be sensitive to temperature changes and tends to agglomerate (which is irreversible) when the temperature increases [241]. The general structure of BSA is shown in Fig. 7.1. The isoelectric point (IEP) of BSA is 4.7 [241] and so this protein is negatively charged at pH 7.4.

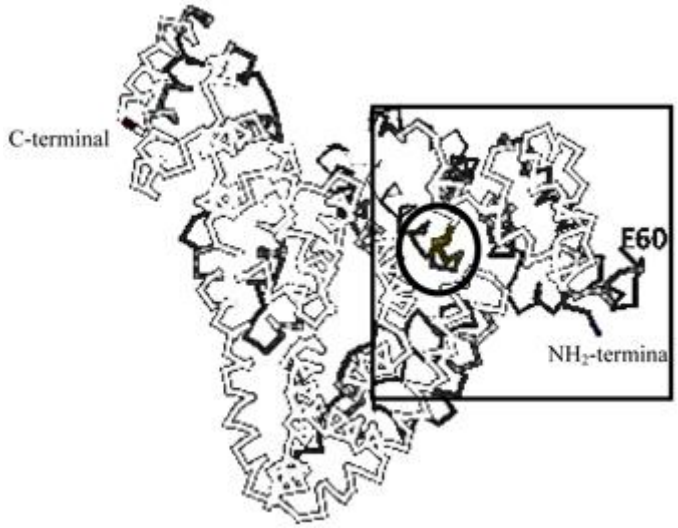


Fig. 7.1 The general structure of BSA [241]

Lysozyme is an of enzyme that can damage bacterial cell walls by hydrolyzing the polysaccharide component of the cell wall, which is part of the innate immune system, where it has been shown that an insufficient level of Lysozyme is associated with bronchopulmonary dysplasia in newborns [242]. It is normally found in secretions such as tears, milk, and saliva and is also present in egg white [243]. The general structure of lysozyme is shown in Fig. 7.2. The Isoelectric point of lysozyme is around pH 10.7 [244] and so this protein is positively charged at pH 7.4.

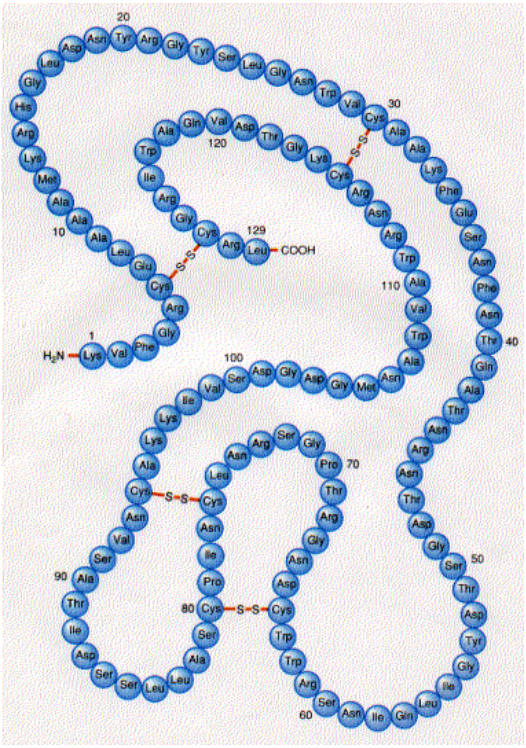


Fig. 7.2 The general structure of lysozyme [244]

7.1.2.2 Layer-by-Layer Self-assembly

The polystyrene particles with size range 483 ± 31 nm (prepared in Chapter 5 2.5 wt %) were used as core templates. To further confirm the proper number of pre-coated PE layers for lysozyme and BSA deposition. Three different samples which consisted of different numbers of polyelectrolyte layers (0, 1 and 3 layers respectively) were prepared via the LbL process. For the capsules consisting of polyelectrolyte and proteins, 2 batches of particle precursors were prepared before the protein's deposition: The first one was coated with 3 polyelectrolyte layers (PDADAMAC/DS/PDADMAC) and the other is coated with only one layer of PDADMAC. For the polymer layers, 5 ml of polystyrene particles were mixed with 10 ml of polyelectrolyte solution (1 mg/ml 0.1 M NaCl) and 10 ml of deionised water. Then the mixture was gently shaken for 1 hr. After shaking, the sample was centrifuged by a series of steps to separate the excess polymers from the coated particles (which followed the same process as that described in Chapter 5). Eventually the remaining particles were re-dispersed in 15 ml of

de-ionised water. After all the pre-coating layers, the particles were exposed to protein solutions to fulfil the whole LBL Self-assembly process. For the protein deposition, the procedure was the same, only the pH was adjusted to the desired pH. Unless otherwise stated all the solutions were of phosphate buffered saline solutions, at pH 7.4. The concentration of BSA solution was 2 mg/ml and for lysozyme was 4 mg/ml of protein. For the capsules consisting only of proteins, lysozyme was the first layer, and the same deposition method for the polyelectrolyte layers was adopted.

7.1.2.3 Core Removal

After the fabrication of the polymer and protein layers, the coated particles were treated with THF to dissolve the core templates. The volume ratio of the particle dispersion to THF was 1:2, and the mixture was kept for 48 hrs. After the dissolving, in order to remove the THF and polystyrene residue, the solution was centrifuged, re-dispersed in de-ionized water, and then dialyzed against de-ionized water. (See Chapter 5 for further details)

7.1.3 Results and Discussion

7.1.3.1 Salt Concentration

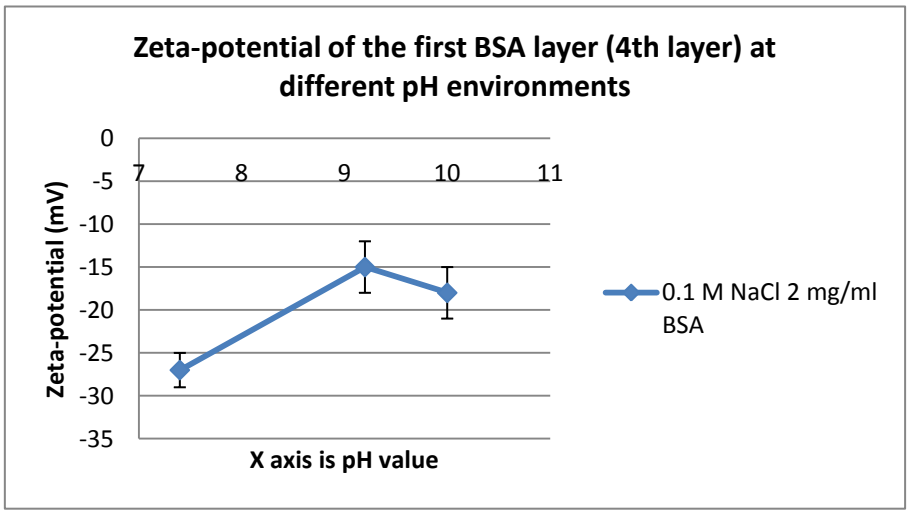
As it was mentioned in Chapter 5, 0.1 M NaCl was the electrolyte concentration used for the polyelectrolyte solutions to prepare the precursors for proteins deposition.

7.1.3.2 The pH Effect on Protein Deposition

As reported in the literature review, at room temperature, the structure and charge of protein mainly depend on the pH value of the solution [245]. Due to the presence of ionic functional groups (-COOH and $–NH_2$), at a certain pH a protein molecule will be

zero charged (called Isoelectric Point: IEP). For any pH value above Isoelectric Point, the protein molecules will be negatively charged while positively charged if it is below. The IEP value for BSA and Lysozyme is 4.7 [241] and 10.7 [244]. Therefore, a pH value between 4.7-10.7 ought to make BSA and Lysozyme charged oppositely. Therefore, 3 buffer solutions (pH7.4, pH9.2, pH10) were tested to explore the optimum pH value for alternating protein layer deposition. For the BSA, since it was negatively charged in the solution, thus, it was employed as the forth layer (after 3 PE layers) and lysozyme which is positively charge was used as the fifth layer (after 3 PE layers and one layer of BSA). The results of the first BSA and Lysozyme layer deposition are given in Fig. 7.3.

(a)



(b)

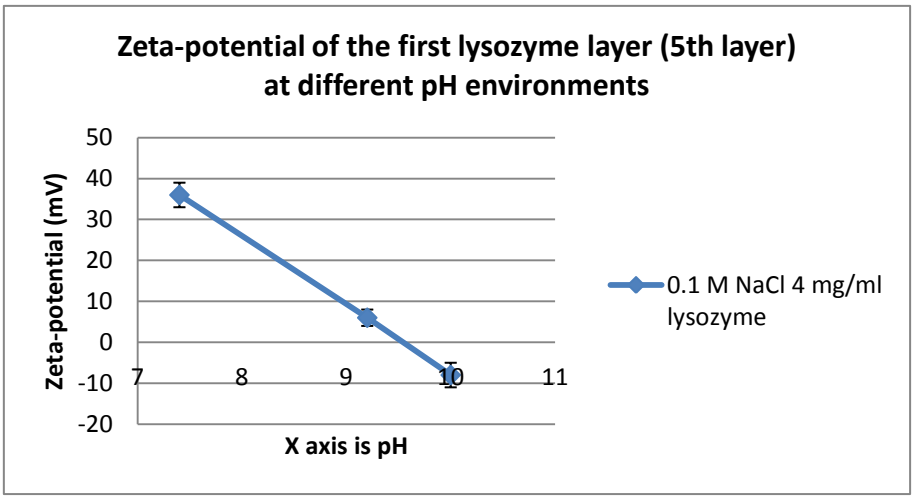


Fig. 7.3 Zeta-potentials of the first protein coating (4th and 5th layer of the coating process) at different pH values (pH7.4, pH9.2, pH10) (a) BSA (b) Lysozyme;

Zeta potential values are given in Appendix Table A.9 and Table A.10

From Fig. 7.3, it can be clearly noticed that compared with pH 9.2 and pH 10, pH 7.4 gave the largest difference in the zeta potential for the two proteins and so this pH was used for all subsequent experiments.

However, it was found that after coating with the lysozyme layers, the particles which were re-dispersed in the de-ionized water (pH 6) exhibited a higher zeta-potential values than those re-dispersed in the buffer solution (pH 7.4). That is because lysozyme was more positively charged in a lower pH medium (DI water pH-6). Therefore, instead of using the buffer solution, the particles with lysozyme as the outer layer were re-dispersed directly into de-ionised water, which provided the coated particles a relatively high zeta-potential value. Thus, the final coating and re-dispersion process is demonstrated as Table 7.1.

Table 7.1 Depositing and re-dispersing solution used in the protein (BSA/lysozyme) deposition experiments (left: dissolving solution, right: re-dispersing solution)

Coating layers	Coating and re-dispersion
Polyelectrolyte layers	0.1 M Salt solution/re-dispersed in deionised water (pH 6)
PDADMAC/BSA	Buffer solution (pH 7.4)/re-dispersed in buffer solution (pH 7.4)
BSA/Lysozyme	Buffer solution (pH 7.4)/re-dispersed in deionised water (pH 6)

7.1.3.3 Nanocapsules Self-assembly

7.1.3.3.1 The Precursor Polyelectrolyte Film and Nanocapsules Fabrication

According to Caruso [116, 172], when coating particles with layers which are not polyelectrolyte layers, (e.g. laponite or other inorganic particles) it is best practise to pre-coat the particles with at least three layers of polyelectrolyte before coating with the other material. Because the polyelectrolyte precursor could make the surface of the particle uniformly charged and smoother and this is necessary for the deposition of large molecules (e.g. proteins and other biomolecules) or nanoparticles (e.g. silica or laponite nanopatilces).

To further confirm whether it was necessary for protein layers, 3 batches of samples were prepared: a) No pre-coating of the particles; b) 1 polyelectrolyte pre-coating of the particles; c) 3 layers pre-coating of the particles sample. For the pre-coating layers,

positively charged PDADMAC and negatively charged DS were used as odd and even layers and for the rest of the layers, positively charged Lysozyme and negatively charged BSA were employed. The results are shown in Fig. 7.4.

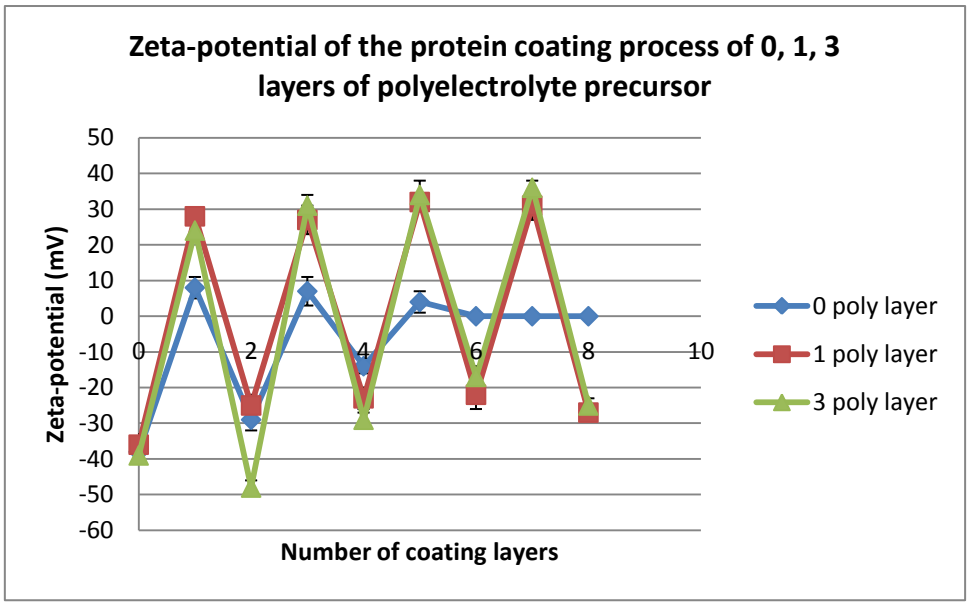


Fig. 7.4 The zeta-potential results of protein (BSA/lysozyme) coating processes started from different layers of polyelectrolyte (PDADMAC/DS) precursors (0, 1, 3 layers).

Zeta-potential values are given in Appendix Table A.11.

In Fig. 7.4, the result of the zeta-potential measurement indicates that if no polyelectrolyte layers were present then the zeta potential of the particles containing protein was low and after 6 layers became zero which led to particle aggregation. However, one layer and 3 layers pre-coated precursors were successfully coated with subsequent protein layers. With suitable buffer solutions and at least one pre-coating polyelectrolyte layer, the zeta-potential of the protein layers were at the similar level of the polyelectrolyte layers, which illustrated that the stability of the protein coated particles was acceptable. However, for the particles without any pre-coatings, it was found that after 6 layers, it was difficult to coat more layers on because the zeta-potential fell to zero, and some aggregation was found in the suspension.

Therefore, after the experiment, it was concluded at least one layer of polyelectrolyte pre-coating needed to fabricate nanocapsules consisting of proteins.

7.1.3.3.2 SEM Examination of the Protein Coated Particles

All the coated polystyrene particles were examined under the SEM to observe the final result of the LBL self-assembly process. Fig. 7.5 to Fig. 7.7 demonstrated the SEM results of the 3 different samples prepared in the last paragraph.

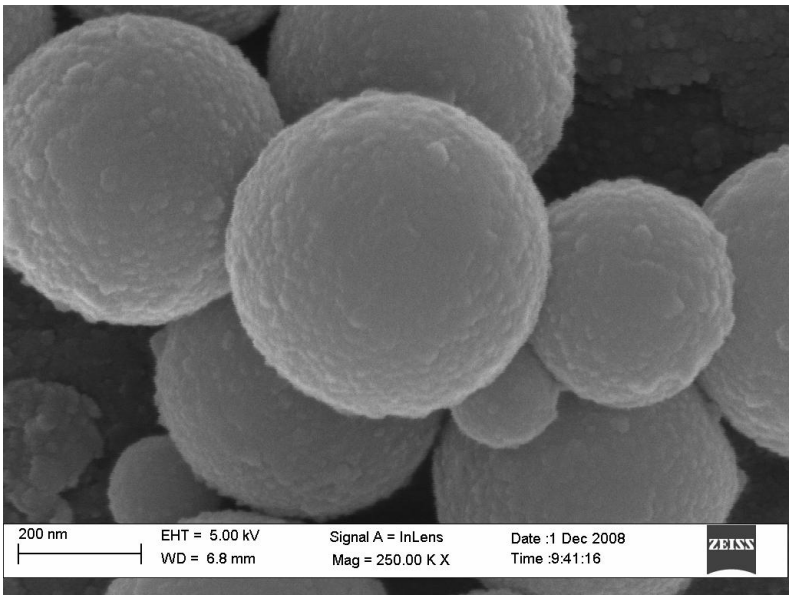


Fig. 7.5 SEM micrographs of polystyrene particles coated with 5 layers of proteins ((lysozyme/BSA)$_2$/lysozyme) without any polyelectrolyte layers

(a) (b)

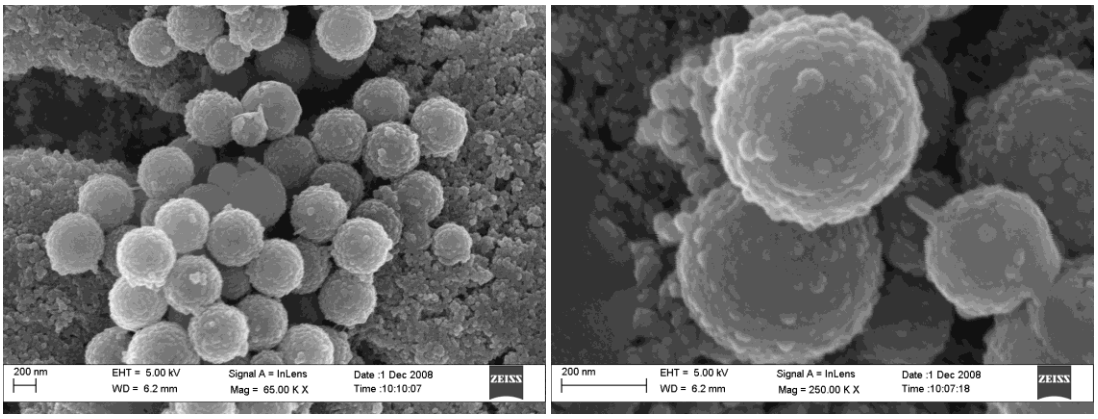


Fig. 7.6 SEM micrographs of polystyrene particles coated with 7 protein layers and 1 polyelectrolyte (PDADMAC/(BSA/lysozyme)$_3$/BSA) pre-coating layer

(a) (b)

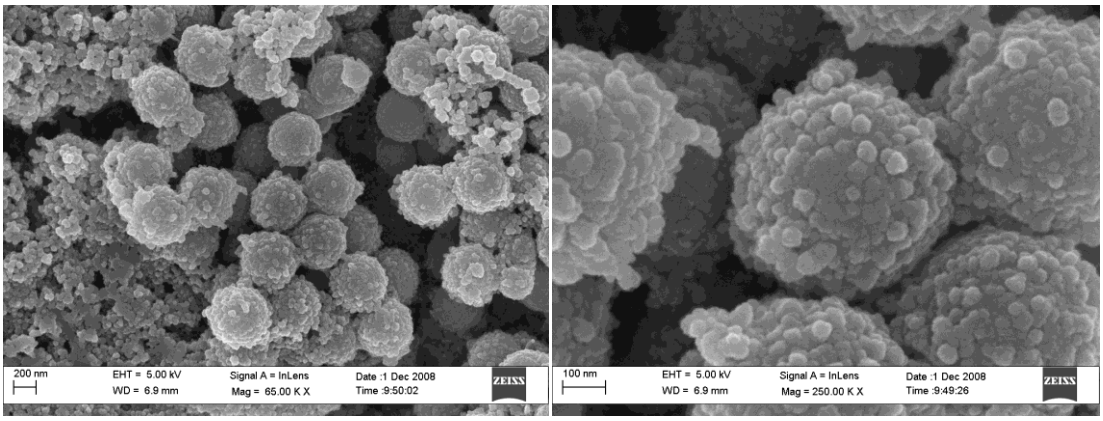


Fig. 7.7 SEM micrographs of polystyrene particles coated with 5 protein layers and 3 polyelectrolyte pre-coating layers (PDADMAC/DS/PDADMAC/(BSA/lysozyme)$_2$/BSA)

Comparing Fig. 7.5 with Fig. 7.6 and Fig. 7.7, the particles in Fig. 7.5 had a much smoother surface than those in Fig. 7.6 and Fig. 7.7. That may indicate the incomplete deposition of the protein layers, and explained why the zeta-potential of these particles fell to zero after 5 layers coating.

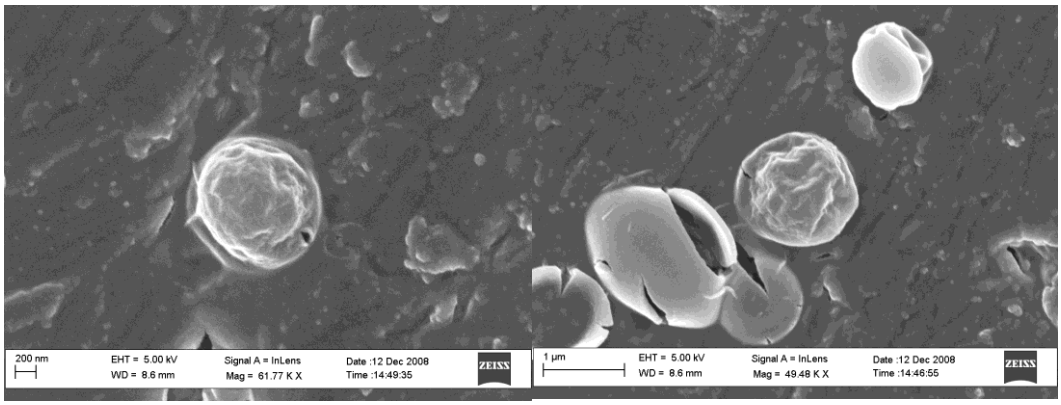
In Fig. 7.6 and Fig. 7.7, the surface of the particles was much rougher compared with particles coated with only polyelectrolyte layers (presented in Chapter 5 Fig. 5.9). That

can be explained by the size difference between protein molecules and polyelectrolyte molecules. Due to the much larger size of the protein molecules, the steric interaction was a barrier for proteins to form a tight and smooth layer as polyelectrolyte. Also, protein molecules had specific 3D structure in the aqueous solution, and this structure can be broken down when dried out the sample for SEM test, which gave the particles a relatively rough surface texture. It can also be noticed that the particles with 3 pre-coating layers of polyelectrolyte have a relatively rougher surface compared the ones with only 1 pre-coating layer. This may indicate that under the same circumstances, the particles with 3 pre-coating layers can adsorb more protein molecules at each stage. In both Fig. 7.6 and Fig. 7.7 there also appear to be some free protein molecules, e.g. particles smaller than 20 nm.

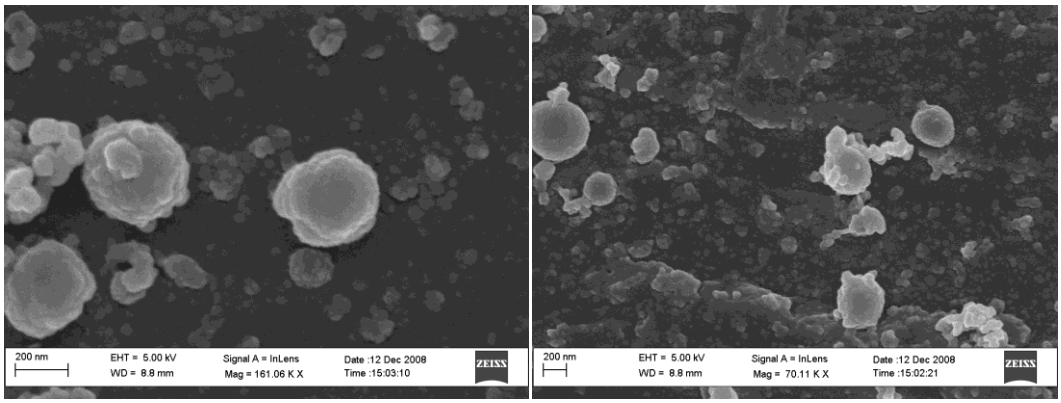
7.1.3.3.3 Core Removal

After dissolving in the THF and dialysed in the de-ionized water, the nano-particles remained in the suspension were investigated under SEM (Fig. 7.8 and Fig. 7.9) to confirm the removal of the core templates.

(a) (b)



(c) (d)



(e)

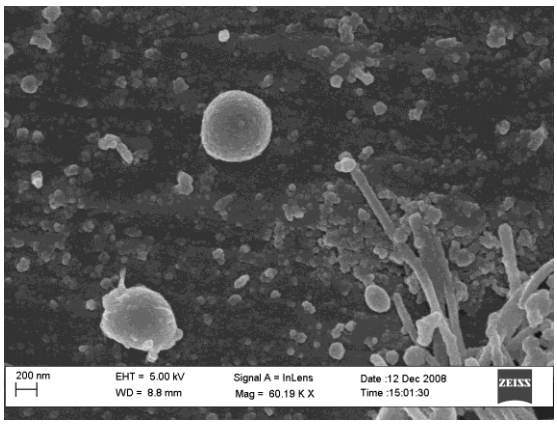


Fig. 7.8 SEM micrographs of capsules prepared from polystyrene particles pre-coated with 3 polyelectrolyte layers and 5 protein layers a) and b) core-removed capsules (deflated) larger than 700 nm, (c)-(e) core-removed capsules smaller than 500 nm

(a) (b)

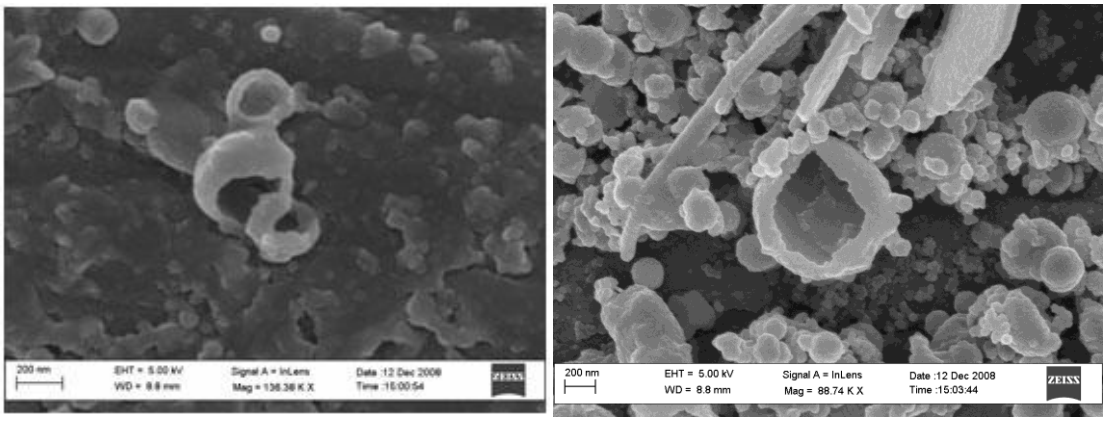


Fig. 7.9 SEM micrographs capsules prepared from polystyrene particles pre-coated with 1 polyelectrolyte layer and 7 protein layers. (a) and (b) are of different magnitude.

For the particles with only 1 polyelectrolyte pre-coating layer, most of the nano-capsules cracked after the core-removal process (Fig. 7.9), whereas, the nanocapsules with 3 pre-coating layers survived from the THF dissolution (Fig. 7.8). This comparison indicates that 3 polyelectrolyte pre-coating layers were better for preparing nano-capsules consisting of proteins. In Fig. 7.8 (a), (b), the 2 nano-capsules had a "deflated balloon" shape, and combined with the result in Fig. 7.9, the removal of the polystyrene particles can be confirmed. Fig. 7.8 (b), it can be noticed that the capsules with a size over 700 nm dried down to the background while the ones around 500 nm or less still held their original shape. In Fig. 7.8 (c)-(e). This may be because the capsules consisting of protein and polyelectrolyte were not as strong as the ones consisting of polyelectrolyte and laponite (Chapter 5). Therefore, if the capsules were too large it would be hard for them to keep the original spherical shape. In both Fig. 7.8 and Fig. 7.9, some rod-shape material can be seen, but before the removal of the polystyrene cores (Fig. 7.6 and Fig. 7.7), there are no such materials. In this case, these rod shaped features might be protein residue from the cracked capsules during the core-removal process.

7.2 Fabrication of Encapsulated Insulin Nanoparticles

After the preparation of the nanocapsules consisting of polyelectrolyte and proteins, the loading of insulin into those capsules is also discussed in this section, however, instead of loading insulin molecules directly into the fabricated nanocapsules, an alternative way which fabricates polyelectrolyte/protein nanocapsules directly onto the insulin nanoparticles is explored. In this method, by coating insulin particles with polyelectrolytes and proteins, the release rate of insulin in vivo could be controlled.

7.2.1 Materials

The chemicals involved in this experiment: Sodium Chloride (99.5% Sigma Aldrich), Dextran Sulfate Sodium Salt (DS) (Sigma), Bovine Serum Albumin (BSA) (≥98% (agarose gel electrophoresis), lyophilized powder, CAS Number 9048-46-8, molecular weight 66 kDa, Sigma-Aldrich), Lysozyme (from chicken egg white, dialyzed, lyophilized powder, 100000 U/mg, mol wt 14.3 kDa, CAS Number 12650-88-3, EC Number 235-747-3, Sigma-Aldrich),, Buffer solution of pH 7.4 (Sigma-Aldrich), Insulin (29USP units/mg, 14011-100MG, LOT#19K177657V, Pcode: 1000855643, CAS No. 11070-73-8) (Sigma-Aldrich). All water used is deionised water.

7.2.2 Methodology

7.2.2.1 Preparation of Insulin Nano-aggregates

Insulin nano-aggregates (100-230 nm in diameter) were prepared by a salting out method. According to Fan et al [17], the optimum salting out method for insulin nano-aggregates was at a pH of 1.1 and a NaCl concentration of 0.6 M. Therefore, in

this experiment, the insulin nano-aggregates were prepared by the following the method:

- 0.01 of g insulin was dissolved in 5 ml HCl solution (pH1.1).
- Then immediately after adding 0.1755 g of NaCl (0.6 M), the sample was stirred in an ice bath for 1 hr to make 2 mg/ml insulin nanoparticles suspension [17].

7.2.2.2 Fabrication of Nanocapsules onto the Insulin Nanoparticles

To separate the insulin nano-aggregates Fan et al. proposed a solution in which polyelectrolytes Poly(α,β-l-malic acid) (PMA) and chitosan were used and combined with ultra-sonicating to get insulin single nanoparticles coated with PMA and chitosan [17]. In this project, protein lysozyme and biocompatible polyelectrolyte dextran sulphate (DS) were employed to fabricate the nanocapsules onto insulin nanoparticles as an innovation.

To keep the insulin particles stable, the optimum condition (pH 1.1 0.6 M NaCl) for insulin precipitation was also applied in the protein and polyelectrolyte solution. Because BSA also salted out at the NaCl concentration of 0.6 M, lysozyme (protein) and dextran sulphate sodium salt (biocompatible polyelectrolyte) were employed as the encapsulating material, and the lysozyme and DS were also dissolved in the same solution (pH 1.1 0.6 M NaCl). Because insulin particles in the suspension were positively charged, DS (1 mg/ml negatively charged) and lysozyme (5 mg/ml positively charged) were used as odd and even layers respectively. 5 ml of 1 mg/ml DS solution were added into 5 ml insulin suspension (2 mg/ml), and the mixture was stirred in the ice bath for 20 min. After that, the suspension was kept in the ultrasonic bath for 2-5 min to ensure the separation of the insulin nanoparticles and the deposition

of the polyelectrolyte/protein. Then the suspension experienced 2 cycles of centrifugation/re-dispersion to remove the excess polyelectrolyte. The particles were centrifuged at 4560 g for 3 min, and re-dispersed in the solution (pH 1.1 0.6 M NaCl) with the aid of an ultra-sonic bath; the re-dispersion time was 5 min. Because all the reactions occurred at a temperature close to 0 ℃, ice was added to the ultra-sonic bath to control the temperature below 4 ℃.

After coating with a DS layer, 5 ml of 5 mg/ml lysozyme was added into the suspension, and followed the same procedure as that used in the DS deposition. By repeating the deposition procedure, 8 layers of polyelectrolyte/protein nanocapsules were built onto the insulin nanoparticles. The 8-layer coated sample was then stored in the refrigerator.

7.2.3 Results and Discussion

7.2.3.1 Preparation of Insulin Nano-aggregates

It had been found that pH and ionic strength were two important factors affecting insulin solubility [17]. It also been indicated by Fan et al. [17] that insulin would dissolve instantly if the pH of the solution was lower than 2.0. That is because the IEP of insulin is 5.5 and at low pH, insulin molecules are more highly charged, therefore, they are more easily to be torn apart by the water molecules. For the ionic strength, it has been found that 0.55 M NaCl is a critical concentration for the insulin precipitation [17]. Any concentration above 0.55 M would lead insulin to precipitate at the pH 1.1. Hence, 0.6 M NaCl and pH 1.1 were chosen to prepare the insulin nanoparticles (size 100-230 nm) Fig. 7.10.

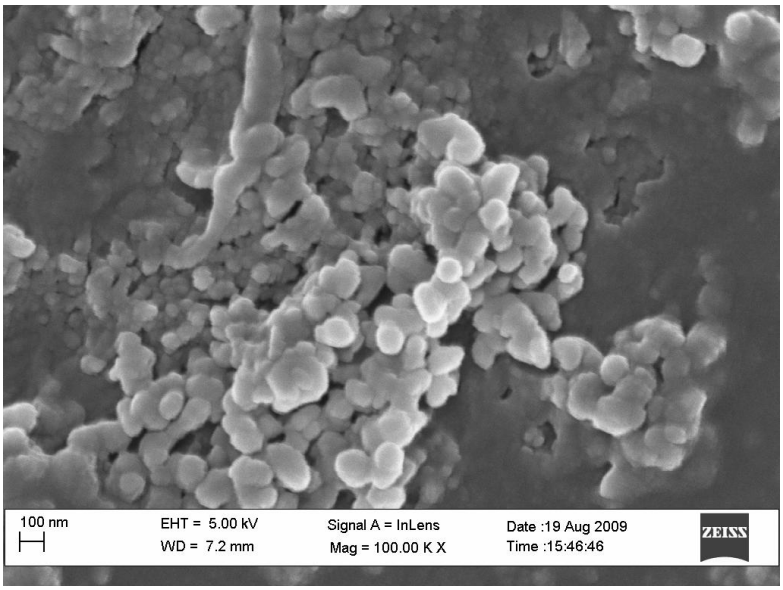


Fig. 7.10 SEM micrograph of insulin micro-aggregates salted out from suspension (0.6 M NaCl, pH 1.1)

From Fig. 7.10 , it can be observed that most of the insulin particles appear aggregated together. Furthermore, light scattering indicated the particle size lay in the μm range, which is different to the experiment carried out by Fan et al [17]. This difference is likely to be because the insulin particles tended to form some micro-aggregates in the suspension. However, the aggregation was reversible as by the addition of dextran sulphate, the insulin particles would de-aggregate and form polyelectrolyte coated single particles. Likewise single particles also formed during successive adsorption of lysozyme and more dextran sulphate layers (Fig. 7.11). As will be seen in the SEM images presented later, the dextran sulfate – lysozyme – ultrasonic treatment was successful in breaking down the insulin nanoparticle aggregates into individual insulin nanoparticles.

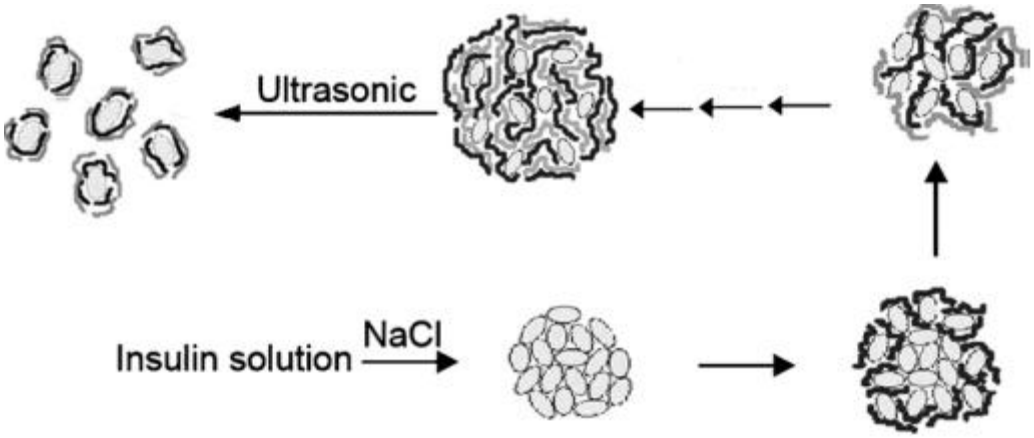


Fig. 7.11 Scheme of the LbL adsorption of negatively charged polyelectrolyte (black strings) and positively charged polyelectrolyte (grey strings) on insulin particles [17].

De-ionised water was used here to test the stability of the insulin aggregates. By simply re-dispersing the insulin aggregates into de-ionised water, it was found that the solution turned transparent, which indicated the release of insulin from the coated aggregates. It was therefore ensured that the acidic condition (0.6 M NaCl pH1.1) was strictly followed during any process involving insulin nano-aggregates. Also de-ionized water can be considered as a releasing medium for the future research.

7.2.3.2 Encapsulation of Insulin Nano-aggregates

7.2.3.2.1 Zeta-potential Measurement

Zeta-potential measurements were used to monitor the deposition of dextran sulfate and lysozyme onto the insulin nanoparticles the results are shown in Fig. 7.12.

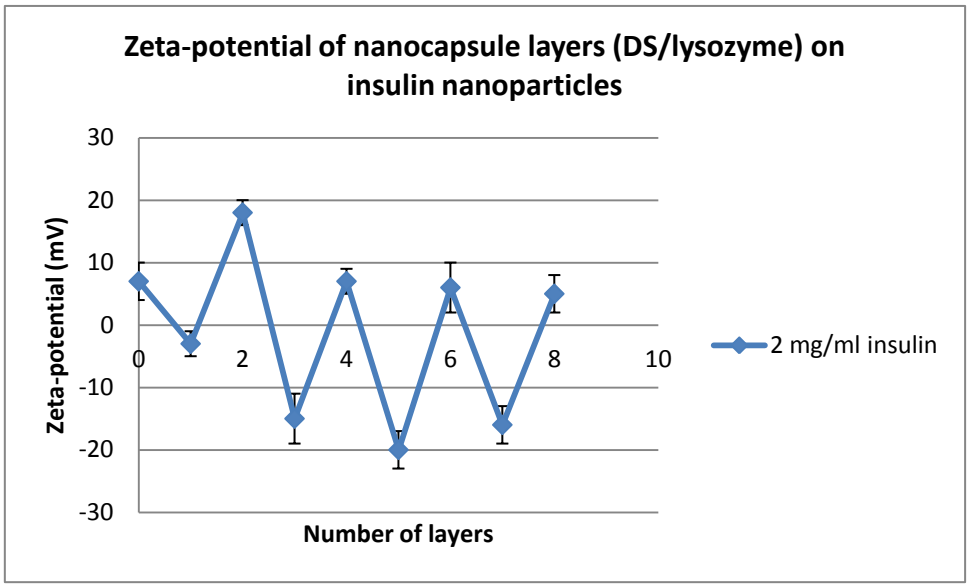


Fig. 7.12 Zeta-potential of the layers (DS/lysozyme) of the coated onto insulin nano-particles.

The values of the zeta-potentials are displayed in the Appendix Table A.12.

From Fig. 7.12, the shift of the zeta-potential confirmed the layer deposition on the insulin nano-particles. The IEP of insulin is 5.5, so the insulin particles were likely to be positively charged in the suspension (0.6 M pH 1.1) and the bare particle zeta-potential was found to be 6 mV. The zeta potential of the insulin particles was low (compared with the polystyrene and silica particles) and accounts for the aggregation of the insulin nanoparticles. The zeta potential was low for the coated particles too however, the particles were very stable during the whole process, and no obvious aggregation was noticed through the whole Layer-by-Layer procedure. Although the zeta-potential was low, charge reversal was occurring, which illustrated most of the particle surface were covered with the new polyelectrolyte or protein after each coating step.

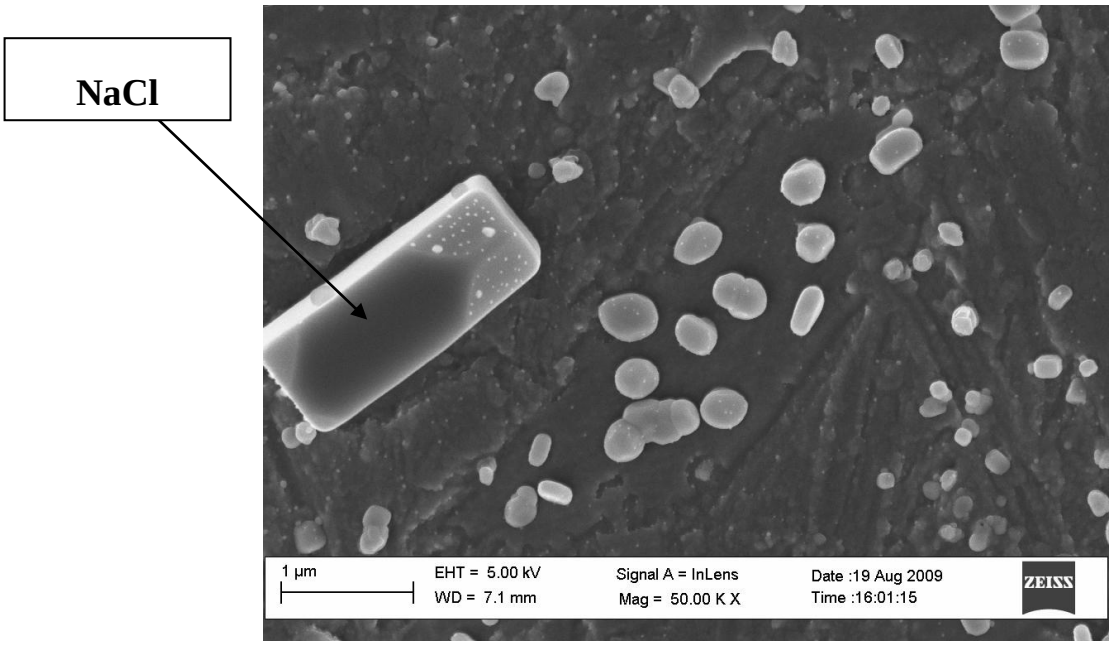
It can be seen from Fig. 7.12 that the zeta-potential of the first layer was relatively lower than the others. This may be because at first, the insulin nano-particles formed micro-aggregates in the suspension and it was hard for the DS molecules to squeeze into the gaps between the particles and cover the whole surface. However, with the deposition of further layers, the insulin particle clusters separated to single insulin particles and more and more polyelectrolyte or protein molecules could be added onto the surface of these particles, which resulted in the zeta-potential staying above 5 mV (absolute value).

7.2.3.2.2 SEM Measurement of the Coated Insulin Particles

After being coated with 8 layers (DS/lysozyme) of polyelectrolyte and protein, the suspension which contained encapsulated insulin nanoparticles was dried out and observed in an SEM to check the result of the Layer-by-layer procedure.

As was stated earlier and illustrated in Fig. 7.11, after coating with polyelectrolyte or protein, the insulin micro-aggregates would separate to single insulin nanoparticles [17]. Fig. 7.13 shows the insulin particles after the Layer-by-Layer procedure. From both micrographs, it can be clearly seen the insulin micro-aggregates disappeared and insulin single particles with a reasonably narrow distribution (50-200 nm) were well dispersed in the suspension.

(a)



(b)

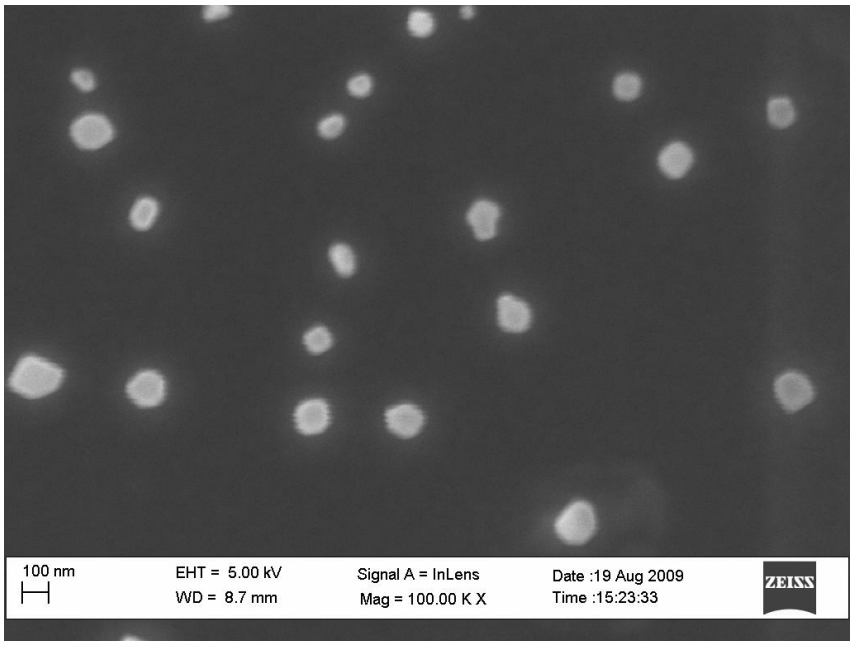


Fig. 7.13 SEM micrographs of 8 layers ((DS/lysozyme)$_4$) coated insulin nano-particles; (a) (b) represent different magnification

From micrographs 7.13 (a), some large crystals were also observed. However, it has been observed by Fan at el [17], that the shape of insulin particles via this salting out method was irregular, mainly elliptical although some can be rhombohedra [17] (Fig. 7.14), so these large particles cannot be insulin particles. Considering the high salt concentration of the suspension, those large crystals are likely to be the crystals of sodium chloride, which were formed during the drying out process. The size of the NaCl crystals varied from hundreds of nanometers to microns (Fig. 7.15). To remove the sodium chloride, the suspension can be centrifuged and the residue can be re-dispersed in the ethanol to avoid the dissolving of insulin nano-particles [17]. Fig. 7.13 a and b show the insulin particles coated 8 layers of polyelectrolyte and protein. The irregular shape of the insulin particles was well observed and despite of the irregular shape, most of the nano-particles stayed within the size range (50-200 nm).

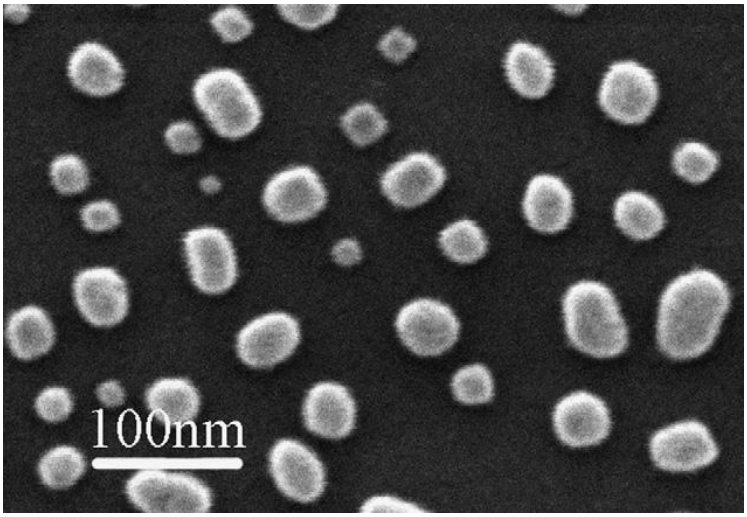


Fig. 7.14 The SEM photograph of the insulin–polyelectrolyte nanoparticles with six polyelectrolyte adsorption cycles from Fan et al.'s work [17]

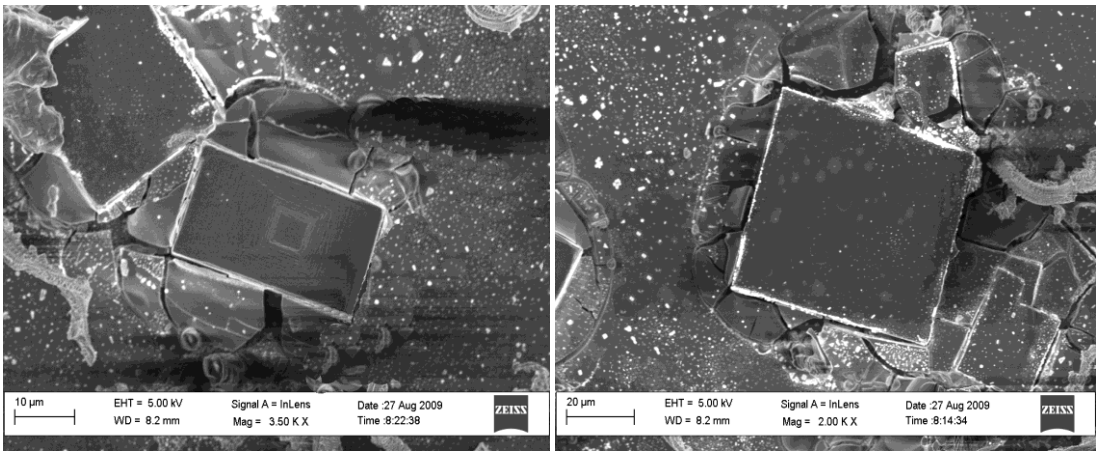


Fig. 7.15 Large NaCl crystals formed during the drying out process

7.3 Conclusion

In this Chapter, the preparation of nanocapsules consisting of polyelectrolyte (as precursor layer) and proteins was discussed. The number of precursor layers was also discussed and 3 paralleled experiments were carried out to testify the optimum number of the precursor layers. It was found 3 precursor layers of PDADMAC/DS/PDADMAC is optimum for the protein layers to deposit. In that case, nanocapsules consisting of 3 precursor layers and 5 layers of protein: BSA/ Lysozyme/BSA/Lysozyme/BSA were fabricated onto the polystyrene particles and hollow capsules were obtained after the core removal process. Furthermore, the application of the polyelectrolyte/protein nanocapsules was discussed. Instead of loading drug molecules directly into the hollow capsules, an alternative way was used in this experiment and insulin as the loading material was treated via salting out method, which produced insulin nanoparticles (50-200 nm). Then the protein and polyelectrolyte layers were deposited onto the insulin nanoparticles and protein/polyelectrolyte nanocapsules loaded with insulin crystals were finally prepared.

Chapter 8 Conclusions and Recommendations for Future Work

8.1 Conclusions

The main objective of this project was to prepare nanocapsules suitable for a drug delivery system. In the experiment, the Layer-by-Layer self-assembly method was employed and combined with core-sacrificial technique to fabricate hollow nanocapsules which consist of biocompatible polyelectrolytes. At first, nanocapsules of a relatively new size range (less than 200 nm) were prepared based on two types of nanoparticles: silica and polystyrene nanoparticles. Then, gold and magnetite particles were used in this project to functionalise the prepared nanocapsules and other combinations of capsule materials (which were also novel innovations of this work): polyelectrolyte/protein, protein/protein were also investigated. Finally, the loading of effective components into the capsules was achieved by encapsulating insulin nanoparticles with polyelectrolyte and protein.

In this thesis, two types of nanoparticles: silica and polystyrene were used as core templates on which to prepare the required nanocapsules. Firstly, the preparation of these two nanoparticles was discussed. The silica nanoparticles were prepared via the hydrolysis of TEOS. Because TEOS and water are immiscible, ethanol was employed as the medium for this reaction and NH_4OH was used as a catalyst. By controlling the ratio of NH_4OH and TEOS, silica nanoparticles of different size range were produced (sizing from 95 ± 14 nm to 250 ± 38 nm). Furthermore, the reaction time was tested and 8 hrs was found to be the minimum length for this reaction. On the other hand, the polystyrene particles were obtained from the polymerization of the styrene monomer. The initiator of the reaction was potassium persulphate; and by preparing the particles

with or without surfactant (SDBS), polystyrene particles of two size ranges (130 ±31nm, 480 ±30 nm) were prepared. After the reaction both of the silica and polystyrene particle suspensions were dialysed against deionised water to remove any unreacted materials.

The silica nanoparticles with size of 95 ±14 nm and 114 ±12 nm were chosen as core templates. Chitosan (CHI) and Dextran sulphate (DS) were employed as capsule materials to fabricate nanocapsules onto the chosen silica nanoparticles. The concentration of sodium chloride of each polyelectrolyte solution was verified and it was found the optimum concentration was 0.1 M. Also the deposition time of each polyelectrolyte layer was tested and a time of 15 min was found to be sufficient for adsorption, although onger times could be used. Following the LbL process, the deposition of 9 layers of polyelectrolyte (CHI/DS) was achieved and each layer's deposition was confirmed by the switch of the zeta potential of the particles surface from negative to positive. After all layers' deposition, the particle suspensions were mixed with HF/NH_4F buffer solution to remove the silica nanoparticles and the hollow nanocapsules were obtained. However, judging from the TEM micrographs (Fig. 4.15, Fig. 4.17), although it was clearly seen that some hollow capsules were formed after the HF dissolution, some of the capsules collapsed due to the lack of strength of the capsules to survive the harsh dissolution conditions. In that situation, the collapsed capsules formed polymer residues and might crosslink the intact capsules together, which could possibly affect the loading and releasing procedure based on these nanocapsules. The reason why these capsules were easily collapsed during the erosion of the acid is because the size of the core templates is less than 200 nm which is much smaller than several hundred nanometres or even microns (as mentioned in earlier literature [131]), and the higher curvature of those capsules resulted in thinner thickness of the capsule which means weaker capsule strength.

Therefore, polystyrene nanoparticles were then used as core templates to prepare stronger nanocapsules. Except for polyelectrolytes, various materials including laponite, proteins, and gold and magnetite nanoparticles were also added onto the polystyrene particles as capsule materials.

Laponite particles which are clay particles were used as capsule layers to strengthen the nanocapsules. By the comparison of the polystyrene particles coated with only polyelectrolytes, one layer of laponite and many layers of laponite, it was found, after the core removal, the nanocapsules comprised of only polyelectrolyte were collapsed, due to the insufficient strength of the nanocapsules and nanocapsules of several laponite layers were also collapsed and formed some bowl-shaped hollow capsules, which might because the wall of the capsules is too thick. In that case, the nanocapsules of one layer of laponite and polyelectrolyte was found to be the most suitable composition and in this experiment nanocapsules consisting of 5 CHI/DS bi-layers plus one CHI/Laponite bi-layer were obtained after the core-removal process.

In order to functionalize the nanocapsules obtained after the removal of the polystyrene particles, further modifications of the capsule surfaces were attempted on the nanocapsules based on the polystyrene nanoparticles of 130 ± 30 nm in this project. Gold nanoparticles and magnetite nanoparticles were both prepared in this experiment. The size of the gold nanoparticles is around 4 nm while it is about 10 nm for the magnetite nanoparticles. The gold and magnetite nanoparticles were deposited onto pre-coated polystyrene nanoparticles separately and after the core removal process, the nanocapsules of 4 layers of CHI/DS bi-layers plus one layer of CHI/Gold and those of 5 layers of CHI/DS bi-layers plus one layer of Magnetite were both obtained.

Then nanocapsules consisting of polyelectrolyte and proteins were prepared. It was found 3 precursor layers is optimum for the protein deposit. Therefore, the polystyrene nanoparticles (480±31 nm) were pre-coated with three layers of polyelectrolyte (PDADMAC/DS/PDADMAC) before any protein molecules' (lysozyme BSA) deposition. In that case, nanocapsules consisting of 3 precursor layers and 5 layers of protein: BSA/ Lysozyme/BSA/Lysozyme/BSA were fabricated onto the polystyrene particles and hollow capsules were obtained after the core removal process.

By the final part of the project, loading drug molecules into the protein/polyelectrolyte nanocapsules was achieved in an alternative way. Insulin which is an effective drug component was salted out to form nanoparticles. The nanoparticles which are within 50 nm to 200 nm were then coated with the polyelectrolyte/protein layers and the nanocapsules loaded with drug molecules were finally obtained.

8.2 Recommendation for Future Work

From the results of this project, the nanocapsules consisting of biocompatible materials were prepared and the insulin loaded nanocapsules were also obtained. Based on the potential use of this area, it is suggested that some further researchin this area be undertaken, which is summarized as follows:

1. In this project, it was found that as a core template, neither silica nor polystyrene were the ideal option. Silica as an inorganic core template could be completely removed from the inner capsule; however, due to the harsh conditions involved in the dissolving process, the productivity of the nanocapsules was relatively low, furthermore the hazardous nature of

hydrofluoric acid would preclude its use for drug delivery. On the other hand, because polystyrene is a high molecular weight material, it is hard to completely remove it by the chemical erosion. Therefore, new core materials are required to overcome those flaws. Calcium phosphate nanoparticles could be employed as an alternative core template because the monodispersed particles are easily to be prepared and could be completely dissolved in diluted HCl.

2. As it was mentioned in the Chapter 5 and 6, the nanocapsules with a high strength are preferable either in surviving from the chemical dissolution or in the further research. Therefore, like Laponite to the polystyrene particles, some new materials which are not sensitive to HF could be introduced to the silica system to strengthen these nanocapsules.

3. Based on the nanocapsules obtained both from silica and polystyrene core templates, the process of loading and releasing of drug molecules could be applied. In order to trace the drug molecules conveniently, the molecules with the property of fluorescence and doxyrubicin are recommended for initial study, due to their ready availability, modest cost, and easy monitoring.

4. Because the insulin molecules had been successfully loaded into the nanocapsules of protein/polyelectrolyte, the active release process could be carried out in the future. By adjusting the pH and salt concentration of the suspension, different release rates of the insulin molecules could be expected.

5. As the insulin molecules were pre-loaded into the nanocapsules, some porous nanoparticles into which insulin could be loaded could also be used in the future, as the required molecules can be loaded into the pores of the

particles before any layer deposition. This process could skip the loading step after the hollow capsules obtained, which assures a high loading rate of the required molecules.

Like the gold and magnetite particles mentioned in Chapter 6, different types of particles or molecules are recommended for the future work to modify the surface of the nanocapsules, which would present new properties to those nanocapsules. For example, the deposition of antibody can lead the capsules more precisely to target site of release.

Appendix

Table A.1 The zeta-potential of each polyelectrolyte layer coated on 95 nm silica particles (CHI/DS)

Number of Layers	Zeta-potential(mV)
0	-38 ±3
1	+28 ±4
2	-32 ±3
3	+58 ±5
4	-26 ±2
5	+51 ±4
6	-30 ±3
7	+53 ±2
8	-25 ±3
9	+56 ±4

Table A.2 The zeta-potential of each polyelectrolyte layer coated on 114 nm silica particles (CHI/DS)

Number of Layers	Zeta-potential(mV)
0	-46 ±2
1	+36 ±1
2	-52 ±3
3	+57 ±2
4	-49 ±4
5	+56 ±2
6	-31 ±2
7	+51 ±3
8	-32 ±4
9	+40 ±5

Table A.3 Zeta-potential of polyelectrolyte layers (PE 1 mg/ml) on polystyrene particles (480 nm) at different salt concentrations

	Zeta-potential		
Layer	0M NaCl	0.1M NaCl	0.5M NaCl
Polystyrene	-48 ±3	-45 ±2	-49 ±3
PDADMAC	+18 ±2	+25 ±3	+24 ±1
DS	-16 ±2	-48 ±2	-36 ±4
PDADMAC	+20 ±1	+31 ±3	+26 ±3

Table A.4 The zeta-potential of each coating layer (consisting of only synthetic polyelectrolytes PDADMAC(odd)/PSS(even)), the concentrations: PE 1 mg/ml, NaCl 0.1 M, Laponite 10 mg/ml on 480 nm PS particles

Number of Layers	Zeta-potential(mV)
0	-48 ±2
1	+45 ±3
2	-47 ±1
3	+52 ±4
4	-46 ±4
5	+49 ±2
6	-41 ±3
7	+52 ±4
8	-41 ±3
9	+48 ±2
10	-40 ±4

Table A.5 The zeta-potential of each coating layer (Consisting of synthetic polyelectrolytes and Laponite particles, PDADMAC/PSS/(PDADMAC/Laponite)$_8$), the concentrations: PE 1 mg/ml, NaCl 0.1 M, Laponite 10 mg/ml on 480 nm PS particles

Number of Layers	Zeta-potential(mV)
0	-46 ±2

1	+43 ±1
2	-45 ±3
3	+52 ±1
4	-23 ±4
5	+46 ±2
6	-24 ±3
7	+50 ±4
8	-31 ±2
9	+46 ±1
10	-29 ±4
11	+46 ±5
12	-25 ±3
13	+36 ±3
14	-34 ±5
15	+36 ±6
16	-26 ±4
17	+32 ±3
18	-31 ±5

Table A.6 The zeta-potential of each coating layer (Consisting of bio-compatible polyelectrolytes and Laponite particles, $(CHI/DS)_5$/CHI/Laponite), the concentrations: PE 1 mg/ml, NaCl 0.1 M, Laponite 10 mg/ml on 480 nm PS particles

Number of Layers	Zeta-potential(mV)
0	-45 ±3
1	+26 ±2
2	-37 ±3
3	+34 ±1
4	-34 ±4
5	+24 ±3
6	-42 ±2
7	+27 ±3
8	-38 ±4
9	+24 ±2
10	-30 ±4
11	+21 ±3
12	-25 ±3

Table A.7 Zeta-potential of nanocapsules consisting of 10 layers of biocompatible polyelectrolyte ($(CHI/DS)_5$) on 130 nm PS particles

Number of Layers	Zeta-potential (mV)
0	-50 ±3
1	+22 ±2
2	-50 ±2
3	+28 ±3
4	-43 ±4
5	+23 ±2
6	-46 ±1
7	+21 ±4
8	-42 ±3
9	+19 ±4
10	-40 ±2

Table A.8 Zeta-potential of nanocapsules consisting of 9-layer biocompatible polyelectrolytes (CHI/DS) and one layer laponite (the 4th layer) on 130 nm PS particles

Number of Layers	Zeta-potential(mV)
0	-48 ±2
1	+25 ±3
2	-50 ±1
3	+26 ±2
4	-34 ±4
5	+25 ±3
6	-42 ±1
7	+19 ±2
8	-39 ±3
9	+23 ±2
10	-37 ±3

Table A.9 The zeta-potential of the first BSA layer (4th layer after 3 polyelectrolyte layers) on PS cores (480 nm) at different pH environments

pH	Zeta-potential(mV)
7.4	-27 ±2
9.2	-15 ±3
10	-18 ±3

Table A.10 The zeta-potential of the first Lysozyme layer (5th layer after 3 polyelectrolyte layers and one BSA layer) on PS cores (480 nm) at different pH environments

pH	Zeta-potential(mV)
7.4	+36 ±3
9.2	+6 ±2
10	-8 ±3

Table A.11 The zeta-potential of the coating process on polystyrene particles contained different number of pre-coating polyelectrolyte (PDADMAC/DS) layers the rest layers are proteins (BSA (-)/lysozyme(+)) on 480 nm PS particles

Number of Layers	Zeta-potential (mV)		
	0 Polyelectrolyte	1 Polyelectrolyte	3 Polyelectrolyte
0	-45 ±2	-48 ±3	-46 ±2
1	+8 ±3	+28 ±2	+24 ±3
2	-29 ±3	-25 ±3	-48 ±2
3	+7 ±4	+27 ±4	+31 ±3
4	-14 ±2	-23 ±3	-29 ±2
5	+4 ±3	+32 ±2	+34 ±4
6	0.00	-22 ±4	-17 ±3
7	0.00	+31 ±4	+36 ±2
8	0.00	-27 ±2	-25 ±2

Table A.12 Zeta-potential of the layers of coated on insulin nano-particles (DS (odd layers)/lysozyme(even layers))

Number of layers	Zeta-potential(mV)
0	+7 ±3
1	-3 ±2
2	+18 ±2
3	-15 ±4
4	+7 ±2
5	-20 ±3
6	+6 ±4
7	-16 ±3
8	+5 ±3

Reference

[1] Caruso F. Hollow capsule processing through colloidal templating and self-assembly. Chem-Eur J 2000;6:413-9.
[2] Daneshpour N, Griffin M, Collighan R, Perrie Y. Targeted delivery of a novel group of site-directed transglutaminase inhibitors to the liver using liposomes: a new approach for the potential treatment of liver fibrosis. Journal of Drug Targeting 2011;19:624-31.
[3] Caruso F, Yang WJ, Trau D, Renneberg R. Microencapsulation of uncharged low molecular weight organic materials by polyelectrolyte multilayer self-assembly. Langmuir 2000;16:8932-6.
[4] Wilcox DL. Hollow and solid spheres and microspheres: science and technology associated with their fabrication and application. the University of Michigan: Material Research Society; 1995.
[5] Letchford K, Burt H. A review of the formation and classification of amphiphilic block copolymer nanoparticulate structures: micelles, nanospheres, nanocapsules and polymersomes. European Journal of Pharmaceutics and Biopharmaceutics 2007;65:259-69.
[6] Antipov AA, Sukhorukov GB. Polyelectrolyte multilayer capsules as vehicles with tunable permeability. Advances in Colloid and Interface Science 2004;111:49-61.
[7] Sahu A, Lambris JD. Structure and biology of complement protein C3, a connecting link between innate and acquired immunity. Immunological Reviews 2001;180:35-48.
[8] Gref R, Domb A, Quellec P, Blunk T, Muller RH, Verbavatz JM, et al. The controlled intravenous delivery of drugs using PEG-coated sterically stabilized nanospheres. Advanced Drug Delivery Reviews 1995;16:215-33.
[9] Douglas SJ, Davis SS, Illum L. Nanoparticles in drug delivery. Critical reviews in therapeutic drug carrier systems 1987;3:233-61.
[10] Moghimi SM, Szebeni J. Stealth liposomes and long circulating nanoparticles: critical issues in pharmacokinetics, opsonization and protein-binding properties. Progress in Lipid Research 2003;42:463-78.
[11] Juliano RL, Stamp D. Effect of particle-size and charge on clearance on clearance rates of liposomes and liposome encapsulated drugs. Biochemical and Biophysical Research Communications 1975;63:651-8.
[12] Senior JH. Fate and behavior of liposomes invivo - a review of controlling factors. Crc Critical Reviews in Therapeutic Drug Carrier Systems 1987;3:123-93.
[13] Vonarbourg A, Passirani C, Saulnier P, Benoit JP. Parameters influencing the stealthiness of colloidal drug delivery systems. Biomaterials 2006;27:4356-73.
[14] Cortez C, Tomaskovic-Crook E, Johnston APR, Scott AM, Nice EC, Heath JK, et al. Influence of size, surface, cell line, and kinetic properties on the specific binding of A33 antigen-targeted multilayered particles and capsules to colorectal cancer cells. ACS Nano 2007;1:93-102.
[15] Cortez C, Tomaskovic-Crook E, Johnston APR, Radt B, Cody SH, Scott AM, et al. Targeting and uptake of multilayered particles to colorectal cancer cells. Advanced Materials 2006;18:1998-+.

[16] Caruso F, Lichtenfeld H, Donath E, Mohwald H. Investigation of electrostatic interactions in polyelectrolyte multilayer films: Binding of anionic fluorescent probes to layers assembled onto colloids. Macromolecules 1999;32:2317-28.
[17] Fan YF, Wang YN, Fan YG, Ma JB. Preparation of insulin nanoparticles and their encapsulation with biodegradable polyelectrolytes via the layer-by-layer adsorption. Int J Pharm 2006;324:158-67.
[18] Muller RH, Keck CM. Challenges and solutions for the delivery of biotech drugs - a review of drug nanocrystal technology and lipid nanoparticles. J Biotechnol 2004;113:151-70.
[19] Paul Ehrlich, Wikipedia, April 8 2012, April 13 2012, http://en.wikipedia.org/wiki/Paul_Ehrlich.
[20] Petkar KC, Chavhan SS, Agatonovik-Kustrin S, Sawant KK. Nanostructured materials in drug and gene delivery: a review of the state of the art. Critical reviews in therapeutic drug carrier systems 2011;28:101-64.
[21] Herlambang S, Kumagai M, Nomoto T, Horie S, Fukushima S, Oba M, et al. Disulfide crosslinked polyion complex micelles encapsulating dendrimer phthalocyanine directed to improved efficiency of photodynamic therapy. Journal of Controlled Release 2011;155:449-57.
[22] Park K. Dendrimer polymeric micelles for enhanced photodynamic cancer treatment. Journal of Controlled Release 2009;133:171-.
[23] Chisholm EJ, Vassaux G, Martin-Duque P, Chevre R, Lambert O, Pitard B, et al. Cancer-specific transgene expression mediated by systemic injection of nanoparticles. Cancer Research 2009;69:2655-62.
[24] Weiner N, Lieb L, Niemiec S, Ramachandran C, Hu Z, Egbaria K. Liposomes - a novel topical delivery system for pharmaceutical and cosmetic applications. Journal of Drug Targeting 1994;2:405-10.
[25] Choudhari KB, Labhasetwar V, Dorle AK. Liposomes as a carrier for oral-administration of insulin - effect of formulation factors. J Microencapsul 1994;11:319-25.
[26] Nguyen S, Hiorth M, Rykke M, Smistad G. The potential of liposomes as dental drug delivery systems. European Journal of Pharmaceutics and Biopharmaceutics 2011;77:75-83.
[27] Homsi J, Simon GR, Garrett CR, Springett G, De Conti R, Chiappori A, et al. Phase I trial of poly-L-glutamate camptothecin (CT-2106) administered weekly in patients with advanced solid malignancies. Clinical Cancer Research 2007;13:5855-61.
[28] Vogel VG. Effects of tamoxifen vs raloxifene on the risk of developing invasive breast cancer and other disease outcomes: The NSABP study of tamoxifen and raloxifene (STAR) P-2 trial (vol 295, pg 2727, 2006). Jama-Journal of the American Medical Association 2007;298:973-.
[29] Vogel VG, Costantino JP, Wickerham DL, Cronin WM, Cecchini RS, Atkins JN, et al. Effects of tamoxifen vs raloxifene on the risk of developing invasive breast cancer and other disease outcomes - The NSABP study of tamoxifen and raloxifene (STAR) P-2 trial. Jama-Journal of the American Medical Association 2006;295:2727-41.
[30] Vogel VG. Effects of tamoxifen vs raloxifene on the risk of developing invasive breast cancer and other disease outcomes: The NSABP study of tamoxifen and raloxifene (STAR) P-2 trial (vol 295, pg 2727, 2006). Jama-Journal of the American Medical Association 2006;296:2926-.

[31] Okada H, Heya T, Igari Y, Ogawa Y, Toguchi H, Shimamoto T. One-month release injectable microspheres of leuprolide acetate inhibit steroidogenesis and genital organ growth in rats. Int J Pharm 1989;54:231-9.
[32] Danielsson I, Lindman B. The definition of micro-emulsion. Colloids and Surfaces 1981;3:391-2.
[33] Moulik SP, Paul BK. Structure, dynamics and transport properties of microemulsions. Advances in Colloid and Interface Science 1998;78:99-195.
[34] Aprahamian M, Michel C, Humbert W, Devissaguet JP, Damge C. Transmucosal passage of polyalkyl cyanoacrylate nanocapsules as a new drug carrier in the small-intestine. Biology of the Cell 1987;61:69-76.
[35] Yoon W. Embolic agents used for bronchial artery embolisation in massive haemoptysis. Expert Opinion on Pharmacotherapy 2004;5:361-7.
[36] Vonarbourg A, Passirani C, Saulnier P, Benoit J-P. Parameters influencing the stealthiness of colloidal drug delivery systems. Biomaterials 2006;27:4356-73.
[37] De Geest BG, De Koker S, Sukhorukov GB, Kreft O, Parak WJ, Skirtach AG, et al. Polyelectrolyte microcapsules for biomedical applications. Soft Matter 2009;5:282-91.
[38] Shu S, Sun C, Zhang X, Wu Z, Wang Z, Li C. Hollow and degradable polyelectrolyte nanocapsules for protein drug delivery. Acta Biomaterialia 2010;6:210-7.
[39] Puri A, Loomis K, Smith B, Lee J-H, Yavlovich A, Heldman E, et al. Lipid-based nanoparticles as pharmaceutical drug carriers: from concepts to clinic. Critical Reviews in Therapeutic Drug Carrier Systems 2009;26:523-80.
[40] Lee J-H, Liao Y-T. Synthesis of polymeric nanofiber and polymeric nanosphere by living free radical polymerization. Journal of Applied Polymer Science 2006;101:3550-8.
[41] Jeon O, Kang JM, Yang HS, Song SJ, Bhang SH, Kang SW, et al. Bone morphogenetic protein-2 delivery using poly(lactic-co-glycolic acid) nanosphere for bone regeneration. Tissue Engineering Part A 2008;14:707-.
[42] Attama AA, Reichl S, Mueller-Goymann CC. Diclofenac sodium delivery to the eye: In vitro evaluation of novel solid lipid nanoparticle formulation using human cornea construct. Int J Pharm 2008;355:307-13.
[43] Attama AA, Mueller-Goymann CC. Effect of beeswax modification on the lipid matrix and solid lipid nanoparticle crystallinity. Colloid Surf A-Physicochem Eng Asp 2008;315:189-95.
[44] Lertsutthiwong P, Noomun K, Jongaroonngamsang N, Rojsitthisak P, Nimmannit U. Preparation of alginate nanocapsules containing turmeric oil. Carbohydrate Polymers 2008;74:209-14.
[45] Stella B, Arpicco S, Rocco F, Marsaud V, Renoir J-M, Cattel L, et al. Encapsulation of gemcitabine lipophilic derivatives into polycyanoacrylate nanospheres and nanocapsules. Int J Pharm 2007;344:71-7.
[46] Gelperina S, Kisich K, Iseman MD, Heifets L. The potential advantages of nanoparticle drug delivery systems in chemotherapy of tuberculosis. Am J Respir Crit Care Med 2005;172:1487-90.
[47] Vauthier C, Bouchemal K. Methods for the preparation and manufacture of polymeric nanoparticles. Pharm Res 2009;26:1025-58.

[48] Shen S, Gu T, Mao D, Xiao X, Yuan P, Yu M, et al. Synthesis of nonspherical mesoporous silica ellipsoids with tunable aspect ratios for magnetic assisted assembly and gene delivery. Chem Mat 2012;24:230-5.
[49] Daum N, Tscheka C, Neumeyer A, Schneider M. Novel approaches for drug delivery systems in nanomedicine: effects of particle design and shape. Wiley Interdisciplinary Reviews-Nanomedicine and Nanobiotechnology 2012;4:52-65.
[50] Tao L, Hu W, Liu Y, Huang G, Sumer BD, Gao J. Shape-specific polymeric nanomedicine: emerging opportunities and challenges. Experimental Biology and Medicine 2011;236:20-9.
[51] Couvreur P, Couarraze, G., Devissaguet, J., Puisieux, F., . Microencapsulation: methods and industrial applications. New York: Marcel Dekker; 1996.
[52] Diederichs JE, Muller RH. Liposomes in cosmetics and pharmaceutical products. Pharmazeutische Industrie 1994;56:267-75.
[53] Barratt G. Colloidal drug carriers: achievements and perspectives. Cell Mol Life Sci 2003;60:21-37.
[54] Sharma A, Sharma US. Liposomes in drug delivery: progress and limitations. Int J Pharm 1997;154:123-40.
[55] Saunders L, Perrin J, Gammack D. Ultrasonic irradiation of some phospholipid sols. The Journal of pharmacy and pharmacology 1962;14:567-72.
[56] Bangham AD, Standish MM, Watkins JC. Diffusion of univalent ions across the lamellae of swollen phospholipids. Journal of Molecular Biology 1965;13:238-52.
[57] Bangham AD, Hill MW, Miller NGA. Preparation and use of liposomes as models of biological membranes: Plenum Press; 1974.
[58] Szoka F, Papahadjopoulos D. Procedure for preparation of liposomes with large internal aqueous space and high capture by reverse-phase evaporation. Proceedings of the National Academy of Sciences of the United States of America 1978;75:4194-8.
[59] Bergenstahl B, Fontell K. Phase-equilibria in the system soybean lecithin water. Progress in Colloid and Polymer Science 1983;68:48-52.
[60] Aboofazeli R, Lawrence MJ. The phase behaviour of quaternary systems containing lecithin. Journal of Pharmacy and Pharmacology 1991;43:87.
[61] Aboofazeli R, Lawrence MJ. Investigations into the formation and characterization of phospholipid microemulsions. 1. pseudo-ternary phase-diagrams of systems containing water-lecithin-alcohol-isopropyl myristate. Int J Pharm 1993;93:161-75.
[62] Aboofazeli R, Lawrence CB, Wicks SR, Lawrence MJ. Investigations into the formation and characterization of phospholipid microemulsions. 3. pseudo-ternary phase-diagrams of systems containing water-lecithin-isopropyl myristate and either an alkanoic acid, amine, alkanediol, polyethylene-glycol alkyl ether or alcohol as cosurfactant. Int J Pharm 1994;111:63-72.
[63] Aboofazeli R, Patel N, Thomas M, Lawrence MJ. Investigations into the formation and characterization of phospholipid microemulsions. 4. pseudo-ternary phase-diagrams of systems containing water-lecithin-alcohol and oil - the influence of oil. Int J Pharm 1995;125:107-16.
[64] Allen TM, Cullis PR. Drug delivery systems: entering the mainstream. Science 2004;303:1818-22.
[65] Allen TM. Liposomes - opportunities in drug delivery. Drugs 1997;54:8-14.

[66] Gregoriadis G. Homing of liposomes to target-cells. Biochemical Society Transactions 1975;3:613-8.
[67] Torchilin VP. Liposomes as delivery agents for medical imaging. Molecular Medicine Today 1996;2:242-9.
[68] Gregoria.G, Leathwoo.Pd, Ryman BE. Enzyme entrapment in liposomes. Febs Letters 1971;14:95-9.
[69] Lasic DD. Liposomes: From physics to applications1993.
[70] Ruysschaert T, Germain M, Gomes J, Fournier D, Sukhorukov GB, Meier W, et al. Liposome-based nanocapsules. Ieee Transactions on Nanobioscience 2004;3:49-55.
[71] Donath E, Sukhorukov GB, Caruso F, Davis SA, Mohwald H. Novel hollow polymer shells by colloid-templated assembly of polyelectrolytes. Angew Chem-Int Edit 1998;37:2202-5.
[72] Soppimath KS, Aminabhavi TM, Kulkarni AR, Rudzinski WE. Biodegradable polymeric nanoparticles as drug delivery devices. Journal of Controlled Release 2001;70:1-20.
[73] Kawahashi N, Matijevic E. Preparation of hollow spherical-particles of yttrium compounds. Journal of Colloid and Interface Science 1991;143:103-10.
[74] Bruinsma PJ, Kim, A. Y., Liu, J., Baskaran, S. Mesoporous silica synthesized by solvent evaporation: spun fibers and spray-dried hollow spheres. Chem Mat 1997;9:2507-12.
[75] Schacht S, Huo Q, VoigtMartin IG, Stucky GD, Schuth F. Oil-water interface templating of mesoporous macroscale structures. Science 1996;273:768-71.
[76] Iida M, Sasaki T, Watanabe M. Titanium dioxide hollow microspheres with an extremely thin shell. Chem Mat 1998;10:3780-2.
[77] Langmuir I. In: Co. GE, editor. US Patent. G01N 21/41 (20060101) ed. United States1941.
[78] Iler RK. Multilayers of colloidal particles. Journal of Colloid and Interface Science 1966;21:569-94.
[79] Decher G, Hong JD. Buildup of ultrathin multilayer films by a self-assembly process. 2. consecutive adsorption of anionic and cationic bipolar amphiphiles and polyelectrolytes on charged surfaces. Berichte Der Bunsen-Gesellschaft-Physical Chemistry Chemical Physics 1991;95:1430-4.
[80] Decher G, Hong JD. Buildup of ultrathin multilayer films by a self-assembly process. 1. consecutive adsorption of anionic and cationic bipolar amphiphiles on charged surfaces. Makromolekulare Chemie-Macromolecular Symposia 1991;46:321-7.
[81] Decher G, Maclennan J, Reibel J, Sohling U. Highly-ordered ultrathin LC multilayer films on solid substrates. Advanced Materials 1991;3:617-9.
[82] Decher G, Hong JD, Schmitt J. Buildup of ultrathin multilayer films by a self-assembly process. 3. consecutively alternating adsorption of anionic and cationic polyelectrolytes on charged surfaces. Thin Solid Films 1992;210:831-5.
[83] Decher G, Maclennan J, Sohling U, Reibel J. Creation and structural comparison of ultrathin film assemblies - transferred freely suspended films and langmuir-blodgett-films of liquid-crystals. Thin Solid Films 1992;210:504-7.
[84] Decher G. Fuzzy nanoassemblies: Toward layered polymeric multicomposites. Science 1997;277:1232-7.
[85] Decher G, Eckle M, Schmitt J, Struth B. Layer-by-layer assembled multicomposite films. Curr Opin Colloid Interface Sci 1998;3:32-9.

[86] Hammond PT. Recent explorations in electrostatic multilayer thin film assembly. Curr Opin Colloid Interface Sci 1999;4:430-42.
[87] Bertrand P, Jonas A, Laschewsky A, Legras R. Ultrathin polymer coatings by complexation of polyelectrolytes at interfaces: suitable materials, structure and properties. Macromolecular Rapid Communications 2000;21:319-48.
[88] Schonhoff M. Self-assembled polyelectrolyte multilayers. Curr Opin Colloid Interface Sci 2003;8:86-95.
[89] Liu WJ, Chen GH, He GH, He ZC, Qian Z. Sacrificial functional polystyrene template to prepare chitosan nanocapsules and in vitro drug release properties. J Mater Sci 2011;46:6758-65.
[90] Zohuriaan-Mehr MJ, Omidian H, Doroudiani S, Kabiri K. Advances in non-hygienic applications of superabsorbent hydrogel materials. J Mater Sci 2010;45:5711-35.
[91] Huang XH, Xu J, Li W, Chen KJ. Preparation of amorphous carbon films by layer-by-layerhydrogen plasma annealing method and their luminescence properties. Thin Solid Films 2002;422:130-4.
[92] Shi LX, Sun JQ, Liu JQ, Shen JC, Gao MY. Site-selective deposition of enzyme/polyelectrolyte multilayer films on ITO electrodes controlled electric fields. Chemistry Letters 2002:1168-9.
[93] Ariga K, Hill JP, Ji QM. Layer-by-layer assembly as a versatile bottom-up nanofabrication technique for exploratory research and realistic application. Phys Chem Chem Phys 2007;9:2319-40.
[94] Anzai J, Kobayashi Y, Nakamura N, Nishimura M, Hoshi T. Layer-by-Layer construction of multilayer thin films composed of avidin and biotin-labeled poly(amine)s. Langmuir 1999;15:221-6.
[95] Cheung JH, Fou AF, Ferreira M, Rubner MF. Molecular self-assembly of conducting polymers-a new Layer-by-Layer thin-film deposition process. Abstr Pap Am Chem Soc 1993;206:364-poly.
[96] Hong JD, Lowack K, Schmitt J, Decher G. Layer-by-Layer deposited multilayer assemblies of polyelectrolytes and proteins-from ultrathin films to protein arrays. In: Laggner PGO, editor. Trends in Colloid and Interface Science Vii1993. p. 98-102.
[97] Byrd H, Pike JK, Talham DR. Inorganic monolayers formed at an organic template-a langmuir-blodgett route to monolayer and multilayer films of zirconium octadecylphosphonate. Chem Mat 1993;5:709-15.
[98] Kayushina R, Lvov Y, Stepina N, Belyaev V, Khurgin Y. Construction and X-ray reflectivity study of self-assembled lysozyme/polyion multilayers. Thin Solid Films 1996;284:246-8.
[99] Fendler JH. Self-assembled nanostructured materials. Chem Mat 1996;8:1616-24.
[100] Sukhorukov GB, Donath E, Lichtenfeld H, Knippel E, Knippel M, Budde A, et al. Layer-by-Layer self assembly of polyelectrolytes on colloidal particles. Colloid Surf A-Physicochem Eng Asp 1998;137:253-66.
[101] Caruso F. Colloids and colloid assemblies: synthesis, modification, organization and utilization of colloidal particles. Weinheim: Wiley-VCH; 2003.
[102] Caruso F, Caruso RA, Mohwald H. Nanoengineering of inorganic and hybrid hollow spheres by colloidal templating. Science 1998;282:1111-4.

[103] Caruso F, Caruso RA, Mohwald H. Production of hollow microspheres from nanostructured composite particles. Chem Mat 1999;11:3309-14.
[104] Caruso F. Hollow inorganic capsules via colloid-templated layer-by-layer electrostatic assembly. Colloid Chemistry Ii 2003;227:145-68.
[105] Caruso F. Generation of complex colloids by polyelectrolyte-assisted electrostatic self-assembly. Aust J Chem 2001;54:349-53.
[106] De Geest BG, Sukhorukov GB, Mohwald H. The pros and cons of polyelectrolyte capsules in drug delivery. Expert Opinion on Drug Delivery 2009;6:613-24.
[107] Johnston APR, Cortez C, Angelatos AS, Caruso F. Layer-by-Layer engineered capsules and their applications. Curr Opin Colloid Interface Sci 2006;11:203-9.
[108] Sukhorukov GB, Antipov AA, Voigt A, Donath E, Mohwald H. pH-controlled macromolecule encapsulation in and release from polyelectrolyte multilayer nanocapsules. Macromolecular Rapid Communications 2001;22:44-6.
[109] Georgieva R, Moya S, Hin M, Mitlohner R, Donath E, Kiesewetter H, et al. Permeation of macromolecules into polyelectrolyte microcapsules. Biomacromolecules 2002;3:517-24.
[110] Khopade AJ, Caruso F. Stepwise self-assembled poly(amidoamine) dendrimer and poly(styrenesulfonate) microcapsules as sustained delivery vehicles. Biomacromolecules 2002;3:1154-62.
[111] Sukhorukov GB, Brumen M, Donath E, Mohwald H. Hollow polyelectrolyte shells: exclusion of polymers and donnan equilibrium. J Phys Chem B 1999;103:6434-40.
[112] Ibarz G, Dahne L, Donath E, Mohwald H. Smart micro- and nanocontainers for storage, transport, and release. Advanced Materials 2001;13:1324-7.
[113] Ye SQ, Wang CY, Liu XX, Tong Z. Multilayer nanocapsules of polysaccharide chitosan and alginate through layer-by-layer assembly directly on PS nanoparticles for release. J Biomater Sci-Polym Ed 2005;16:909-23.
[114] Sukhorukov G, Dahne L, Hartmann J, Donath E, Mohwald H. Controlled precipitation of dyes into hollow polyelectrolyte capsules based on colloids and biocolloids. Advanced Materials 2000;12:112-5.
[115] Tao X, Chen H, Sun XJ, Chen HF, Roa WH. Formulation and cytotoxicity of doxorubicin loaded in self-assembled bio-polyelectrolyte microshells. Int J Pharm 2007;336:376-81.
[116] Caruso F, Trau D, Mohwald H, Renneberg R. Enzyme encapsulation in Layer-by-Layer engineered polymer multilayer capsules. Langmuir 2000;16:1485-8.
[117] Trau D, Yang WJ, Seydack M, Caruso F, Yu NT, Renneberg R. Nanoencapsulated microcrystalline particles for superamplified biochemical assays. Analytical Chemistry 2002;74:5480-6.
[118] Balabushevitch NG, Sukhorukov GB, Moroz NA, Volodkin DV, Larionova NI, Donath E, et al. Encapsulation of proteins by Layer-by-Layer adsorption of polyelectrolytes onto protein aggregates: factors regulating the protein release. Biotechnology and Bioengineering 2001;76:207-13.
[119] Bobreshova ME, Sukhorukov GB, Saburova EA, Elfimova LI, Shabarchina LI, Sukhorukov BI. Lactate dehydrogenase in interpolyelectrolyte complex. Function and stability. Biofizika 1999;44:813-20.

[120] Dai ZF, Heilig A, Zastrow H, Donath E, Mohwald H. Novel formulations of vitamins and insulin by nanoengineering of polyelectrolyte multilayers around microcrystals. Chem-Eur J 2004;10:6369-74.
[121] Shenoy DB, Sukhorukov GB. Engineered microcrystals for direct surface modification with Layer-by-Layer technique for optimized dissolution. European Journal of Pharmaceutics and Biopharmaceutics 2004;58:521-7.
[122] Qiu XP, Leporatti S, Donath E, Mohwald H. Studies on the drug release properties of polysaccharide multilayers encapsulated ibuprofen microparticles. Langmuir 2001;17:5375-80.
[123] Ye SQ, Wang CY, Liu XX, Tong Z, Ren B, Zeng F. New loading process and release properties of insulin from polysaccharide microcapsules fabricated through Layer-by-Layer assembly. Journal of Controlled Release 2006;112:79-87.
[124] Ye SQ, Wang CY, Liu XX, Tong Z. Deposition temperature effect on release rate of indomethacin microcrystals from microcapsules of Layer-by-Layer assembled chitosan and alginate multilayer films. Journal of Controlled Release 2005;106:319-28.
[125] Wang YJ, Caruso F. Enzyme encapsulation in nanoporous silica spherest. Chem Commun 2004:1528-9.
[126] Wang YJ, Caruso F. Mesoporous silica spheres as supports for enzyme immobilization and encapsulation. Chem Mat 2005;17:953-61.
[127] Volodkin DV, Petrov AI, Prevot M, Sukhorukov GB. Matrix polyelectrolyte microcapsules: new system for macromolecule encapsulation. Langmuir 2004;20:3398-406.
[128] Yu AM, Wang YJ, Barlow E, Caruso F. Mesoporous silica particles as templates for preparing enzyme-loaded biocompatible microcapsules. Advanced Materials 2005;17:1737-+.
[129] Wang YJ, Yu AM, Caruso F. Nanoporous polyelectrolyte spheres prepared by sequentially coating sacrificial mesoporous silica spheres. Angew Chem-Int Edit 2005;44:2888-92.
[130] Zhu YF, Shi JL, Shen WH, Dong XP, Feng JW, Ruan ML, et al. Stimuli-responsive controlled drug release from a hollow mesoporous silica sphere/polyelectrolyte multilayer core-shell structure. Angew Chem-Int Edit 2005;44:5083-7.
[131] Itoh Y, Matsusaki M, Kida T, Akashi M. Enzyme-responsive release of encapsulated proteins from biodegradable hollow capsules. Biomacromolecules 2006;7:2715-8.
[132] Harrison TS, Goa KL. Long-acting risperidone - a review of its use in schizophrenia. Cns Drugs 2004;18:113-32.
[133] Angelatos AS, Radt B, Caruso F. Light-responsive polyelectrolyte/gold nanoparticle microcapsules. J Phys Chem B 2005;109:3071-6.
[134] Radt B, Smith TA, Caruso F. Optically addressable nanostructured capsules. Advanced Materials 2004;16:2184-+.
[135] De Geest BG, Skirtach AG, De Beer TRM, Sukhorukov GB, Bracke L, Baeyens WRG, et al. Stimuli-responsive multilayered hybrid nanoparticle/polyelectrolyte capsules. Macromolecular Rapid Communications 2007;28:88-95.
[136] Lu ZH, Prouty MD, Guo ZH, Golub VO, Kumar C, Lvov YM. Magnetic switch of permeability for polyelectrolyte microcapsules embedded with Co@Au nanoparticles. Langmuir 2005;21:2042-50.

[137] De Geest BG, Skirtach AG, Mamedov AA, Antipov AA, Kotov NA, De Smedt SC, et al. Ultrasound-triggered release from multilayered capsules. Small 2007;3:804-8.
[138] Skirtach AG, De Geest BG, Mamedov A, Antipov AA, Kotov NA, Sukhorukov GB. Ultrasound stimulated release and catalysis using polyelectrolyte multilayer capsules. J Mater Chem 2007;17:1050-4.
[139] Tao X, Li JB, Mohwald H. Self-assembly, optical behavior, and permeability of a novel capsule based on an azo dye and polyelectrolytes. Chem-Eur J 2004;10:3397-403.
[140] De Geest BG, Sanders NN, Sukhorukov GB, Demeester J, De Smedt SC. Release mechanisms for polyelectrolyte capsules. Chem Soc Rev 2007;36:636-49.
[141] Skirtach AG, Antipov AA, Shchukin DG, Sukhorukov GB. Remote activation of capsules containing Ag nanoparticles and IR dye by laser light. Langmuir 2004;20:6988-92.
[142] Skirtach AG, Dejugnat C, Braun D, Susha AS, Rogach AL, Parak WJ, et al. The role of metal nanoparticles in remote release of encapsulated materials. Nano Letters 2005;5:1371-7.
[143] Skirtach AG, Javier AM, Kreft O, Koehler K, Alberola AP, Moehwald H, et al. Laser-induced release of encapsulated materials inside living cells. Angew Chem-Int Edit 2006;45:4612-7.
[144] Skirtach AG, Karageorgiev P, Bedard MF, Sukhorukov GB, Moehwald H. Reversibly permeable nanomembranes of polymeric microcapsules. J Am Chem Soc 2008;130:11572-+.
[145] Skirtach AG, Karageorgiev P, De Geest BG, Pazos-Perez N, Braun D, Sukhorukov GB. Nanorods as wavelength-selective absorption centers in the visible and near-infrared regions of the electromagnetic spectrum. Advanced Materials 2008;20:506-+.
[146] Gerasimov OV, Boomer JA, Qualls MM, Thompson DH. Cytosolic drug delivery using pH- and light-sensitive liposomes. Advanced Drug Delivery Reviews 1999;38:317-38.
[147] Shum P, Kim JM, Thompson DH. Phototriggering of liposomal drug delivery systems. Advanced Drug Delivery Reviews 2001;53:273-84.
[148] Thompson DH, Gerasimov OV, Wheeler JJ, Rui YJ, Anderson VC. Triggerable plasmalogen liposomes: improvement of system efficiency. Biochimica Et Biophysica Acta-Biomembranes 1996;1279:25-34.
[149] Zhang ZY, Smith BD. Synthesis and characterization of NVOC-DOPE, a caged photoactivatable derivative of dioleoylphosphatidylethanolamine. Bioconjugate Chemistry 1999;10:1150-2.
[150] Bisby RH, Mead C, Morgan CC. Wavelength-programmed solute release from photosensitive liposomes. Biochemical and Biophysical Research Communications 2000;276:169-73.
[151] Spratt T, Bondurant B, O'Brien DF. Rapid release of liposomal contents upon photoinitiated destabilization with UV exposure. Biochimica Et Biophysica Acta-Biomembranes 2003;1611:35-43.
[152] Goodwin AP, Mynar JL, Ma YZ, Fleming GR, Frechet JMJ. Synthetic micelle sensitive to IR light via a two-photon process. J Am Chem Soc 2005;127:9952-3.
[153] Jiang JQ, Tong X, Zhao Y. A new design for light-breakable polymer micelles. J Am Chem Soc 2005;127:8290-1.
[154] Javier AM, del Pino P, Bedard MF, Ho D, Skirtach AG, Sukhorukov GB, et al. Photoactivated release of cargo from the cavity of polyelectrolyte capsules to the cytosol of Cells. Langmuir 2008;24:12517-20.

[155] Tiourina OP, Antipov AA, Sukhorukov GB, Larionova NL, Lvov Y, Mohwald H. Entrapment of alpha-chymotrypsin into hollow polyelectrolyte microcapsules. Macromolecular Bioscience 2001;1:209-14.
[156] Qiu XP, Donath E, Mohwald H. Permeability of ibuprofen in various polyelectrolyte multilayers. Macromolecular Materials and Engineering 2001;286:591-7.
[157] Antipov AA, Sukhorukov GB, Leporatti S, Radtchenko IL, Donath E, Mohwald H. Polyelectrolyte multilayer capsule permeability control. Colloid Surf A-Physicochem Eng Asp 2002;198:535-41.
[158] Tiourina OP, Sukhorukov GB. Multilayer alginate/protamine microsized capsules: encapsulation of alpha-chymotrypsin and controlled release study. Int J Pharm 2002;242:155-61.
[159] Shchukin DG, Sukhorukov GB, Mohwald H. Smart inorganic/organic nanocomposite hollow microcapsules. Angew Chem-Int Edit 2003;42:4472-5.
[160] Balabushevich NG, Tiourina OP, Volodkin DV, Larionova NI, Sukhorukov GB. Loading the multilayer dextran sulfate/protamine microsized capsules with peroxidase. Biomacromolecules 2003;4:1191-7.
[161] Antipov AA, Sukhorukov GB, Mohwald H. Influence of the ionic strength on the polyelectrolyte multilayers' permeability. Langmuir 2003;19:2444-8.
[162] Dai ZF, Voigt A, Leporatti S, Donath E, Dahne L, Mohwald H. Layer-by-layer self-assembly of polyelectrolyte and low molecular weight species into capsules. Advanced Materials 2001;13:1339-42.
[163] Mendelsohn JD, Barrett CJ, Chan VV, Pal AJ, Mayes AM, Rubner MF. Fabrication of microporous thin films from polyelectrolyte multilayers. Langmuir 2000;16:5017-23.
[164] Schuler C, Caruso F. Decomposable hollow biopolymer-based capsules. Biomacromolecules 2001;2:921-6.
[165] Caruso F, Schuler C, Kurth DG. Core-shell particles and hollow shells containing metallo-supramolecular components. Chem Mat 1999;11:3394-9.
[166] Khopade AJ, Caruso F. Two-component, ultrathin microcapsules prepared by a core-mediated layer-by-layer approach. Chem Mat 2004;16:2107-12.
[167] Gao CY, Moya S, Lichtenfeld H, Casoli A, Fiedler H, Donath E, et al. The decomposition process of melamine formaldehyde cores: the key step in the fabrication of ultrathin polyelectrolyte multilayer capsules. Macromolecular Materials and Engineering 2001;286:355-61.
[168] Gao CY, Liu XY, Shen JC, Mohwald H. Spontaneous deposition of horseradish peroxidase into polyelectrolyte multilayer capsules to improve its activity and stability. Chem Commun 2002:1928-9.
[169] Gao CY, Moya S, Donath E, Mohwald H. Melamine formaldehyde core decomposition as the key step controlling capsule integrity: optimizing the polyelectrolyte capsule fabrication. Macromolecular Chemistry and Physics 2002;203:953-60.
[170] Caruso F, Mohwald H. Preparation and characterization of ordered nanoparticle and polymer composite multilayers on colloids. Langmuir 1999;15:8276-81.
[171] Kato N, Schuetz P, Fery A, Caruso F. Thin multilayer films of weak polyelectrolytes on colloid particles. Macromolecules 2002;35:9780-7.

[172] Caruso F, Mohwald H. Protein multilayer formation on colloids through a stepwise self-assembly technique. J Am Chem Soc 1999;121:6039-46.
[173] Kato N, Caruso F. Homogeneous, competitive fluorescence quenching immunoassay based on gold nanoparticle/polyelectrolyte coated latex particles. J Phys Chem B 2005;109:19604-12.
[174] Dejugnat C, Prevot M, Sukhorukov GB. Stimuli-responsive properties of nano-engineered polyelectrolyte microcapsules. Abstr Pap Am Chem Soc 2004;227:U549-U50.
[175] Zhu HG, Stein EW, Lu ZH, Lvov YM, McShane MJ. Synthesis of size-controlled monodisperse manganese carbonate microparticles as templates for uniform polyelectrolyte microcapsule formation. Chem Mat 2005;17:2323-8.
[176] Antipov AA, Shchukin D, Fedutik Y, Petrov AI, Sukhorukov GB, Mohwald H. Carbonate microparticles for hollow polyelectrolyte capsules fabrication. Colloid Surf A-Physicochem Eng Asp 2003;224:175-83.
[177] Quinn JF, Johnston APR, Such GK, Zelikin AN, Caruso F. Next generation, sequentially assembled ultrathin films: beyond electrostatics. Chem Soc Rev 2007;36:707-18.
[178] Sukhishvili SA. Responsive polymer films and capsules via Layer-by-Layer assembly. Curr Opin Colloid Interface Sci 2005;10:37-44.
[179] Fukui Y, Fujimoto K. The preparation of sugar polymer-coated nanocapsules by the Layer-by-Layer deposition on the liposome. Langmuir 2009;25:10020-5.
[180] Song W, He Q, Moehwald H, Yang Y, Li J. Smart polyelectrolyte microcapsules as carriers for water-soluble small molecular drug. Journal of Controlled Release 2009;139:160-6.
[181] Schwertmann U, Cornell RM. Iron oxides in the laboratory: preparation and characterization2000.
[182] Poyard S, Jaffrezic-Renault N, Martelet C, Cosnier S, Labbe P. Optimization of an inorganic/bio-organic matrix for the development of new glucose biosensor membranes. Analytica Chimica Acta 1998;364:165-72.
[183] de Melo JV, Cosnier S, Mousty C, Martelet C, Jaffrezic-Renault N. Urea biosensors based on immobilization of urease into two oppositely charged clays (Laponite and Zn-Al layered double hydroxides). Analytical Chemistry 2002;74:4037-43.
[184] Shan D, Cosnier S, Mousty C. HRP/ Zn-Cr-ABTS redox clay-based biosensor: design and optimization for cyanide detection. Biosensors & Bioelectronics 2004;20:390-6.
[185] What is zeta potential? : Microtec co., January 1st 2011, October 20th 2011, ltd. http://nition.com/en/products/zeecom_s.htm.
[186] Schwer C, Kenndler E. Electrophoresis in fused-silica capillaries-the influence of organic-solvents on the electroosmotic velocity and the zeta-potential. Analytical Chemistry 1991;63:1801-7.
[187] Bockris J O'M RAKN. Modern electrochemistry. New York: Plenum Press; 1970.
[188] J G. Colloids and Interfaces with surfactants and polymers - an introduction. West Sussex: John Wiley & Sons Ltd.; 2004.
[189] Zeta-Meter TES, "Home Page". Zeta Potantial: A complete Course in 5 Minutes", June 07 2010, October 25 2011,. Zeta-Meter, Inc, www.zeta-meter.com.; 2010.
[190] J KB. Micro- and nanoscale fluid mechanics: transport in microflidic devices. New York, NY: Cambridge University Press; 2010.

[191] Berne BJ, Pecora, R. Dynamic light scattering. New York: Wiley; 1976.
[192] R P. Doppler shifts in light scattering from pure liquids and polymer solutions. Journal of Chemical Physics 1964;40:1604.
[193] Cummins HZ, Knable N, Yeh Y. Observation of diffusion broadening of rayleigh scattered light. Physical Review Letters 1964;12:150-3.
[194] Urban C, Schurtenberger P. Characterization of turbid colloidal suspensions using light scattering techniques combined with cross-correlation methods. Journal of Colloid and Interface Science 1998;207:150-8.
[195] Clark N A LJH, Benedek G B. A study on brownian motion using light scattering. American Journal of Physics 1970;38:575-85.
[196] E KD. Analysis of macromolecular polydispersity in intensity correlation spectroscopy-method of cumulants. Journal of Chemical Physics 1972;57:4814-&.

[197] A E. Investigations on the theory of Brownian Movement. New York: Dover Publ. Inc.; 1956.
[198] Dynamic light scattering, Wikipedia, December 17 2011, December 23 2011, http://en.wikipedia.org/wiki/Dynamic_light_scattering.
[199] Rudenberg HG, Rudenberg PG. Origin and background of the invention of the electron microscope: commentary and expanded notes on memoir of reinhold rudenberg. In: Hawkes PW, editor. Advances in Imaging and Electron Physics, Vol 1602010. p. 207-86.
[200] Erni R, Rossell MD, Kisielowski C, Dahmen U. Atomic-resolution imaging with a sub-50-pm electron probe. Physical Review Letters 2009;102.
[201] Electron Microscope, Wikipedia, July 9 2012, August 2 2012, http://en.wikipedia.org/wiki/Electron_microscope.
[202] Goodhew P J HJ, Beanland R. Electron microscopy and analysis, 3rd edition. London: Taylor & Francis; 2001.
[203] Suzuki E. High-resolution scanning electron microscopy of immunogold-labelled cells by the use of thin plasma coating of osmium. Journal of Microscopy-Oxford 2002;208:153-7.
[204] Scanning electron microscope, Wikipedia, December 4 2011, December 23 2011, http://en.wikipedia.org/wiki/Scanning_electron_microscopy.
[205] McMullan D. Scanning electron microscopy 1928–1965. Scanning 1995;17:175.
[206] Scanning Electron Microscope, Purdue University, July 10 2012, August 2 2012, http://www.purdue.edu/rem/rs/sem.htm.
[207] Transmission electron microscopy, Wikipedia, November 28 2011, December 23 2011, http://en.wikipedia.org/wiki/Transmission_electron_microscope.
[208] D GM. Introduction to conventional transmission electron microscopy. Cambridge: Cambridge University Press; 2003.
[209] F ER. Physical principles of electron microscopy: an introduction to TEM, SEM, and AEM. USA: Springer; 2005.
[210] transmission electron microscope, Encyclopedia Britannica, Inc., January 1 2012, August 2 2012, http://www.britannica.com/EBchecked/media/110686/Transmission-electron-microscope.
[211] CPS disc centrifuge, CPS Instruments Inc., January 01 2011, August 02 2012, http://www.cpsinstruments.eu/pdf/General%20Brochure.pdf.
[212] H L. Hydrodynamics 6th edition ed. Cambridge: Cambridge University Press; 1994.

[213] Stokes' law, Wikipedia, May 30 2012, August 02 2012, http://en.wikipedia.org/wiki/Stokes%27_law.
[214] Nanoparticle Size Analyser, CPS Instruments Europe, analytikLtd., July 10 2012, August 2 2012, http://www.analytik.co.uk/nanoparticle-size-analysis.htm.
[215] A. NR. Squire's fundamentals of radiology 5th edition. USA: Harvard University Press; 1997.
[216] Introduction to X-ray Powder Diffraction, Connolly J R, January 1 2007, August 02 2012, http://epswww.unm.edu/xrd/xrdclass/01-XRD-Intro.pdf.
[217] Langford J I LD. Powder diffraction. Reports on Progress in Physics 1996;59:131-24.
[218] Geochemical Instrumentation and Analysis, Integrating Research and Education, June 22 2012, August 02 2012, http://serc.carleton.edu/research_education/geochemsheets/techniques/XRD.html.
[219] Powder diffraction, Wikipedia, July 31 2012, August 02 2012, http://en.wikipedia.org/wiki/Powder_diffraction.
[220] C WAJ. X-ray optics: the diffraction of X-rays by finite an imperfect crystals. 2nd edition. London: Methuen; 1962.
[221] Patterson AL. The scherrer formula for X-ray particle size determination. Physics Review 1939;56:978-82.
[222] Sun J, Zhou S, Hou P, Yang Y, Weng J, Li X, et al. Synthesis and characterization of biocompatible Fe3O4 nanoparticles. J Biomed Mater Res Part A 2007;80A:333-41.
[223] Shape factor (X-ray diffraction), Wikipedia, May 05 2012, August 02 2012, http://en.wikipedia.org/wiki/Shape_factor_%28X-ray_diffraction%29.
[224] Stöber W, Fink, A., Bohn, E. Controlled growth of monodisperse silica spheres in the micron size range. Journal of colloid and interface science 1968;26.
[225] Schonhoff M. Layered polyelectrolyte complexes: physics of formation and molecular properties. Journal of Physics-Condensed Matter 2003;15:R1781-R808.
[226] Goodwin JW, Hearn J, Ho CC, Ottewill RH. The preparation and characterisation of polymer latices formed in the absence of surface active agents. British Polymer Journal 1973;5:347-62.
[227] Goodwin JW, Hearn J, Ho CC, Ottewill RH. Studies on preparation and characterization of monodispersed polystyrene lattices .3. Preparation without added surface-active agents. Colloid and Polymer Science 1974;252:464-71.
[228] Chung-li Y, goodwin J, Ottewill R. Studies on the preparation and characterisation of monodisperse polystyrene latices

Kolloidchemie heute II. In: Kohlschütter H, Müller F, Weiss A, editors.: Springer Berlin / Heidelberg; 1976. p. 163-75.
[229] Rockwood company, 2001,Chembrief, vol 1, issue 2.
[230] http://www.Laponite.com/science.htm. Rockwood Additives; 2003.
[231] Mourchid A, Delville A, Lambard J, Lecolier E, Levitz P. Phase-diagram of colloidal dispersions of anisotropic charged-particles - equilibrium properties, structure, and rheology of laponite suspensions. Langmuir 1995;11:1942-50.
[232] Mourchid A, Lecolier E, Van Damme H, Levitz P. On viscoelastic, birefringent, and swelling properties of Laponite clay suspensions: Revisited phase diagram. Langmuir 1998;14:4718-23.

[233] Arys X, Laschewsky A, Jonas AM. Ordered polyelectrolyte "multilayers". 1. Mechanisms of growth and structure formation: A comparison with classical fuzzy "multilayers". Macromolecules 2001;34:3318-30.
[234] Buron CC, Filiatre C, Membrey F, Bainier C, Charraut D, Foissy A. Early steps in layer-by-layer construction of polyelectrolyte films: the transition from surface/polymer to polymer/polymer determining interactions. Journal of Colloid and Interface Science 2007;314:358-66.
[235] Dejeu J, Buisson L, Guth MC, Roidor C, Membrey F, Charraut D, et al. Early steps of the film growth mechanism in self-assembled multilayers of PAH and PSS on silica - Polymer uptake, charge balance and AFM analysis. Colloid Surf A-Physicochem Eng Asp 2006;288:26-35.
[236] Musyanovych A, Rossmanith R, Tontsch C, Landfester K. Effect of hydrophilic comonomer and surfactant type on the colloidal stability and size distribution of carboxyl- and amino-functionalized polystyrene particles prepared by miniemulsion polymerization. Langmuir 2007;23:5367-76.
[237] Duff DG, Baiker A, Edwards PP. A new hydrosol of gold clusters .1. formation and particle-size variation. Langmuir 1993;9:2301-9.
[238] Scherrer P. Bestimmung der Grösse und der inneren Struktur von Kolloidteilchen mittels Röntgenstrahlen. Nachrichten von der Gesellschaft der Wissenschaften zu Göttingen 1918;2.
[239] Patterson AL. The scherrer formula for X-ray particle size determination. Physical Review 1939;56.
[240] Bovine serum albumin, Wikipedia, November 22 2011, December 23 2011, http://en.wikipedia.org/wiki/Bovine_serum_albumin.
[241] http://www.sigmaaldrich.com/sigma/product%20information%20sheet/a3912pis.pdf
[242] Revenis ME, Kaliner MA. Lactoferrin and lysozyme deficiency in airway secretions - association with the development of bronchopulmonary dysplasia. Journal of Pediatrics 1992;121:262-70.
[243] Lysozyme, Wikipedia, December 15 2011, December 23 2011, http://en.wikipedia.org/wiki/Lysozyme.
[244] Lysozyme, Lysozyme.co.uk, October 10 2011, December 23 2011, http://lysozyme.co.uk/.
[245] Protein, Wikipedia, August 23 2012, August 13 2012, http://en.wikipedia.org/wiki/Protein.